

JAERI - M
83-005

JAPANESE CONTRIBUTIONS TO THE JAPAN-US WORKSHOP
ON BLANKET DESIGN/TECHNOLOGY

(Exchange B-39 in the Japan-US Fusion

Cooperation Program, November 10-11, 1982)

February 1983

Tatsuzo TONE, Yasushi SEKI, Akio MINATO*¹

Takeshi KOBAYASHI*², Seiji MORI*²

Hiromitsu KAWASAKI*³ and Kenji SUMITA*⁴

日本原子力研究所
Japan Atomic Energy Research Institute

JAERI-Mレポートは、日本原子力研究所が不定期に公刊している研究報告書です。
入手の間合わせは、日本原子力研究所技術情報部情報資料課（〒319-11茨城県那珂郡東海村）あて、お申しこしてください。なお、このほかに財団法人原子力弘済会資料センター（〒319-11茨城県那珂郡東海村日本原子力研究所内）で複写による実費頒布をおこなっております。

JAERI-M reports are issued irregularly.

Inquiries about availability of the reports should be addressed to Information Section, Division of Technical Information, Japan Atomic Energy Research Institute, Tokai-mura, Naka-gun, Ibaraki-ken 319-11, Japan.

©Japan Atomic Energy Research Institute, 1983

編集兼発行 日本原子力研究所
印 刷 いばらき印刷㈱

Japanese Contributions to the Japan-US Workshop
on Blanket Design/Technology
(Exchange B-39 in the Japan-US Fusion
Cooperation Program, November 10-11,1982)

Tatsuzo TONE, Yasushi SEKI, Akio MINATO^{*1}
Takeshi KOBAYASHI^{*2}, Seiji MORI^{*2}
Hiromitsu KAWASAKI^{*3} and Kenji SUMITA^{*4}

Division of Large Tokamak Development
Tokai Research Establishment, JAERI
(Received January 17, 1983)

This report describes Japanese papers presented at the Japan-US Workshop on Blanket Design/Technology which was held at Argonne National Laboratory, November 10-11, 1982. Overview of Fusion Experimental Reactor(FER), JAERI's activities related to first wall/blanket/shield, summary of FER blanket and its technology development issues and summary of activities at universities on fusion reactor blanket engineering are covered.

Keywords: Nuclear Fusion, Japan-US Fusion Cooperation, Exchange Program, Tokamak, Fusion Experimental Reactor, First Wall/Blanket/Shield Design

*1 On leave from Kawasaki Heavy Industries,Ltd.

*2 Kawasaki Heavy Industries,Ltd.

*3 Century Research Center Corp.,Ltd.

*4 Osaka University

ブランケット設計／技術に関する日米ワークショップ
における日本側提出論文
(日米核融合研究協力・交換計画 B-39)

日本原子力研究所東海研究所大型トカマク開発部
東稔達三・関 泰・湊 章男^{*1}・小林武司^{*2}
森 清治^{*2}・川崎弘光^{*3}・住田健二^{*4}

(1983年1月17日受理)

本報告書は、1982年11月10-11日に米国のアルゴンヌ国立研究所において開催された、「ブランケット設計／技術」に関する日米ワークショップに日本側が提出した論文をとりまとめたものである。内容は、核融合実験炉（FER）の概要、第1壁／ブランケット／遮蔽に関連した原研の研究開発の現況、FERブランケット設計の概要と技術的課題、及び大学における核融合炉ブランケットの研究の概要で構成されている。

-
- * 1 出向職員，川崎重工（株）
 - * 2 川崎重工（株）
 - * 3 センチュリー・リサーチ・センター（株）
 - * 4 大阪大学

Contents

I. Overview of the Fusion Experimental Reactor (FER) (T. Tone) ...	1
II. Research and Development Activities Related to First Wall/Blanket/Shield at JAERI (T. Tone)	10
1. INTRODUCTION	10
2. FUSION NEUTRONICS SOURCE FACILITY	12
3. EVALUATED NUCLEAR DATA FILE	18
4. NEUTRONICS COMPUTER CODES AND LIBRARIES	20
5. STRUCTURAL MATERIALS	29
6. BREEDING MATERIAL	31
7. ELECTROMAGNETIC ENGINEERING	44
7.1 Development of Analysis Methods and Computer Codes for Eddy Current	44
7.2 Experiments on Magnetomechanical Behavior of Toroidal Coils and Vacuum Vessel	51
8. THERMOMECHANICAL ENGINEERING	54
8.1 Surface Heat Flux Test Facility	54
8.2 Thermal Cycle Test of a Composite Divertor Plate	56
III. Outline of FER Blanket Concept (Y. Seki, A. Minato [*] , S. Mori ^{**} , T. Tone)	60
IV. Neutronics Design of FER Blanket/Shield (Y. Seki, S. Mori ^{**} , H. Kawasaki ^{***})	79
V. Thermomechanical Design of the FER Blanket (T. Kobayashi ^{**}) ...	103
VI. Technology Issues of the FER Blanket Development	127
VII. Studies on the Fusion Reactor Blanket Engineering at Universities in Japan, 1980-1982 (K. Sumita [†])	134
Acknowledgement	135

* On leave from Kawasaki Heavy Industries, Ltd.

** Kawasaki Heavy Industries, Ltd.

*** Century Research Center Corp., Ltd.

† Osaka University

目 次

I. 核融合実験炉 (FER) の概要 (東稔)	1
II. 原研における第 1 壁 / ブランケット / 遮蔽に関する研究開発 (東稔)	10
1. 序	10
2. 核融合炉物理用中性子源	12
3. 核データファイル	18
4. ニュートロニクス計算コードと断面積ライブラリ	20
5. 構造材	29
6. 増殖材	31
7. 電磁気解析と実験	44
7.1 渦電流の解析コード	44
7.2 トロイダルコイルと真空容器に及ぼす電磁力実験	51
8. 熱構造	54
8.1 表面熱流束試験装置	54
8.2 ダイバータ板の熱サイクル試験	56
III. FER ブランケットの概要 (関, 湊, 森, 東稔)	60
IV. FER ブランケット / 遮蔽のニュートロニクス (関, 森, 川崎)	79
V. FER ブランケットの熱構造設計 (小林)	103
VI. FER ブランケット開発の技術課題	127
VII. 大学における核融合炉ブランケットに関する研究の概要 (住田)	134
謝 辞	135

I. Overview of the Fusion Experimental Reactor (FER)

1. Long-Term Program

In June 1982, the Atomic Energy Commission issued its Long-Term Program of the Development and the Utilization of Atomic Energy, in which a long-range plan for fusion reactor development was laid out. This concluded a series of processes of deliberation which started in March 1980 when the Nuclear Fusion Council of the Atomic Energy Commission established its Review Subcommittee for Long-Term Strategy. Upon submission of a report from the Subcommittee in March 1981, the Council conducted its review and presented its report to the Commission in September 1981.

The Fusion Experimental Reactor (FER) defined in the new long-term program has an objective of achieving self-ignition and demonstrating its engineering feasibility of a fusion reactor in the latter half of 1990's as a next generation tokamak succeeding the JT-60.

2. Reactor Design Studies

Design studies of near-term Tokamak fusion reactors at JAERI until about 1980 were carried out in line with an approach in which serial development of two reactors, the first (PETF: Plasma Engineering Test Facility)⁽¹⁾ with a mission of achieving a self-ignited plasma and a limited test of reactor technologies and the second (JXFR: JAERI Experimental Fusion Reactor)⁽²⁾ for an integrated test of reactor technologies. Since about 1980, however, a difference approach was considered and replaced the above, in which a single reactor (FER)⁽³⁾, with possible staged operation, carries a comprehensive mission of achievement of self-ignition and integrated test of fusion technologies.

Design studies of the INTOR have also been intensively carried out at JAERI since the phase-zero in 1979. The design concepts of FER and INTOR have been interrelatedly developed, in particular, for common features.

3. Objectives of the FER

Major requirements of the Fusion Experimental Reactor identified by the Review Subcommittee on Long-Term Strategy are:

1. to show engineering feasibility of the fusion reactor and its plausibility as energy source,
2. to take reasonable step from present technology and the expectable future developments and to be designed flexible to allow the staged progress to reach objectives, and
3. to be designed with cost/benefit considerations.

The objectives of the FER in order to realize these missions were formulated in the following terms by the Review Subcommittee:

1. Self-ignition,
2. D-T burning for about one hundred seconds,
3. Definitive demonstration of essential fusion technologies such as systems integration, plasma heating technology, plasma control technology, superconducting magnet technology, and tritium technology, etc., and
4. Integral test of technologies concerned with future fusion reactors in the areas of materials, tritium production technology, remote maintenance technology, safety, reliability and durability, and availability improvement.

The design of the FER is being carried out under the following additional requirements:

5. Tritium breeding ratio of about unity,
6. Moderate neutron wall loading of approximately 1 MW/m^2 , and
7. Staged operation scenarios, for example, of installing the breeding blanket in the second stage, should be evaluated.

4. The FER Design Concept

The reference design of the FER is based on a dee-shaped tokamak plasma configuration with a double-null divertor. The major design parameters are listed in Table 1. Figure 1 shows the vertical view of the FER designed in 1981.⁽³⁾ The heating is provided by neutral beam injection and radiofrequency heating. The superconducting coil system with the poloidal coils placed external to the toroidal coils

is enclosed in a semi-permanent common cryostat vacuum chamber (belljar type). The plasma vacuum chamber is made of a semi-permanent toroidal structure and torus sectors which fit within this structure. The assembly/disassembly of the torus sectors can be made without disturbing these semi-permanent components.

The design of the FER which shares the above features is made with emphasis placed on reducing the reactor size, while keeping good accessibility for maintenance and assembly/disassembly procedures. This effort is particularly important, since the FER, in contrast to other near-term reactors, aims at achieving a tritium breeding ratio of unity and hence requires a breeding blanket fully enclosing the plasma volume leading to a larger blanket/shield structure. Tritium breeding blanket with Li_2O as breeding material is installed all around the plasma and at the back sides of divertor chambers to enhance breeding ratio.

In order to reduce the size of toroidal coils, each of the blanket/shield sectors is divided into three modules which can be removed through a space between the adjacent toroidal coils; the central module is drawn out by a single radial motion and the two side modules are first moved toroidally and then drawn radially, as shown in Fig. 2. Furthermore, special attention is paid to the shield design to reduce the coil size. In a conventional design, unified blanket/shield sectors provide radiation shielding for both coils and biological purposes. The idea is to reduce the outboard thickness of the blanket/shield sectors to a value required for the coil shielding and to place an additional shield for biological purposes at a space between the outer legs of the adjacent toroidal coils. This design concept reduces the size of the sector and hence allows a substantial decrease in the size of the toroidal coils. Bore of the FER toroidal coils is $9.1 \text{ m} \times 6.1 \text{ m}$.

Employment of a vacuum boundary which is common to both the plasma vacuum chamber and the cryostat vacuum chamber also helps to reduce the reactor size and simplifies the assembly/disassembly procedure because the plasma vacuum chamber can be sealed at a more open space between the toroidal coils. It also simplifies the connection of adjacent blanket/shield sectors, since they can be mechanically jointed by insulated bolts with no need for vacuum tightness.

A double-null divertor configuration, instead of the single-null, is employed to reduce the major reactor radius and also to improve the coupling between OH coils and the plasma, since it will have a thinner scrape-off layer at the inboard plasma surface. Three divertor modules cover a space of two sectors and they are drawn out through a maintenance port located at a bay of the vacuum chamber. This allows a wide open space available for maintenance activity. The assembly/disassembly procedure of divertor modules was analyzed in detail using scaled models.

The design study for the reference concept based on a double-null divertor is in more detail being made. On the other hand, in parallel with the reference design optional design studies with a few attractive features based on advanced concepts such as pumped limiter and RF current drive are in progress.

A design alternative of the FER has been made applying the concept of the Swimming Pool Type Tokamak Reactor (SPTR). The vertical view of the FER-SPTR⁽⁴⁾ is shown in Fig. 3. The reactor is submerged in a water pool. The SPTR concept excludes the huge and heavy solid shield structure protecting superconducting magnets which brings about great difficulties in repair and maintenance. The water plays a role of bulk shield and eases the problem of radiation streaming shielding. The elimination of the solid shield reduces greatly the radioactive waste disposal. Replacement of solid shield structures by the water shield allows better space utilization and reduces the size of the toroidal coils. The size of the toroidal coil of the FER-SPTR is 9.1 m × 6.1 m in bore, the same as in the FER.

The reduction of the vacuum chamber in size and weight is another benefit resulting from this concept. The assembly/disassembly of the plasma vacuum chamber is made by running a remotely-operated welder/cutter a short way around the vacuum chamber in a space where the water is normally filled. Technical issues associated with this concept such as corrosion, tritium leak into the water, and failure mode analysis are being assessed. A design study to develop the SPTR concept to a commercial tokamak power reactor (SPTR-P) is in progress.⁽⁵⁾

An optional concept of utilizing water only as bulk shield in the solid shield space of the FER without submerging the whole reactor in a water pool is being studied in comparison with the FER and the FER-SPTR.

References

- (1) T. Hiraoka, et al.: "Conceptual Studies of Plasma Engineering Test Facility", JAERI-M 8198 (1979).
- (2) K. Sako, et al.: "First Preliminary Design of an Experimental Fusion Reactor", JAERI-M 7300 (1977) (in Japanese), and "Second Preliminary Design of JAERI Experimental Fusion Reactor (Interim Report)", JAERI-M 8286 (1979).
- (3) K. Tomabechi, et al.: "Concept of the Next Tokamak", Proc. IAEA 3rd Technical Committee Meeting and Workshop on Fusion Reactor Design and Technology, Tokyo, 1981, II-5 (in press), and "Fusion Experimental Reactor Development at JAERI", 9th Int. Conf. on Plasma Phys. and Controlled Nucl. Fusion Research, Baltimore, September 1982, IAEA-CN-41/E-4.
- (4) K. Sako, et al.: "Next Tokamak Design (Swimming Pool Type)", Proc. IAEA 3rd Technical Committee Meeting and Workshop on Fusion Reactor Design and Technology, Tokyo, 1981, II-6 (in press), and "Design Study of Swimming Pool Type Tokamak Reactor (SPTR)", J. Nucl. Sci. Technol., 19, 6 (1982) 491.
- (5) T. Tone, et al.: "Design Study of a Tokamak Power Reactor", Proc. IAEA 3rd Technical Committee Meeting and Workshop on Fusion Reactor Design and Technology, Tokyo, 1981, II-8 (in press).

Table 1 Major Design Parameters

Power	
Fusion power (MW)	440
Average neutron wall loading (MW/m ²)	1.0
Operation	
Burn time (s)	100
Duty factor (%)	50 ~ 70
Availability (%)	25 ~ 50
Plasma	
Major radius (m)	5.5
Plasma radius (m)	1.1
Plasma elongation	1.5
Burn average beta (total) (%)	4
Plasma current (MA)	5.3
Average ion temperature (keV)	10
Average ion density (m ⁻³)	1.4×10^{20}
Energy confinement time (s)	1.4
Toroidal field on plasma axis (T)	5.7
Heating	
NBI power (MW)	30
RF power (MW)	30
Impurity Control	
Method	double-null poloidal divertor
Power to divertor plate (MW)	45
Breeding Blanket	
Structural material	316 SS
Breeding material	Li ₂ O
Breeder temperature (°C)	400 ~ 1000
Tritium breeding ratio	1.05
Coolant	H ₂ O
Toroidal Field Coils (TFC)	
Number	14
Bore (m)	$6.1^W \times 9.1^H$
Conductor	Nb ₃ Sn, NbTi
Maximum field (T)	12
Poloidal Field Coils (PFC)	
Location	external to TFC
Conductor	NbTi
Maximum field (T)	8

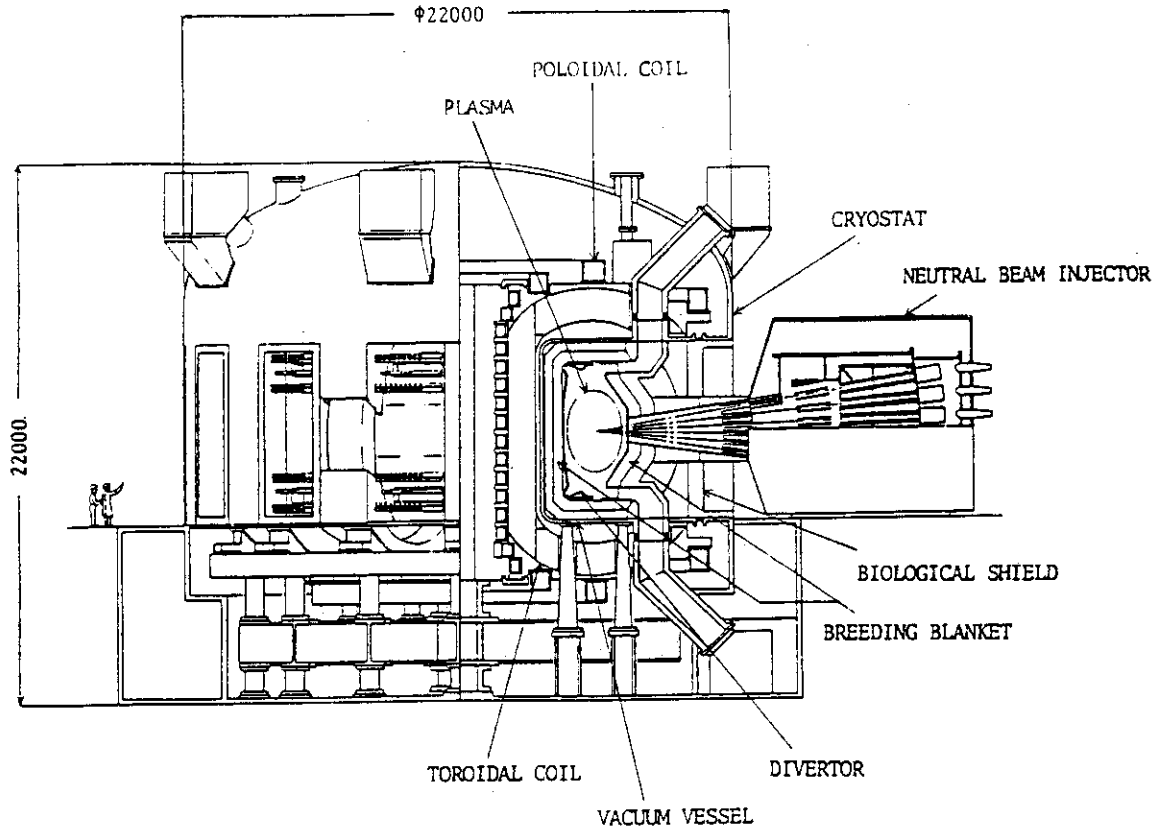


Fig. 1 Vertical view of the FER

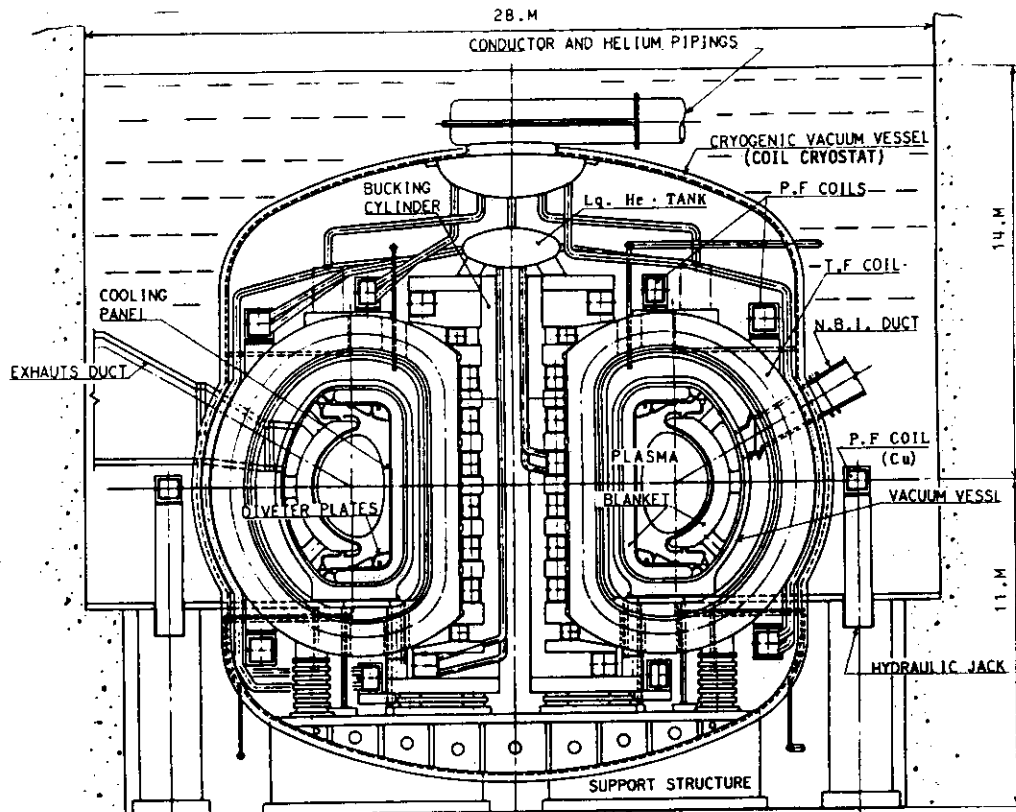


Fig. 3 Vertical view of the FER-SPTR

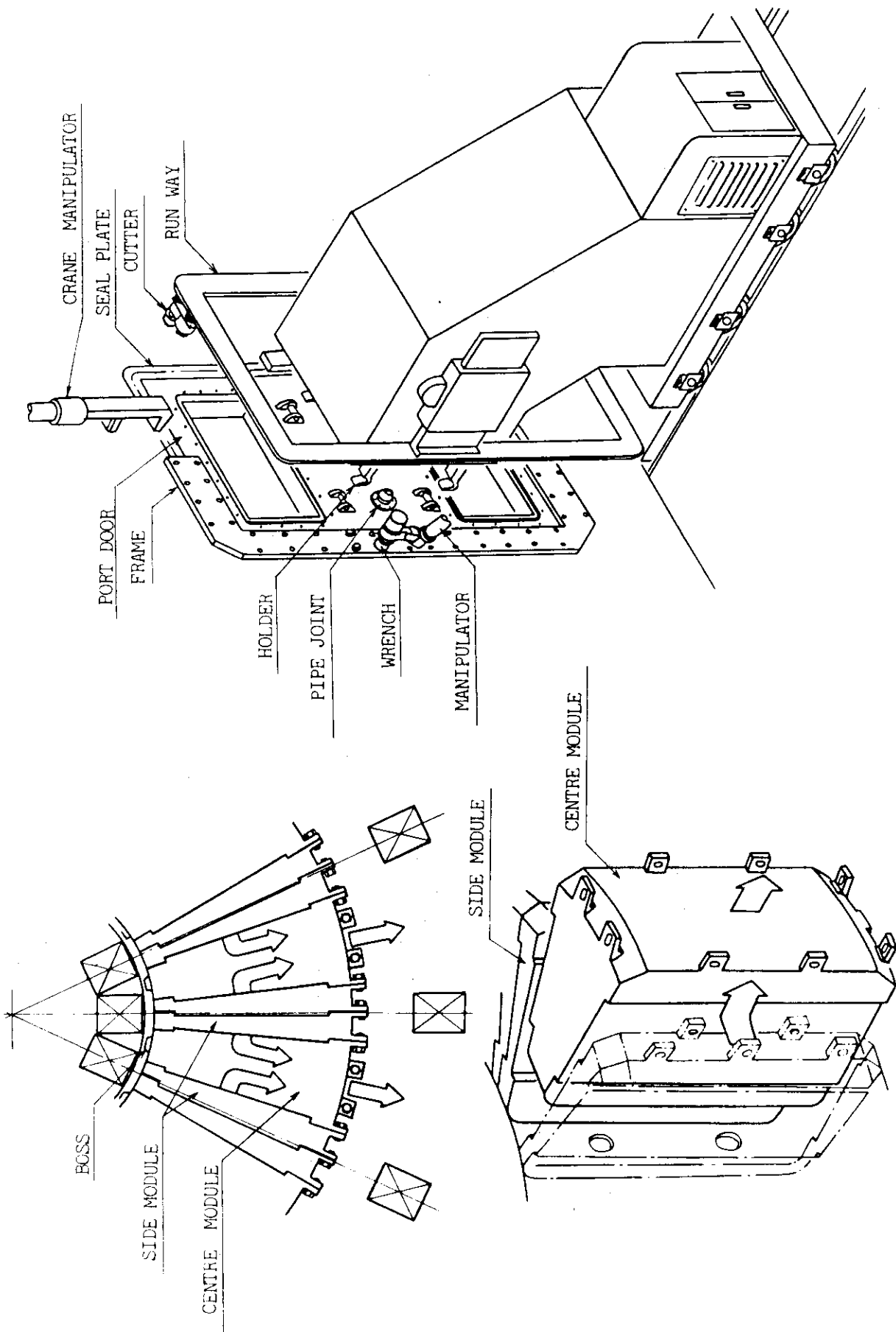
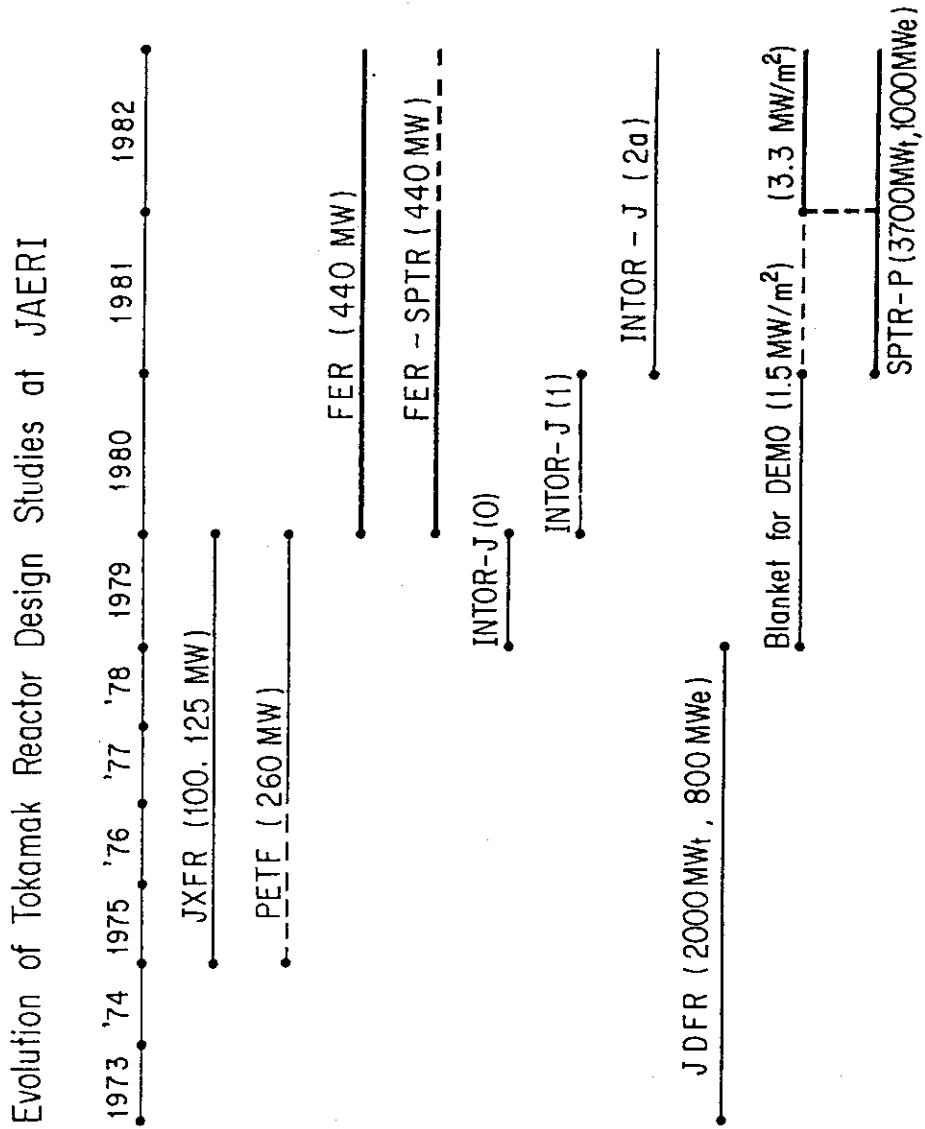


Fig. 2(b) Maintenance port opening machine

Fig. 2(a) Module exchange

Appendix (View graphs presented)



II. Research and Development Activities Related to First Wall/Blanket/Shield at JAERI

1. INTRODUCTION

First wall/blanket/shield comprising a torus system surrounding a plasma are essentially important structures as a reactor core. The development of first wall/blanket/shield technologies is, however, behind that of technologies directly related to plasma development, such as superconducting magnet and NBI and RF heating. In order to develop first wall/blanket/shield concepts it is required to establish an engineering data base for their design and construction.

Among a number of important development areas are neutronics, materials, and electromagnetic and thermomechanical engineering. Current activities on these areas conducted at JAERI are described in this paper, though some of them are in preliminary stages.

Blanket/shield neutronics requires an integrated approach consisting of experiments, developments of computer codes and nuclear data file, and comprehensive design efforts. Blanket/shield experiments have started with the Fusion Neutronics Source (FNS) Facility which is an intense D-T neutron source recently completed. Various neutronics computer codes have been developed for experiment analysis and reactor neutronics design. A nuclear data file for use in fusion researches is being developed among a series of JENDLs (Japanese Evaluated Nuclear Data Library).

In order to develop the breeder blanket concept of the Fusion Experimental Reactor (FER) it is important to timely select the most promising one among a number of candidate breeder materials and to establish the requisite data base. Development activities of tritium breeder at JAERI are focused on the solid Li_2O in view of tritium release, breeding performance, safety and thermomechanical design of blanket. Typical experimental results concerned with the blanket design are described in chapter 6.

The structural material used in the FER first wall/blanket is Type 316 austenitic stainless steel which has a relatively large data base for a neutron fluence of about $3 \text{ MW}\cdot\text{y}/\text{m}^2$ supposed in the FER operation. Neutron irradiation tests with High Flux Isotope Reactor (HFIR) and Oak Ridge Research Reactor (ORR) planned under the Japan-US

Fusion Cooperation Program and irradiation test data from JOYO (experimental fast breeder reactor in Japan) are expected to be available. Irradiation tests of welded materials planned in HFIR will improve the current poor data base of this area. To improve the austenitic stainless steel the development of the prime candidate alloy (PCA) and five other candidates has been initiated. Their fundamental materials properties were examined.

Various computer codes for eddy current analysis are described in this paper. They were mainly developed for JT-60 and some of them have been applied to the eddy current analysis for electromagnetic force and plasma positional controllability in fusion reactor designs. Small-scale experiments on magnetomechanical effects are to be conducted in collaboration with the University of Tokyo.

Surface heat flux testing of first wall materials is planned. The test facility to be installed is equipped with a 30 kW electron beam system. On the other hand a test stand with a plasma generator has been completed and experiments on thermal cycle of a divertor plate will first of all start.

Finally the author would like to thank the following people for their collaboration to prepare this paper: (1) Fusion Neutronics Source Facility - T. Nakamura (2) Evaluated Nuclear Data File - T. Asami and Y. Seki (3) Neutronics Computer Codes and Libraries - Y. Seki, M. Nakagawa and T. Suzuki (4) Structural Materials - K. Shiraishi (5) Breeding Material - H. Watanabe (6) Development of Analysis Methods and Computer Codes for Eddy Current - S. Nishio (7) Experiments on Magnetomechanical Behavior of Toroidal Coils and Vacuum Vessel - K. Miya (the University of Tokyo) and A. Minato (8) Surface Heat Flux Test Facility - Y. Murakami (9) Thermal Cycle Test of a Composite Divertor Plate - H. Kawamura.

2. FUSION NEUTRONICS SOURCE FACILITY

The Fusion Neutronics Source Facility (FNS) has a capability to allow wide range of experiments with good accuracy by its various neutron production modes and by a well-designed arrangement of target locations, experimental equipments and ports⁽¹⁾.

2.1 Experimental Facility

The FNS consists basically of a high current electrostatic deuteron accelerator, tritium metal target assemblies, tritium handling and processing devices, experimental equipments and a building which plays an important role in experimental program with its shield structure and ports incorporated in it⁽²⁾⁽³⁾.

The accelerator of 400 keV Cockcroft-Walton type has two ion sources — for high and low current —, pre- and post-acceleration pulsing devices and two drift tubes in the direction of 0° and 80° to the axis of acceleration. Each beam transport lines lead to the separate target room surrounded by thick concrete shield: a 15 m × 15 m large target room #1 for the 80° beam line and a small 5 m × 5 m target room #2 for the 0° one. Four types of tritium metal target assemblies have been prepared: LLL-type rotating, small-sized rotating, water-cooled stationary and air-cooled stationary targets.

A variety of source conditions for experiments can be realized by suitable choices in ion sources, beam lines, operation modes — DC and pulse — and target types, high intensity continuous source of initial yield up to 5×10^{12} n/sec for a sample irradiation in target room #2 or 2 ns neutron pulse with peak intensity of 10^{13} n/sec for time-of-flight experiment in target room #1 for example. The performance characteristics of the FNS generator is summarized in Table 1.

All tritium gas released from the target into the vacuum system is transferred to a tritium removal and monitoring unit via leak-free lines. Tritium containing exhaust gas is once kept in a storage tank and then recirculated through a reactor for oxidation and a molecular sieve dryer where tritium is fixed in the form of water.

The FNS is provided with a lot of experimental equipments as:

1) a time-of-flight tube facility with detector stations at 11 m and 36 m, 2) a 25×25 matrix structure where the experimental media are assembled in various shapes and sizes, 3) a movable deck to carry experimental system on and to locate it in a right position relative to the target, 4) a dual rotatable measuring deck which bears a collimator and a detector shield and rotates around the target from 0° to 110° to the direction of d^+ beam and 5) a pneumatic sample transfer system between target and measuring rooms. The illustration of the main part of the FNS facility is shown in Fig. 1. Absolute source yield is determined by measuring associated alpha-particles emitted to back angle with a small SSD incorporated in the beam line. Auxiliary monitors are a long counter and Th-fission chambers.

2.2 Experimental Program

The experimental program is divided roughly in four categories as follows:

a) Experiments on blanket and shield bench-mark systems

They are experiments on simple composition and simple geometry systems to examine the nuclear data and the calculational methods in a manner as straight-forward as possible. Detailed spectrum measurements by using scintillation spectrometer and time-of-flight method, and detailed reaction rate measurement, especially of tritium production, are major items. 14 MeV cross section measurements are also performed. Target room #1 and 80° beam line is used for this purpose. The experiments on Li_2O system have been initiated.

b) Experiments on modelled blanket and shield modules

A series of experiments on integrated assembly of first-wall, breeder and reflector/shield is planned utilizing the experimental hole connecting target rooms #1 and #2. This is expected to provide experimental verification on the accuracy of nuclear calculation in the current design work. A modelled module is set in or outside of the experimental hole. Spatial reaction and dose distribution are to be measured. Streaming experiment combined with this assembly is also of interest.

c) Experiments on shielding making use of building structure

Duct streaming, deep penetration and sky-shine experiments can be performed by using target room entrance tunnel, shield doors and various experimental ports. In this case doses and/or spectra of neutron and secondary gamma-ray are of major concern.

d) Experiments on induced activities

Experiments on induced activities of various materials used in fusion reactor are planned to examine the results of the calculation code THIDA which evaluates the shut-down dose in INTOR and FER designs. Samples are irradiated directly in 14 MeV beam or inserted in the medium such as Li_2O surrounding the target to vary the spectrum environment and resultant gamma ray spectra are measured for different combination of irradiation time and cooling time.

These four categories are related each other and play complementary roles.

2.3 Experiments

Two blanket and a shield experiments have been performed since the initial D-T neutron operation in August 1981. Tritium production rate and other reaction rate distributions were measured in a pseudo-spherical lithium oxide system with a graphite reflector as the first in a series of blanket benchmark experiment⁽²⁾. The experimental arrangement is shown in Fig. 2. Secondary, time-of-flight measurement conducted for the angular-dependent flux spectra of the fast neutrons emitted from the surface of lithium-oxide slab assemblies of different thickness.

A large-scale duct streaming experiment was performed by using a personnel access tunnel to the target room; dose and spectrum distributions were obtained for neutron and gamma-ray in the duct. The layout of the duct is shown in Fig. 3. Preliminary experiment on the beam profile at the edge of the hole was undertaken. The cross section of the experimental hole is given in Fig. 4.

As a preliminary test, 316 SS sample was irradiated in the inside edge of Li_2O blanket bench-mark system, and the results contributed to the correction of inadequate gamma data library of THIDA.

The purpose of these experiments was to provide the experimental

data used in examining the calculational techniques applied in the prediction of nuclear performances in the FER design at JAERI⁽⁴⁾. Especially there has been no integral experiment data on lithium oxide that is a promising candidate for blanket material due to high Li atom density to achieve good tritium breeding gain, before our experiments.

References

- (1) T. Nakamura, H. Maekawa: 9th Conf. on Plasma Physics and Controlled Nuclear Fusion Research, Baltimore, September 1982, IAEA-CN-41/O-4
- (2) T. Nakamura, et al.: "Fusion Neutronics Source (FNS)", pp.55-56, Proc. 3rd Sym. on Accelerator Science and Technology, Aug. 27-29, 1980, Osaka Univ., Osaka, Japan.
- (3) "Reactor Engineering Division Annual Report", pp. 137-153, JAERI-M 9672 (1981).
- (4) K. Tomabechi, et al.: 9th Conf. on Plasma Physics and controlled Nuclear Fusion Research, Baltimore, September 1982, IAEA-CN-41/E-4

Table 1 Performance characteristics of FNS

Acceleration voltage : 400 kV					
Beam characteristics :			B beam line		
DC Mode	A beam line	B beam line	Pulse Mode	Bunching	Sweeping
Max. Beam current	23 mA	3.0 mA	Pulse Width	1.6 ns	20ns-8 μ s
Target type	23 cm ϕ RT [*]	HSWCST ^{**}	Interval	0.5-256 μ s	2-512 μ s
³ T amount	1,000 C _i	25 C _i	Peak Current	45 mA	3.0 mA
Max. neutron Yield	5 \times 10 ¹² n/s	5 \times 10 ¹¹ n/s	On/Off Ratio	4 \times 10 ⁵	2 \times 10 ⁵

* : Rotating Target, ** : High Speed Water Cooled Stationary Target

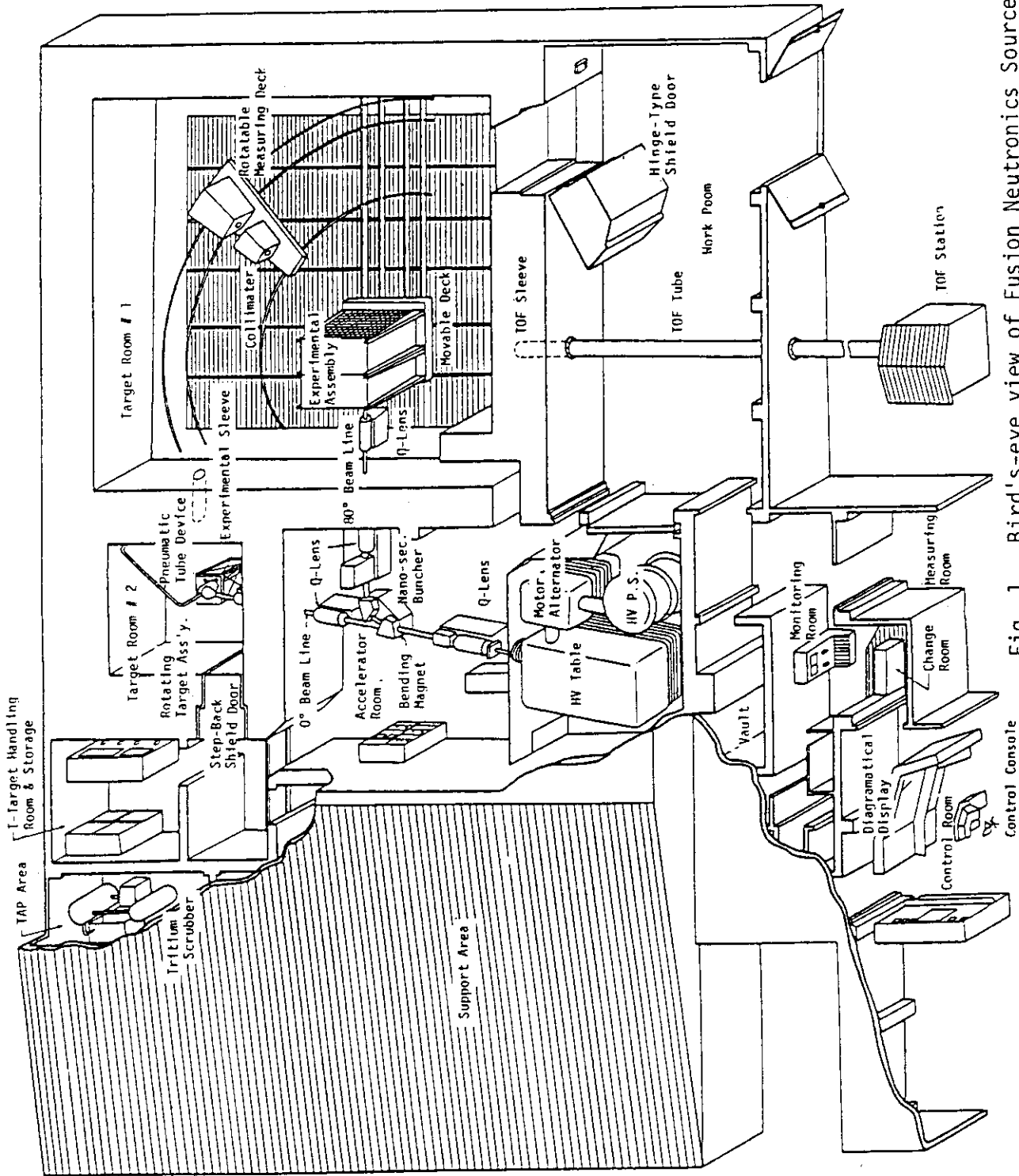


Fig. 1 Bird's-eye view of Fusion Neutronics Source Facility

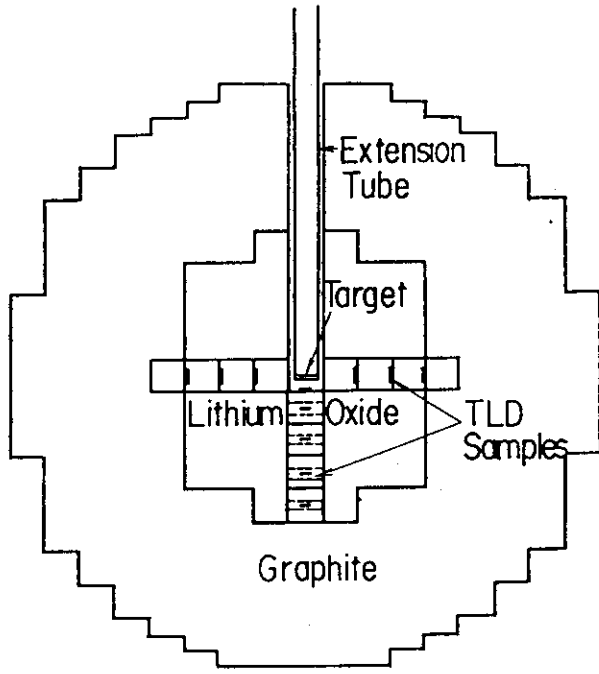


Fig.2 Horizontal cross-section across the center of Li_2O-C assembly

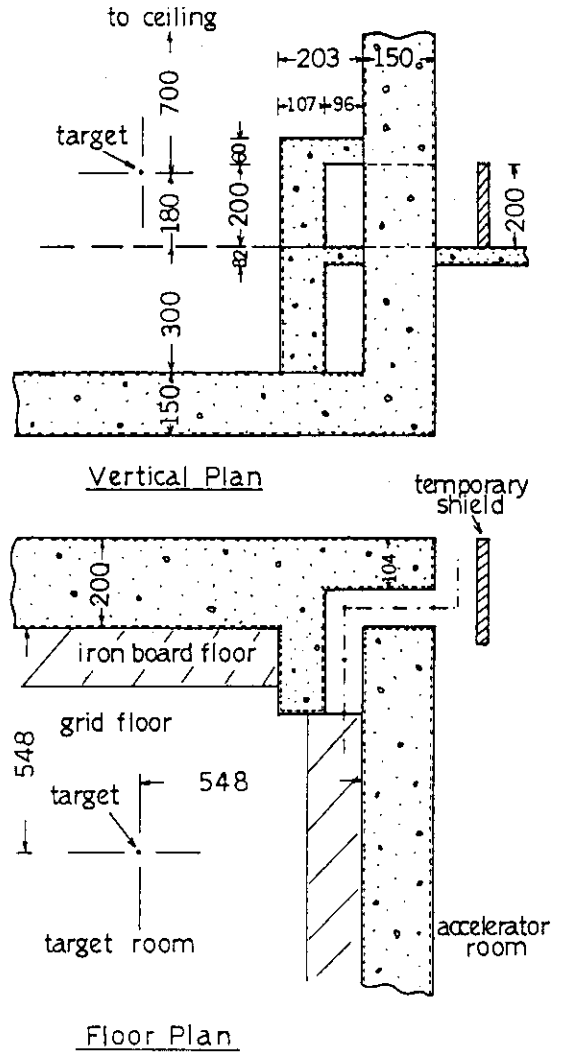


Fig.3 Duct streaming experiment layout (personnel access-way)

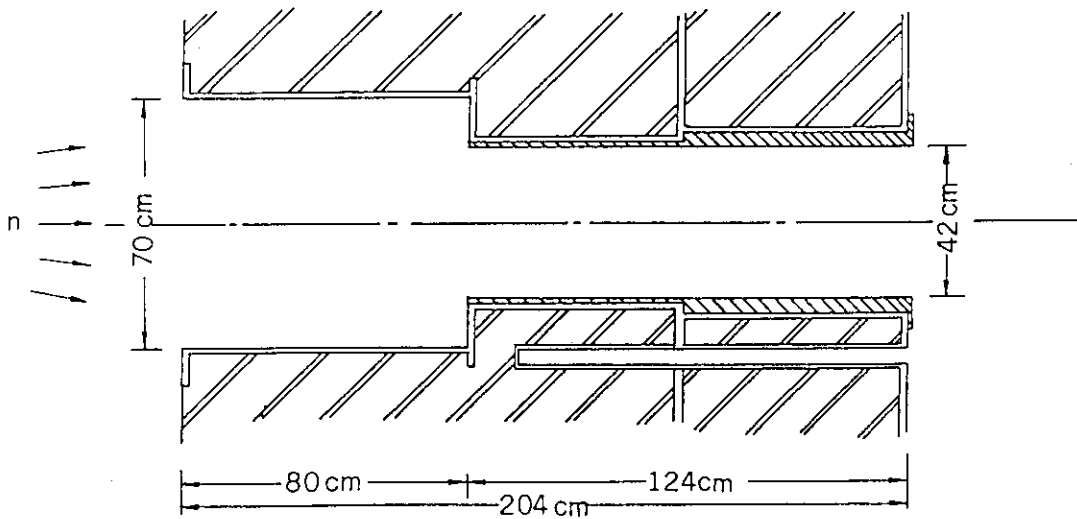


Fig.4 Cross-sectional view of experimental hole

3. EVALUATED NUCLEAR DATA FILE

Japanese Evaluated Nuclear Data Library (JENDL) has been developed by Japanese Nuclear Data Committee and JAERI Nuclear Data Center. The first version of JENDL, JENDL-1, which was released in 1977, has been compiled to use mainly for fast-reactor development. The second version, JENDL-2 has aimed for use in wider fields including fusion researches, shielding calculations, etc., and its compilation is in progress. It is scheduled to be released by the end of 1982. At the same time a plan for the compilation of JENDL-3 has been completed. The JENDL-3 will be compiled by the end of 1984, benchmark-tested by the end of 1985 and released in 1986. It will contain some 180 nuclides listed in Table 1.

Main feature of the JENDL-3 are as follows.

- (i) The upper bound neutron energy will be kept at 20 MeV.
- (ii) The improvement of accuracy in data will have priority over the increase in the number of nuclides to be stored.
- (iii) Gamma-ray production cross sections will be included.
- (iv) The accuracy of high energy (10 - 20 MeV) will be improved.

Table 1 List of nuclides to be stored in JENDL-3

Z	Element	Z	Element	Z	Element
1	^1_1H , ^2_1H , ^3_1H	29	$^{63}_{29}\text{Cu}$, $^{65}_{29}\text{Cu}$	59	$^{141}_{59}\text{Pr}$
2	^3_2He , ^4_2He	30	$^{64}_{30}\text{Zn}$, $^{66}_{30}\text{Zn}$, $^{67}_{30}\text{Zn}$, $^{68}_{30}\text{Zn}$, $^{70}_{30}\text{Zn}$	60	$^{142}_{60}\text{Nd}$, $^{143}_{60}\text{Nd}$, $^{144}_{60}\text{Nd}$, $^{145}_{60}\text{Nd}$, $^{146}_{60}\text{Nd}$, $^{148}_{60}\text{Nd}$, $^{150}_{60}\text{Nd}$
3	^6_3Li , ^7_3Li	31	$^{69}_{31}\text{Ga}$, $^{71}_{31}\text{Ga}$	62	$^{144}_{62}\text{Sm}$, $^{147}_{62}\text{Sm}$, $^{148}_{62}\text{Sm}$, $^{149}_{62}\text{Sm}$, $^{150}_{62}\text{Sm}$, $^{152}_{62}\text{Sm}$, $^{154}_{62}\text{Sm}$
4	^9_4Be	35	$^{79}_{35}\text{Br}$, $^{81}_{35}\text{Br}$	63	$^{151}_{63}\text{Eu}$, $^{153}_{63}\text{Eu}$
5	$^{10}_5\text{B}$, $^{11}_5\text{B}$	37	$^{85}_{37}\text{Rb}$, $^{87}_{37}\text{Rb}$	64	$^{152}_{64}\text{Gd}$, $^{154}_{64}\text{Gd}$, $^{155}_{64}\text{Gd}$, $^{156}_{64}\text{Gd}$, $^{157}_{64}\text{Gd}$, $^{158}_{64}\text{Gd}$, $^{160}_{64}\text{Gd}$
6	$^{12}_6\text{C}$	38	$^{84}_{38}\text{Sr}$, $^{86}_{38}\text{Sr}$, $^{87}_{38}\text{Sr}$, $^{88}_{38}\text{Sr}$	65	$^{159}_{65}\text{Tb}$
7	$^{14}_7\text{N}$	39	$^{89}_{39}\text{Y}$	72	$^{174}_{72}\text{Hf}$, $^{176}_{72}\text{Hf}$, $^{177}_{72}\text{Hf}$, $^{178}_{72}\text{Hf}$, $^{179}_{72}\text{Hf}$, $^{180}_{72}\text{Hf}$
8	$^{16}_8\text{O}$	40	$^{90}_{40}\text{Zr}$, $^{91}_{40}\text{Zr}$, $^{92}_{40}\text{Zr}$, $^{94}_{40}\text{Zr}$, $^{96}_{40}\text{Zr}$	73	$^{181}_{73}\text{Ta}$
9	$^{19}_9\text{F}$	41	$^{93}_{41}\text{Nb}$, $^{94}_{41}\text{Nb}$	74	$^{180}_{74}\text{W}$, $^{182}_{74}\text{W}$, $^{183}_{74}\text{W}$, $^{184}_{74}\text{W}$, $^{186}_{74}\text{W}$
11	$^{23}_{11}\text{Na}$	42	$^{92}_{42}\text{Mo}$, $^{94}_{42}\text{Mo}$, $^{95}_{42}\text{Mo}$, $^{96}_{42}\text{Mo}$, $^{97}_{42}\text{Mo}$, $^{98}_{42}\text{Mo}$, $^{100}_{42}\text{Mo}$	82	$^{204}_{82}\text{Pb}$, $^{206}_{82}\text{Pb}$, $^{207}_{82}\text{Pb}$, $^{208}_{82}\text{Pb}$
12	$^{24}_{12}\text{Mg}$, $^{25}_{12}\text{Mg}$, $^{26}_{12}\text{Mg}$	43	$^{99}_{43}\text{Tc}$	90	$^{228}_{90}\text{Th}$, $^{230}_{90}\text{Th}$, $^{232}_{90}\text{Th}$, $^{233}_{90}\text{Th}$, $^{234}_{90}\text{Th}$
13	$^{27}_{13}\text{Al}$	44	$^{96}_{44}\text{Ru}$, $^{98}_{44}\text{Ru}$, $^{99}_{44}\text{Ru}$, $^{100}_{44}\text{Ru}$, $^{101}_{44}\text{Ru}$, $^{102}_{44}\text{Ru}$, $^{104}_{44}\text{Ru}$	91	$^{231}_{91}\text{Pa}$, $^{233}_{91}\text{Pa}$
14	$^{28}_{14}\text{Si}$, $^{29}_{14}\text{Si}$, $^{30}_{14}\text{Si}$	45	$^{103}_{45}\text{Rh}$	92	$^{232}_{92}\text{U}$, $^{233}_{92}\text{U}$, $^{234}_{92}\text{U}$, $^{235}_{92}\text{U}$, $^{236}_{92}\text{U}$, $^{238}_{92}\text{U}$
15	$^{31}_{15}\text{P}$	46	$^{102}_{46}\text{Pd}$, $^{104}_{46}\text{Pd}$, $^{105}_{46}\text{Pd}$, $^{106}_{46}\text{Pd}$, $^{108}_{46}\text{Pd}$, $^{110}_{46}\text{Pd}$	93	$^{237}_{93}\text{Np}$, $^{239}_{93}\text{Np}$
16	$^{32}_{16}\text{S}$, $^{33}_{16}\text{S}$, $^{34}_{16}\text{S}$, $^{36}_{16}\text{S}$	47	$^{107}_{47}\text{Ag}$, $^{109}_{47}\text{Ag}$	94	$^{236}_{94}\text{Pu}$, $^{238}_{94}\text{Pu}$, $^{239}_{94}\text{Pu}$, $^{240}_{94}\text{Pu}$, $^{241}_{94}\text{Pu}$, $^{242}_{94}\text{Pu}$
17	$^{35}_{17}\text{Cl}$, $^{37}_{17}\text{Cl}$	48	$^{106}_{48}\text{Cd}$, $^{108}_{48}\text{Cd}$, $^{110}_{48}\text{Cd}$, $^{111}_{48}\text{Cd}$, $^{112}_{48}\text{Cd}$, $^{113}_{48}\text{Cd}$, $^{114}_{48}\text{Cd}$, $^{116}_{48}\text{Cd}$	95	$^{241}_{95}\text{Am}$, $^{242}_{95}\text{Am}$, $^{243}_{95}\text{Am}$
18	$^{40}_{18}\text{Ar}$	49	$^{113}_{49}\text{In}$, $^{115}_{49}\text{In}$	96	$^{242}_{96}\text{Cm}$, $^{243}_{96}\text{Cm}$, $^{244}_{96}\text{Cm}$, $^{245}_{96}\text{Cm}$
19	$^{39}_{19}\text{K}$, $^{40}_{19}\text{K}$, $^{41}_{19}\text{K}$	51	$^{121}_{51}\text{Sb}$, $^{123}_{51}\text{Sb}$, $^{124}_{51}\text{Sb}$		
20	$^{40}_{20}\text{Ca}$, $^{42}_{20}\text{Ca}$, $^{43}_{20}\text{Ca}$, $^{44}_{20}\text{Ca}$, $^{46}_{20}\text{Ca}$, $^{48}_{20}\text{Ca}$	52	$^{120}_{52}\text{Te}$, $^{122}_{52}\text{Te}$, $^{123}_{52}\text{Te}$, $^{124}_{52}\text{Te}$, $^{125}_{52}\text{Te}$, $^{126}_{52}\text{Te}$, $^{128}_{52}\text{Te}$, $^{130}_{52}\text{Te}$		
22	$^{46}_{22}\text{Ti}$, $^{47}_{22}\text{Ti}$, $^{48}_{22}\text{Ti}$, $^{49}_{22}\text{Ti}$, $^{50}_{22}\text{Ti}$	53	$^{127}_{53}\text{I}$		
23	$^{50}_{23}\text{V}$, $^{51}_{23}\text{V}$	54	$^{124}_{54}\text{Xe}$, $^{126}_{54}\text{Xe}$, $^{128}_{54}\text{Xe}$, $^{129}_{54}\text{Xe}$, $^{130}_{54}\text{Xe}$, $^{131}_{54}\text{Xe}$, $^{132}_{54}\text{Xe}$, $^{134}_{54}\text{Xe}$		
24	$^{50}_{24}\text{Cr}$, $^{52}_{24}\text{Cr}$, $^{53}_{24}\text{Cr}$, $^{54}_{24}\text{Cr}$	55	$^{135}_{55}\text{Xe}$		
25	$^{55}_{25}\text{Mn}$	56	$^{133}_{56}\text{Ba}$		
26	$^{54}_{26}\text{Fe}$, $^{56}_{26}\text{Fe}$, $^{57}_{26}\text{Fe}$, $^{58}_{26}\text{Fe}$	57	$^{130}_{57}\text{La}$, $^{132}_{57}\text{La}$, $^{134}_{57}\text{La}$, $^{135}_{57}\text{La}$, $^{136}_{57}\text{La}$, $^{137}_{57}\text{La}$, $^{138}_{57}\text{La}$		
27	$^{59}_{27}\text{Co}$	58	$^{138}_{58}\text{Ce}$, $^{139}_{58}\text{Ce}$, $^{140}_{58}\text{Ce}$, $^{142}_{58}\text{Ce}$		
28	$^{58}_{28}\text{Ni}$, $^{60}_{28}\text{Ni}$, $^{61}_{28}\text{Ni}$, $^{62}_{28}\text{Ni}$, $^{64}_{28}\text{Ni}$				

----- Nuclides stored in JENDLE-1

----- Nuclides stored in JENDLE-2

4. NEUTRONICS COMPUTER CODES AND LIBRARIES

Fusion reactor neutronics R&D activities in JAERI are summarized in Fig. 1. In Fig. 1, cross section libraries and computer codes developed or under development are described with wavy underlines. Some of the activities are briefly described in the following.

4.1 PROF-GROUCH-G/B

A code system for generating group constants library as described in APPENDIX 4.1.

4.2 GICX40

A 42-group neutron, 21-group gamma ray cross section set for 40 nuclides of interest in terms of fusion reactor design.

4.3 BERMUDA-1DN and BERMUDA-2DN

One and two-dimensional neutron transport code using the direct integration method in a multi-group model described in APPENDIX 4.1.

4.4 MORSE-DDX

Monte Carlo code using multi-group double differential cross section library described in APPENDIX 4.2.

4.4 MORSE-I

Monte Carlo code which can treat toroidal geometry and with improved point detector techniques as described in APPENDIX 4.3.

4.5 THIDA

A code system which calculated Transmutation, Hazard potential, Induced activity, Dose rate and After heat.

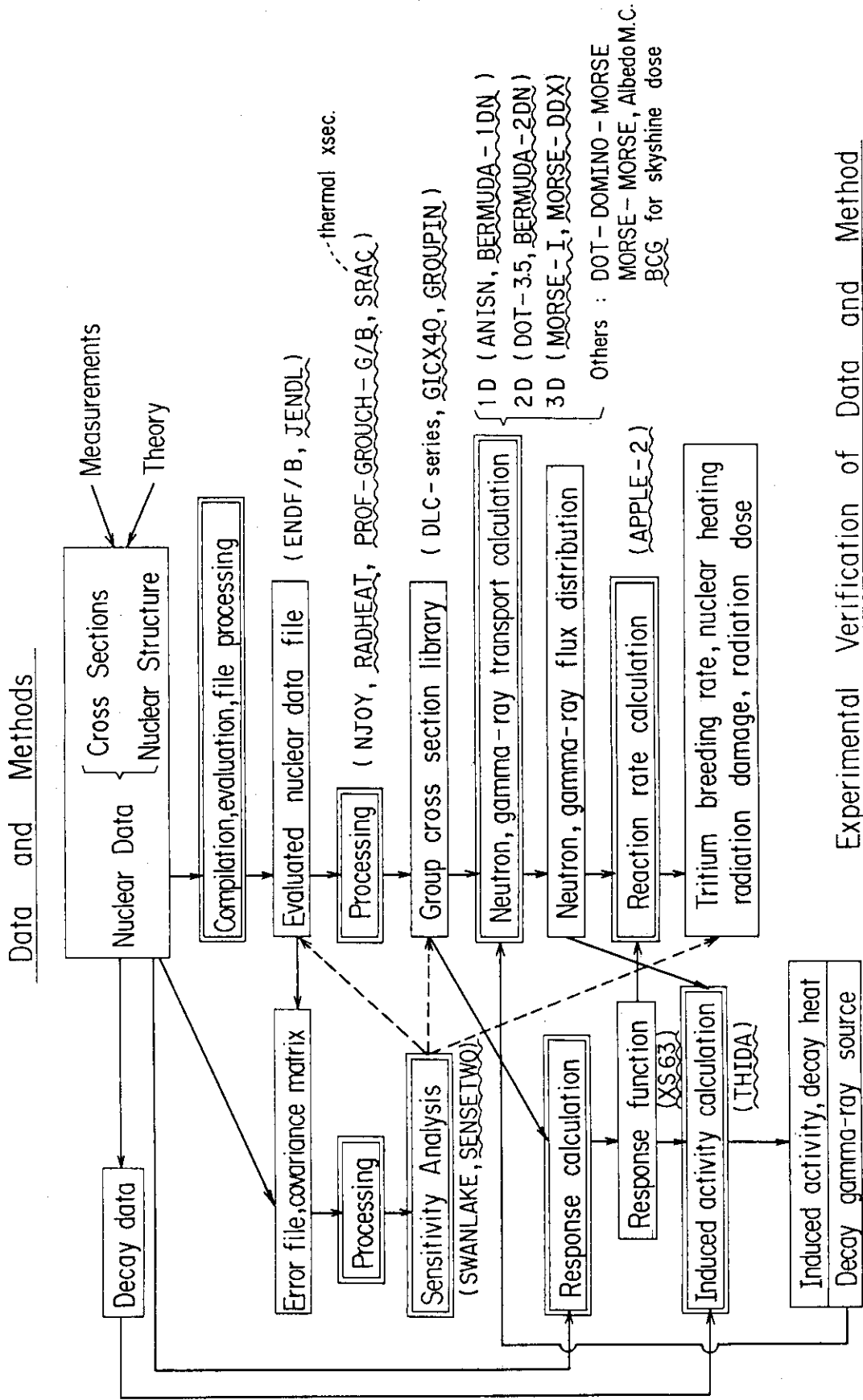


Fig. 1 Reactor neutronics activities in JAERI

APPENDIX 4.1

BERMUDA-2DN : A Two-Dimensional Neutron Transport Code

Tomoo SUZUKI , Akira HASEGAWA ,
Toshimi MORI , Takeharu ISE

Japan Atomic Energy Research Institute
Tokai-mura , Japan

The two-dimensional neutron transport code BERMUDA-2DN has been developed from the one-dimensional code PALLAS-TS (BERMUDA-1DN). The main purpose of the present code is to analyze the fusion blanket neutronics experiments for plane or cylindrical assemblies, into which D-T neutrons are injected from the outside along the z-axis. The time-independent transport equation is solved for two-dimensional, cylindrical, multi-regional geometry using the direct integration method in a multigroup model. In addition, group-transferance kernels are accurately obtained from the double-differential cross section data, without the Legendre polynomial expansion, but with the energy and scattering angle correlation relation.

A library file of group constants for the present code has been prepared using a collapsing utility code CONDENSE-2DN from the 120-group library of PALLAS-TS. Any group structure is available through this utility code to adopt user's requirement. For more consistent treatment of generating group constants library, we are developing a code system PROF-GROUCH-G/B. This system intends to furnish cross sections not only to shielding applications but also to core analyses or sensitivity analyses from selected nuclear data through the Evaluated Data File Storage and Retrieval Systems (EDFSRS) using the same procedures. The EDFSRS is a general utility system for the world-wide evaluated nuclear data files such as ENDF/B, ENDL, JENDL, UK and KEDAK.

For angular discrete ordinates, a set of fourty points are selected over the hemisphere made by unit direction vectors. Not only latitudes but also longitudes are taken into account in calculating the weight of azimuthal angle of scattering. For the

outer point source which is located on the z-axis of the cylinder or on the extension of the z-axis, the uncollided (direct beam) flux is initially obtained at each spatial mesh point in the point kernel model. The first collision source distribution with angular dependence is determined by the uncollided flux. The transport equation is solved for this first collision source plus slowing down source from upper groups, using iteration technique and neutron rebalancing scheme. Thus the angular flux distribution is obtained as the sum of the solution and the uncollided flux values.

At an intense D-T neutron source FNS, measurements were performed on the angular dependence of leakage spectra from Li_2O slab assemblies. A test calculation by the BERMUDA-2DN has shown to represent fairly well the observed values.

A typical observed angular flux spectrum is shown in Fig. 1 along with the calculated one. The measured source spectrum was used in the calculation. The experimental errors of energy and flux were estimated to be $+4.7\%$ and -3 to $+5\%$ for systematic error, and $\pm 4.5\%$ and $\pm(5$ to $20)\%$ for random error, respectively. Though the results were compared absolutely and there exist discrepancies partially, the calculational spectra agree fairly well with the experimental ones in the whole. It is clear that the BERMUDA code was demonstrated to be able to apply the fusion neutronics and shielding calculations.

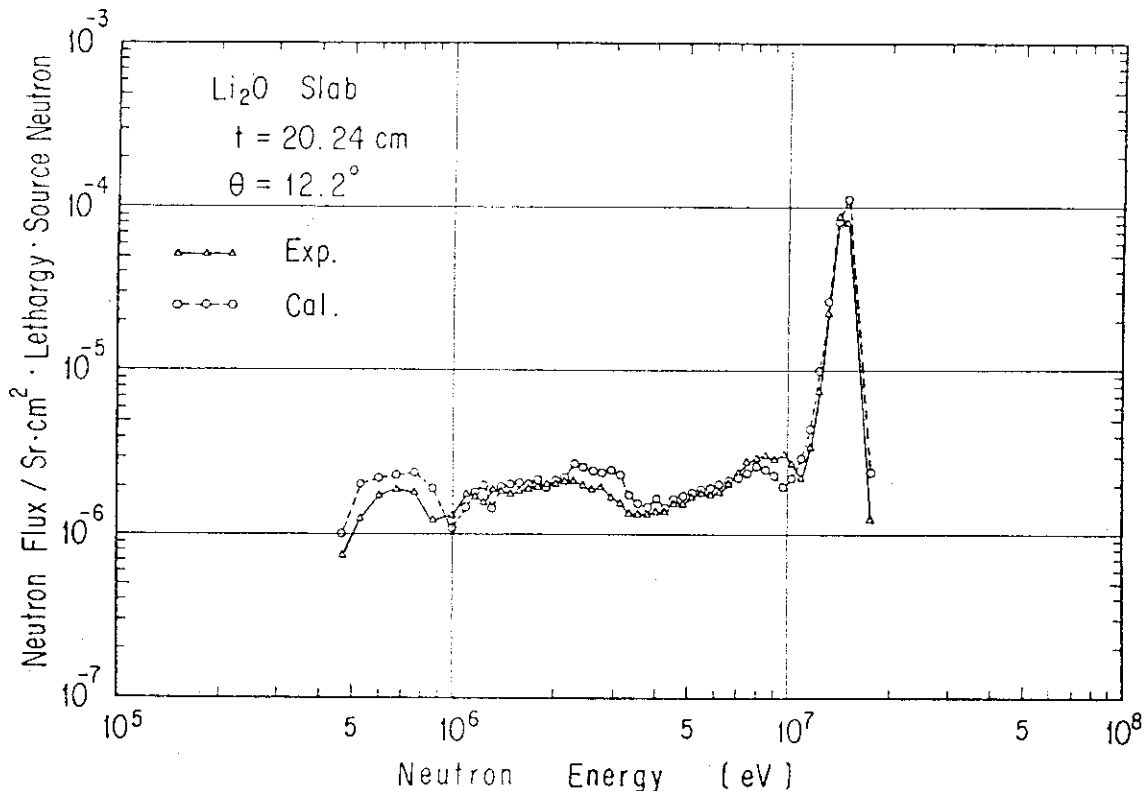


Fig. 1 Typical angle-dependent neutron leakage spectrum in Li_2O assembly

APPENDIX 4.2

Development of Monte Carlo Code Using Multi-group
Double Differential Cross Section Library and Its Application
to Shielding Calculation for Fusion Materials

Masayuki Nakagawa, Takamasa Mori and Yukio Ishiguro
Japan Atomic Energy Research Institute, Tokai Establishment
Tokai-mura, Ibaraki-ken, Japan

The anisotropy of scattering angular distribution plays an important role in the neutron energy and angular distributions at the higher energy region as encountered in fusion blanket neutronics. The conventional multi-group methods using the P_1 expansion for the anisotropic scattering sometimes significantly mispredict the neutron transport phenomena in the materials with highly anisotropic scattering cross sections. The use of the lower order P_1 expansion of the angular distributions leads to negative energy transfer matrices, hence sometimes to negative flux.

In order to overcome such problems, the use of the double differential form of scattering cross sections (DDX) was proposed for the accurate treatment of the energy-angle correlated kinematics by Takahashi et al.. The transport codes using this type of cross sections can treat accurately the strong anisotropic scattering observed in the fusion blanket and shielding materials. Investigations have been made for producing the multi-group DDX library and applying it in the general Monte Carlo transport calculations. A simplified form of the DDX has been derived to produce the multi-group cross section library from the ENDF/B type nuclear data file. The DDX library production code, PROF-DDX, has been developed for neutronics calculations. This code produces partial cross sections,

σ_x^g , neutron production cross section, σ_{pr}^g , and energy-angle correlated scattering probability matrix, $I(\mu_k, g', g)$, in the energy range from 16.5 MeV to 0.32 eV. The scattering probability is calculated in a fine mesh structure based on the collision kinematics. The angular mesh points, μ_k , are taken to be 20 with an equal width $\Delta\mu$. The anisotropy of scattering is taken into account both for the elastic and the inelastic scatterings.

The general purpose Monte Carlo code, MORSE-CG has been modified to be able to treat the DDX library as multi-group cross sections. In the random walk routines, the energy and angle after a collision are determined by using the probability table $I(\mu_k, g', g)$ which is calculated for constituent materials. Since the scattering angle can be selected from the continuous distribution, the ray effect is not observed in this method. The computation time by the present method is comparable with that by the P_8 expansion.

The availability of the DDX library and Monte Carlo method has been examined by analysing the neutron spectra measured with use of a 14 MeV neutron source in several materials by Hansen et al. In the analysis, the results by the conventional P_8 cross sections produced by the SUPERTOG code and the present DDX have been compared with the measured spectra. The present method shows significant improvements for ${}^7\text{Li}$, graphite and oxygen, though the differences between two methods are not so larger for heavy materials such as iron and lead. The analysis has been also carried out for the neutron angular spectrum in Li_2O assemblies measured at FNS facility. The present method can predict fairly well the measured spectrum.

APPENDIX 4.3 Computational Data and Methods Used in the Nuclear Design of Fusion Reactors

Nuclear design⁽¹⁾ of INTOR-J⁽²⁾, the JAERI proposal for the International Tokamak Reactor (INTOR)⁽³⁾ has been carried out using one dimensional (1D) S_N code ANISN⁽⁴⁾, two dimensional (2D) S_N code DOT-3.5⁽⁵⁾ and three dimensional (3D) Monte Carlo code MORSE-I⁽⁶⁾. A 42 group-neutron 21 group-gamma coupled cross-section library for 40 nuclides GICX40⁽⁷⁾, which is based on ENDF/B-III and IV⁽⁸⁾ for neutron data and POPOP4 Library⁽⁹⁾ for gamma-ray production data, was used.

The 1D calculations were used in preliminary calculations and parametric surveys on tritium breeding⁽¹⁰⁾ and magnet shielding design. Neutron and gamma-ray fluxes, radiation damage rates and nuclear heating rate distributions were calculated with cylindrical models.

Gamma dose rates after reactor shutdown were also calculated using 1D model and THIDA code system⁽¹¹⁾. THIDA is a code system which calculates Transmutation, Hazard potential, Induced activity, Dose rate and Afterheat. It consists of the following: induced activity calculation code; activation chain, activation cross section, radionuclide gamma-ray energy/intensity and gamma-ray group constant files; and gamma-ray flux to exposure dose rate conversion coefficients.

The 2D calculations were carried out to investigate the effect of neutron streaming through the divertor channel. As a result, the streaming effect is found to cause about two times as much nuclear heating rate in the magnet than the case without divertor channel.

Poloidal distributions of 14 MeV neutron flux, helium production, displacement damage and nuclear heating rates in the first wall system were calculated⁽¹²⁾ using Monte Carlo transport code MORSE-I⁽⁶⁾. The peaking factors of 14 MeV neutron flux and helium production rate distributions were found to be about 1.3 and those of displacement damage and nuclear heating a little smaller. The peaks were always in the outboard side of the first wall.

An albedo Monte Carlo method was developed in order to evaluate the neutron streaming through neutral beam injector (NBI) ports⁽¹³⁾. Preliminary results of the evaluation suggest that nuclear heating and radiation damage in the NBI seems to be tolerable but the induced activation necessitates remote operation for the repair and maintenance of NBI components around the ion source.

The Monte Carlo Transport Code MORSE has been improved. MORSE-I is a revision of the MORSE-GG code⁽¹⁴⁾. The following improvements are made.

- (1) MORSE-I can treat a torus geometry which is represented by using surface of fourth order while original MORSE-GG treats those which can be represented by surfaces of second order. The number of surfaces allowed in a block is increased from 17 to 35.⁽⁶⁾
- (2) Point-detector technique is improved
 - (2)-1 Computational time required is reduced significantly by the Score Point Selection technique.⁽¹⁵⁾
 - (2)-2 Specular reflection boundaries can be used as symmetric boundaries. Proper usage of this boundary also reduces computational time practically.⁽¹⁶⁾
 - (2)-3 Infinite variance is eliminated by the Small Density Perturbation technique.⁽¹⁷⁾

References

- (1) Seki, Y., Iida, H., Yamauchi, M., Kitamura, M. and Kawasaki, H.: Proc. 1980 Annual Meeting of the Atomic Energy Soc. of Japan, D29 (1980) (in Japanese)
- (2) Sako, K., Tone, T., Seki, Y., Iida, H., Yamato, H., et al.: Engineering Aspects of the JAERI Proposal for INTOR (I) and (II), JAERI-M 8503 and 8518 (1980)
- (3) INTOR (International Tokamak Reactor), Division of Research and Laboratories, IAEA, Vienna (1980)
- (4) Engle, W.W., Jr.: A User's Manual for ANISN, A One-Dimensional Discrete Ordinates Transport Code With Anisotropic Scattering, K-1693, Oak Ridge Gaseous Diffusion Plant (1967)
- (5) RSIC Computer Code Collection: DOT-3.5, Two Dimensional Discrete Ordinates Transport Code, CCC-276, Radiation Shielding Information Center, Oak Ridge National Laboratory (1976)
- (6) Iida, H. and Yamauchi, M.: Proc. 1978 Fall Meeting of the Atomic Energy Soc. of Japan, B35 (1978) (in Japanese)
- (7) Seki, Y. and Iida, H.: Coupled 42-Group Neutron and 21-Group Gamma Ray Cross Section Sets for Fusion Reactor Calculations, JAERI-M 8818 (1980)

- (8) Drake, M.K.: Data Formats and Procedures for the ENDF Neutron Cross Section Library, BNL-50274 (T-601, TID-4500) (1970) Rev. 1974
- (9) Ford, W.E., III.: The POPOP4 Library of Neutron-Induced Secondary Gamma-Ray Yield and Cross Section Data, CTC-42 (1970)
- (10) Iida, H. and Seki, Y.: Studies on Increasing Tritium Breeding Ratios of JXFR and INTOR-J Blankets, JAERI-M 8896 (1980) (in Japanese)
- (11) Iida, H. and Igarashi, M.: THIDA - Code System for Calculation of the Exposure Dose Rate Around a Fusion Device - , JAERI-M 8019 (1978) (in Japanese)
- (12) Iida, H., Seki, Y., Yamamoto, T. and Kawasaki, K.: Poloidal Distributions of Neutron Flux, Radiation Damage and Nuclear Heating Rate in a First Wall System of INTOR-J, JAERI-M 8517 (1979)
- (13) Yamauchi, M., Iida, H. and Murata, T.: Calculation of Neutron and Gamma-Ray Streaming Through the Neutral Beam Injector Port of INTOR-J, to be published in Proc. 11th Symposium on Fusion Technology, Oxford Sept. 15-19 (1980)
- (14) Straker, W.A., Stevens, P.N., Irving, D.C. and Cain, V.C. : The MORSE Code - A Multigroup Neutron and Gamma-Ray Monte Carlo Transport Code, ORNL-4585 (1970)
- (15) Iida, H. and Seki, Y.: Reduction of Computational Time for Point Detector Estimator in Monte Carlo Transport Code, Nucl. Sci. Eng., 74, 213 (1980)
- (16) Iida, H. and Seki, Y.: Simple Method of Eliminating Infinite Variance in Point Detector Problem of Monte Carlo Calculation, J. Nucl. Sic. Tech. 17, 315 (1980)
- (17) Iida, H. and Seki, Y.: A Point Detector Scoring Method Compatible with Monte Carlo Transport Calculations of Specularly Reflected Particles, Nucl. Sci. Eng., 76, 302(1980).

5. STRUCTURAL MATERIALS

The Research Committee on Fusion Reactor Materials in JAERI has initiated an alloy development program to provide materials data for reactor design by 1990. The program is divided into two phases — Phase I is the period extending to 1985 and Phase II to 1990.

The alloy development for the first wall and blanket structural materials is concentrated on austenitic stainless steel and a heat of the prime candidate alloy (PCA) of about 1,000 kg was prepared for testing in Phase I on the fundamental properties required for reactor design study. The testing is being made also on five candidate alloys to be a reference to the PCA in water-coolant environment; The PCA might suffer from stress corrosion cracking in the environment. Chemical compositions of the candidate alloys are given in Table 1. The five candidates (A to K in Table 1) alloys were designed to achieve less susceptibility of stress corrosion cracking in water-coolant environment.

All the alloys showed reasonable strength and good ductility as expected in tensile testing up to 650°C. Short-term creep testing at temperatures of 550°C to 650°C revealed that PCA had much higher strength than Type 316 stainless steel in both solution annealed and cold worked conditions. No serious problem was disclosed for weldability of the alloys by Vareststraint hot cracking and high temperature ductility tests. All the alloys are now being heated to prove phase stability in the temperature ranged from 400°C to 650°C.

As to the resistance to stress corrosion cracking in water-coolant environment, PCA has been examined in parallel with the other alloys by Streicher test, slow strain rate test (SSRT), electrochemical potentiokinetic reactivation method (EPR) and double U-bend test. Low carbon alloys (C, J and K) showed naturally better resistance to intergranular corrosion in EPR test and stress corrosion cracking in double U-bend test than the other alloys. Furthermore, the tests indicated that increase in nickel and chromium contents and addition of niobium were beneficial for increasing the corrosion resistance. It is also evident from the examinations that PCA can be used in controlled water-coolant environment. The susceptibility of stress corrosion cracking for PCA is continued to be examined with alloys K and C to evaluate endurance

limit in the water-coolant environment.

In addition to the corrosion study, the examination for establishing the welding procedure of PCA and fatigue testing at temperatures of 300°C to 500°C are planned in the next fiscal year. The prime candidate alloy is also planned to be irradiated in HFIR and ORR under US-Japan fusion energy collaboration program, to obtain data for evaluating the lifetime of the first wall as a function of operating temperature by the end of Phase II. Tensile test, testings on fatigue properties and microstructural observations are included in the post-irradiation examination. In-pile creep test with pressurized tubes will also be carried out in ORR.

Irradiation test data from JOYO are expected to become available from a program done in cooperation with Power Reactor and Nuclear Fuel Corporation. The integrity of the PCA as a structural member is intended to be verified in Phase II, and materials data needed for reactor design are expected to be documented in a materials handbook. FMIT is desired to supply high energy neutron damage data by the end of Phase II.

On ferritic steels, scoping study has been started in relation to development of wrapper materials in fast breeder reactor. Selection of the prime candidate alloy is scheduled to be made by the end of Phase I, and irradiation tests will be performed in Phase II. For advanced alloys beyond austenitic and ferritic steels, fundamental studies are left to universities and other governmental laboratories.

Table 1 Chemical compositions of candidate alloys (wt %)

alloy	C	Si	Mn	P	S	Ni	Cr	Mo	Ti	Nb	B	N
PCA	0.06	0.53	1.79	0.027	0.009	16.22	14.51	2.37	0.24	-	0.0035	-
A	0.05	0.52	1.55	0.018	0.007	16.2	16.1	2.6	0.25	0.12	-	0.004
B	0.06	0.49	1.54	0.016	0.006	16.2	16.2	2.6	0.24	0.21	-	0.005
C	0.02	0.5	0.5	0.015	≤0.01	16	16	2.5	0.25	0.1	-	-
J	0.02	0.51	1.47	0.015	0.005	15.92	15.96	2.52	0.296	-	-	0.003
K	0.02	0.48	1.46	0.015	0.005	17.56	17.99	2.6	0.298	-	-	0.004

6. BREEDING MATERIAL

Studies of physical and chemical properties and irradiation behavior have been carried out since 1975, in order to clarify the feasibility. These studies have included many principal aspects for the characteristics of Li_2O . Recent works for preparation, physical and thermodynamical properties, compatibilities and tritium release behavior are described below⁽¹⁾.

6.1 Preparation of Lithium Oxide Pellet

Sintered Li_2O pellets with various kinds of density (84 to 98 % TD) and grain size (5 to 100 μm) were prepared by a presssintering method at a certain temperature of 1373 to 1623 K as shown in Fig. 1⁽²⁾. In this preparation, Li_2O powders were produced by thermal decomposition of Li_2CO_3 as a starting material. Occasionally Li_2O powder was purchased.

6.2 Physical and Thermodynamic Properties

The high thermal conductivity is one of advantages of Li_2O over the other candidate solid breeding materials as shown in Fig. 2. The thermal diffusivity of Li_2O pellets having the wide range of density (70.8 to 93.4 % TD) was measured using a laser pulse method in the temperature range from 473 to 1173 K⁽³⁾. The porosity dependence of thermal conductivity was fitted with the modified Maxwell-Eucken equation and Loeb equation.

The heat capacity of Li_2O was measured in the temperature range from 306 to 1073 K using an adiabatic scanning calorimeter⁽⁴⁾. The heat capacity equation obtained by the least squares method was shown below,

$$C_p = 75.24 + 9.55 \times 10^{-3} T - 25.05 \times 10^{-5} T^{-2} \text{ (J/mol}\cdot\text{K)}.$$

The thermal expansion of zone-refined crystals (100 % TD) and sintered pellets of Li_2O was measured in the temperature range from

298 to 1273 K. The thermal expansion coefficient increased with density above 87 % TD. The thermal expansion curve for the fused Li_2O single crystal is shown in Fig. 3(a) and for the sintered samples in Fig. 3(b) (5).

The solubility and diffusivity of hydrogen in Li_2O have been measured by an equilibrium-quenching and hot-extraction method (6). The dissolved amount of hydrogen in Li_2O was found to be proportional to the square root of hydrogen pressure, according with Sivert's law. The dissolved amount was measured to be $(6 \sim 11) \times 10^{-5}$ atom $\text{mol}^{-1} \cdot \text{atom}^{-1/2}$, which was equal to $2 \sim 4$ wppm at 1 atm, in the temperature range from 770 to 970 K. This result suggests that the dissolved state of hydrogen in Li_2O lattice is not molecular but atomic or ionic. On the other hand, hydrogen is confirmed to be scarcely dissolved in the form of atomic state, according to an electron spin resonance measurement (7).

The diffusion coefficient of hydrogen was determined to be from 5×10^{-16} to 10^{-15} m^2/sec in the temperature range from 850 to 1050 K, and its activation energy was 34 KJ/mol.

6.3 Compatibility

(1) He ion backscattering spectroscopy study

In order to get fundamental knowledges of compatibility, each surface reaction of Li_2O pellets coated with Fe, Cr and Ni which were typical elements of candidate container materials, was studied (8). Specimens were heated in vacuum in the temperature range from 770 to 1070 K for 600 to 3600 sec. Depth profiles of coated elements in the specimens were determined by He ion backscattering spectroscopy using a 2 MV Van de Graff accelerator at JAERI. In the case of the pellets coated with iron, the formation of a more volatile product Li_5FeO_4 was observed, which has been confirmed to be produced by a reaction between Li_2O and Fe in the compatibility test.

When Li_2O pellets coated with chromium were heated above 870 K, chromium layer was oxidized to form Cr_2O_3 at the surface by residual oxygen in vacuum during heat treatment. From the relationship between the thickness and heat treatment time, the formation of Cr_2O_3 or LiCrO_2 layers was found to occur by a diffusion-limited reaction.

In respect to the spectra of Li_2O pellets coated with nickel,

the width of nickel peak increased with heat treatment time above 820 K, while the height of the peak reduced, resulting in conservation of the area of nickel peak. In the compatibility test between Li_2O and nickel described in (2), no reaction product was found below 1023 K by X-ray diffraction. This fact and nickel peak-broadening with time suggest that nickel atoms diffuse in Li_2O were determined to be about 3×10^{-18} and 7×10^{-18} m^2/sec at 920 and 970 K, respectively.

(2) Compatibility test

The reaction of sintered Li_2O discs with several commercial heat resistance alloys (304 SS, 316 SS, Incoloy 800, Hastelloy X-R and Inconel 600) has been investigated under static He gas atmosphere of 3.3×10^4 Pa in the temperature range from 773 to 1023 K⁽⁹⁾. The temperature dependence of the weight gain of alloys is shown in Fig. 4. The weight gain of alloys was proportional to the square root of reaction time, which is known as the parabolic law, as shown in Fig. 5. In the case of 304 SS, 316 SS, and Incoloy 800, the weight gain of these alloys was higher than the weight loss of corresponding Li_2O discs. Such an excess weight gain may be attributed to oxidation of alloys by oxygen existing in the surrounding as an impurity. As shown in Fig. 4, the reactivity of Incoloy 800, 304 SS, 316 SS, Hastelloy X-R and Inconel 600 decreased in turn in the temperature of 773 to 1023 K.

In contrast with the Fe-Ni-Cr alloys, Ni metal did not react with the sintered Li_2O discs. It was confirmed that Ni plating on 316 SS improved the compatibility⁽¹⁰⁾.

(3) Reaction of Li_2O with moisture in He atmosphere

It is important to clarify the effect of moisture in He purge gas on the chemical stability of Li_2O , as Li_2O is very hygroscopic. It is pointed out, recently, that the amount of vaporization of Li_2O in He atmosphere containing moisture is not negligibly small for design of tritium producing blanket⁽¹¹⁾. The weight change of Li_2O powder at high temperatures has been measured using a thermobalance in the flowing He gas containing various amounts of moisture. Outline of the experimental apparatus is shown in Fig. 6.

Figure 7 shows the partial pressures of water vapor above LiOH

and Li_2O as the present work (A). In addition, the equilibrium pressures of water vapor above LiOH and Li_2O which have been measured by an effusion method using Knudsen cell, are shown as the present work (B). These value of our present work (A) are lower than ones of Gregory et al. (12)

The apparent vapor pressure of Li_2O , which is calculated by using the transpiration method, are shown in Table 1. Since our experiment does not satisfy the condition keeping the saturated vapor pressure around specimen, the rate of vaporization loss seems to be larger than that of Tetenbaum (11).

Vaporized substances from Li_2O powder were observed to be mostly deposited on the surface of nickel foil lapped inside a quartz tube, and did not deposit on the cold parts of the quartz tube. Since the region of nickel foil is kept at high temperature enough to decompose LiOH , the precipitates of LiOH does not retain. There may be no problem that the vaporization of Li_2O under He atmosphere containing moisture affects the tritium inventory.

6.4 Tritium Release

As summarized in Table 2, the tritium produced in Li_2O by the ${}^6\text{Li}(n,\alpha)\text{T}$ reaction was released mostly in the form of HTO through heat treatment (13) ~ (16). The irradiated materials were heated under vacuum for 20 min at each temperature, which was raised stepwise from 473 to 870 K at 100 K intervals. The following facts are noticed in this table: (1) The HTO fraction released from Li_2O powder decreased with increasing neutron fluence (nvt) and inversely the HT fraction increased. (2) The HT fraction from the sintered Li_2O pellet (76.5 % TD) was larger than that from the powder and the percentage of tritium retained in the pellet was higher than that in the powder. (3) The distribution of tritiated species released from LiOH powder seemed nearly independent of the neutron fluence and the HTO fraction was larger than that of Li_2O powders.

The diffusion coefficients for tritium in Li_2O powder irradiated to 8.1×10^{16} n/cm² and in the pellet irradiated to 5.4×10^{15} n/cm² are shown in Fig. 8 in comparison with those obtained for Li_2O powders by Guggi et al. (17) and Vasiliev et al. (18)

From a series of studies on the chemical behavior of tritium in Li_2O , a tritium release scenario is conclusively written as follows: In Li_2O containing no protium impurities, tritium atoms or ions produced by the ${}^6\text{Li}(n,\alpha)\text{T}$ reaction are trapped as interstitials in the crystal. The LiOT formation at the initial recoil events is also conceivable, although the contribution of high energy or hot reactions of tritium in Li_2O is still a subject to be investigated further. During heat treatment the interstitial tritium migrates through the lattice outward and leaves the crystalline surface principally in the form of T_2 . In the practical case, however, protium impurity (LiOH) is present in the vicinity of the surface and the interstitial tritium must be substituted for H, turning into LiOT before leaving the surface. Hence, almost all tritium produced in Li_2O is released in the form of $\text{HTO}(\text{g})$ and diffusion of tritium appears to be a rate-determining step.

In-pile experiments with in-situ tritium recovery have been identified as one of high priority items. At present in-pile tests are planned in thermal neutron fluences of 10^{18} and 10^{20} n/cm^2 using the sweep gas capsules in order to elucidate a radiation effect on the tritium release process and tritium inventory at the steady-state. The flow diagram of the in-pile tritium release experiment is shown in Fig. 9.

References

- (1) H. Watanabe, H. Kudo: Proc. 3rd IAEA Technical Committee Meeting and Workshop on Fusion Reactor Design and Technology, Tokyo, October 1981.
- (2) T. Takahashi, et al.: Annual Meeting of Atomic Energy Soc. of Japan, J-15 (1981), in Japanese.
- (3) T. Takahashi, et al.: J. Nucl. Mater. 91 (1980) 93.
- (4) T. Tanifuji, et al.: J. Nucl. Mater. 78 (1978) 422.
- (5) T. Kurasawa: J. Nucl. Mater. 107 (1982) 334.
- (6) H. Katsuta, et al.: Internal Report (1981)
- (7) K. Noda: Private Communications
- (8) K. Noda, et al.: J. Nucl. Mater., submitted.
- (9) T. Kurasawa, et al.: J. Nucl. Mater. 92 (1980) 67.

- (10) F.A. Finn, T. Kurasawa, et al.: Proc. 9th IEEE Symp. on Engineering Problems of Fusion Research, Chicago, October 1981.
- (11) M.A. Abdou, et al.: FED-INTOR/TRIT/81-01.
- (12) N. Gregory, R. Mohr: J. Am. Chem. Soc. 77 (1955) 2142.
- (13) H. Kudo, K. Tanaka: Radiochem. Radioanal. Letters 23.
- (14) S. Nasu, et al.: J. Nucl. Mater. 68 (1977) 261.
- (15) H. Kudo, et al.: J. Inorg. Nucl. Chem. 40 (1978) 363.
- (16) H. Kudo, K. Okuno: J. Nucl. Mater., 101 (1981) 38.
- (17) D. Guggi: Proc. 9th Symp. on Fusion Technology (Garmisch-Partenkirchen, June 14-18, 1976) Pergamon Press, PP.337-344.
- (18) V.G. Vasiliev, et al.: US/USSR Workshop on Engineering and Economic Problems of ETF (Moscow and Leningrad, Sept. 10-21, 1979).

Table 1 Apparent vapor pressure of Li_2O in He flow

Vppm H_2O in He	Apparent vapor pressure*, atm	
	1173K	1273K
12	3.0×10^{-5}	1.7×10^{-4}
30	4.7×10^{-5}	1.8×10^{-4}
113	1.8×10^{-4}	$6.6 \times 10^{-5} \text{ **}$ (115ppm, at 1268K)
290	3.2×10^{-4}	9.5×10^{-4}
420	$3.7 \times 10^{-5} \text{ **}$	$1.0 \times 10^{-4} \text{ **}$ (440ppm, at 1263K)

* Calculated using the transpiration equation

$$P = (w/u)(RT/M) \times 2$$

w : the rate of weight loss (g/min)

u : He flow rate (cm^3/min)RT : $22.4 \times 10^3 \text{ cm}^3 \cdot \text{atm}/\text{mol}$ M : molecular weight of Li_2O , 30g/mol

** Values measured by M.Tetenbaum et al.

Table 2 Distribution of tritiated species released from neutron-irradiated Li_2O heated up to 870 K under vacuum

Material	Neutron fluence cm^{-2}	Distribution of tritiated species (%)				
		HTO	HT	CH_3T	$\text{C}_2\text{H}_{2n-1}\text{T}$ (n=1,2,3)	Retained in material
Li_2O powder	5.4×10^{15}	99.1	0.4	0.1	0.2	0.2
	3.6×10^{16}	98.0	0.9	0.9	0.1	0.1
	8.1×10^{16}	97.6	1.8	0.4	0.1	0.1
	8.9×10^{17}	93.4	5.6	0.7	0.1	0.1
Li_2O pellet (76.5 %TD)	5.4×10^{15}	95.4	3.5	0.5	0.03	0.6
LiOH powder	3.6×10^{16}	99.4	0.3	0.1	0.2	0.01
	8.9×10^{17}	99.1	0.8	0.1	0.01	0.03

The samples were heated for 20 min at each temperature which was raised stepwise from 473 to 870 K at 100 K interval.

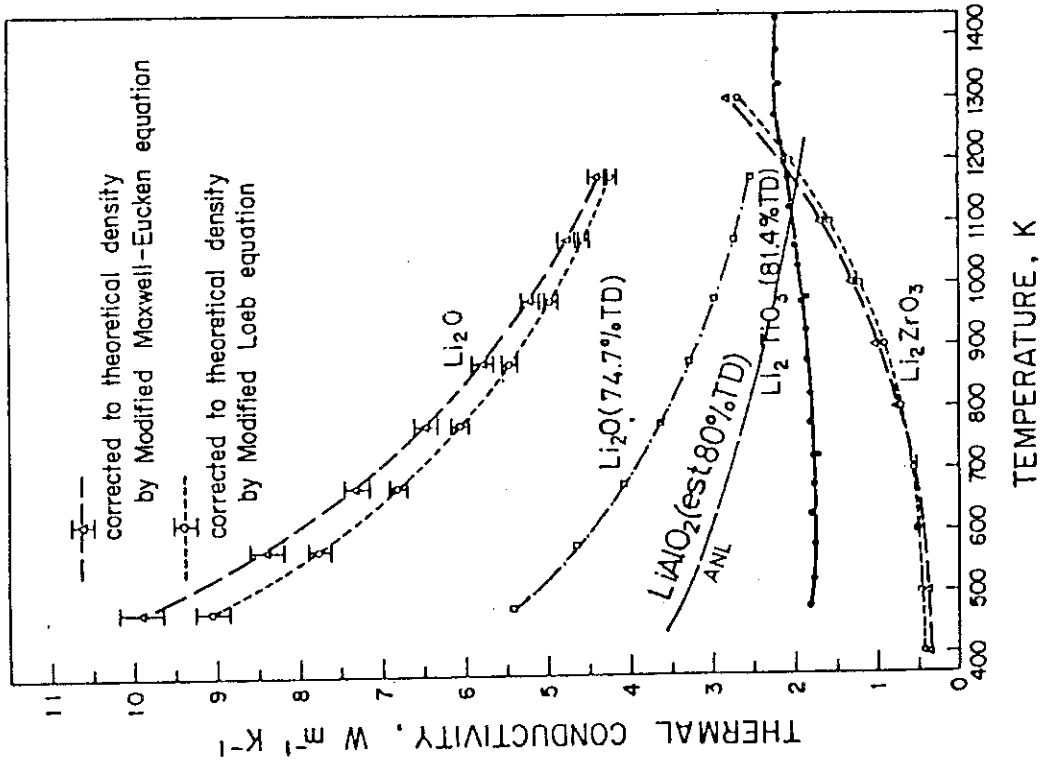


Fig. 2 Thermal conductivity of candidate solid breeder materials

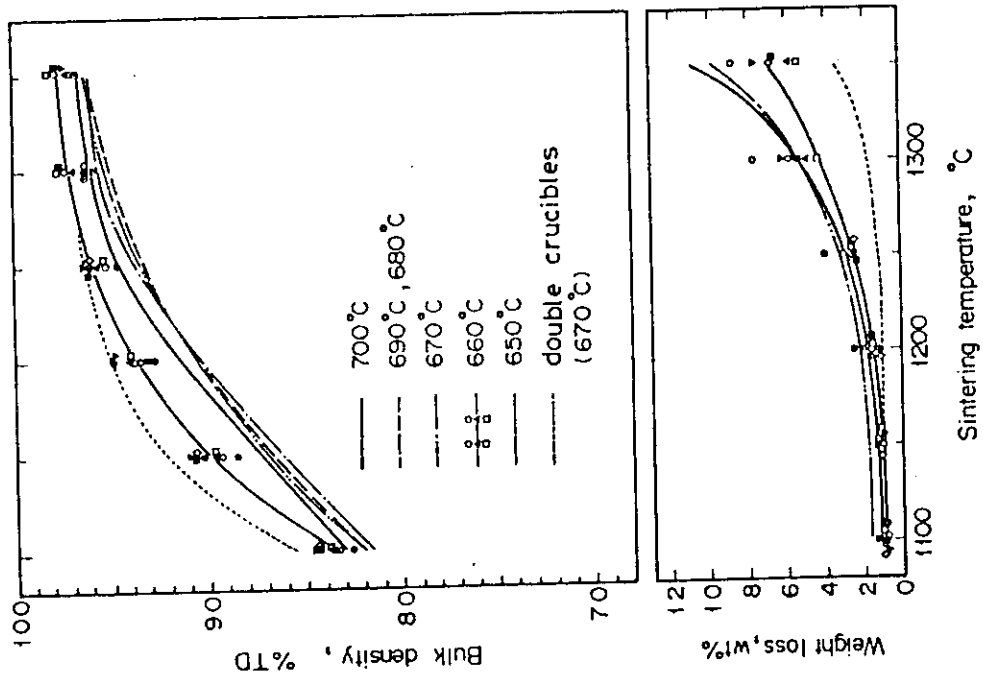


Fig. 1 Relation between pellet density/weight loss and sintering temperature

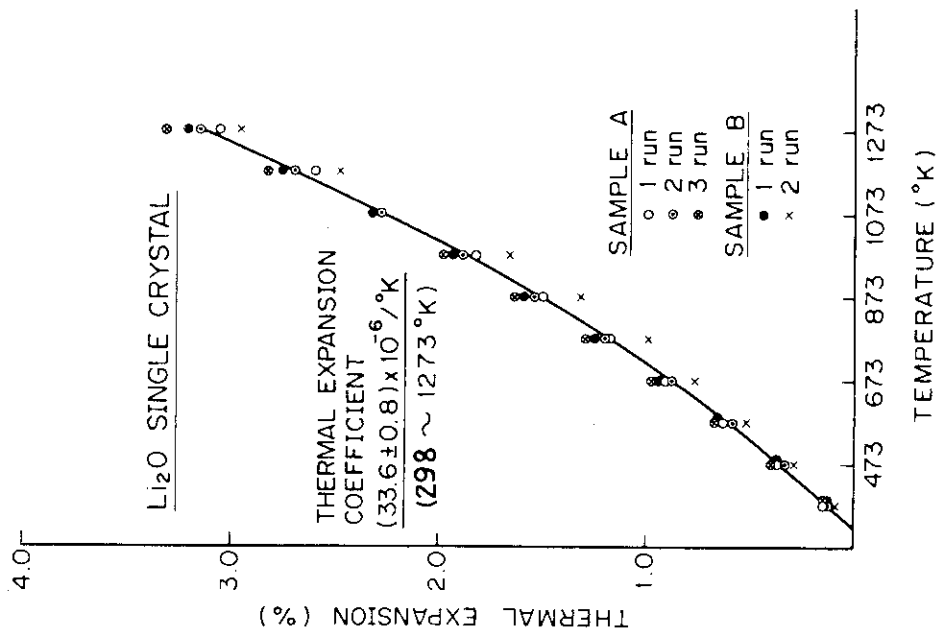


Fig. 3(a) The thermal expansion curve of a fused Li₂O single crystal. A and B samples were cutted from the same rod.

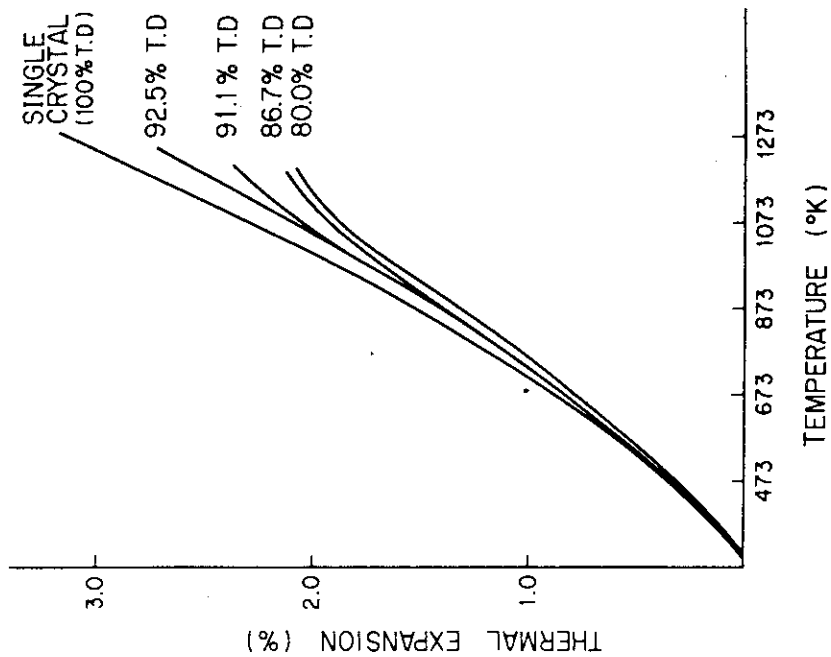


Fig. 3(b) Thermal expansion curves of fused and sintered samples. The curve of the 75.5% TD sample was omitted because it overlapped the curve of the 80.0% TD sample.

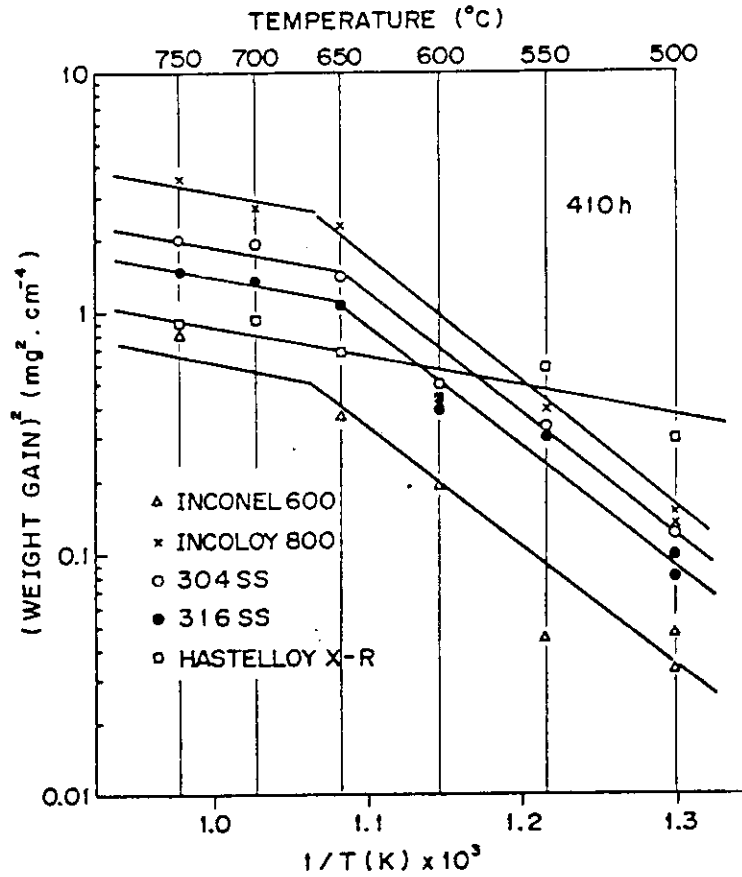


Fig. 4 Temperature dependence of weight gain of Fe-Ni-Cr alloys.

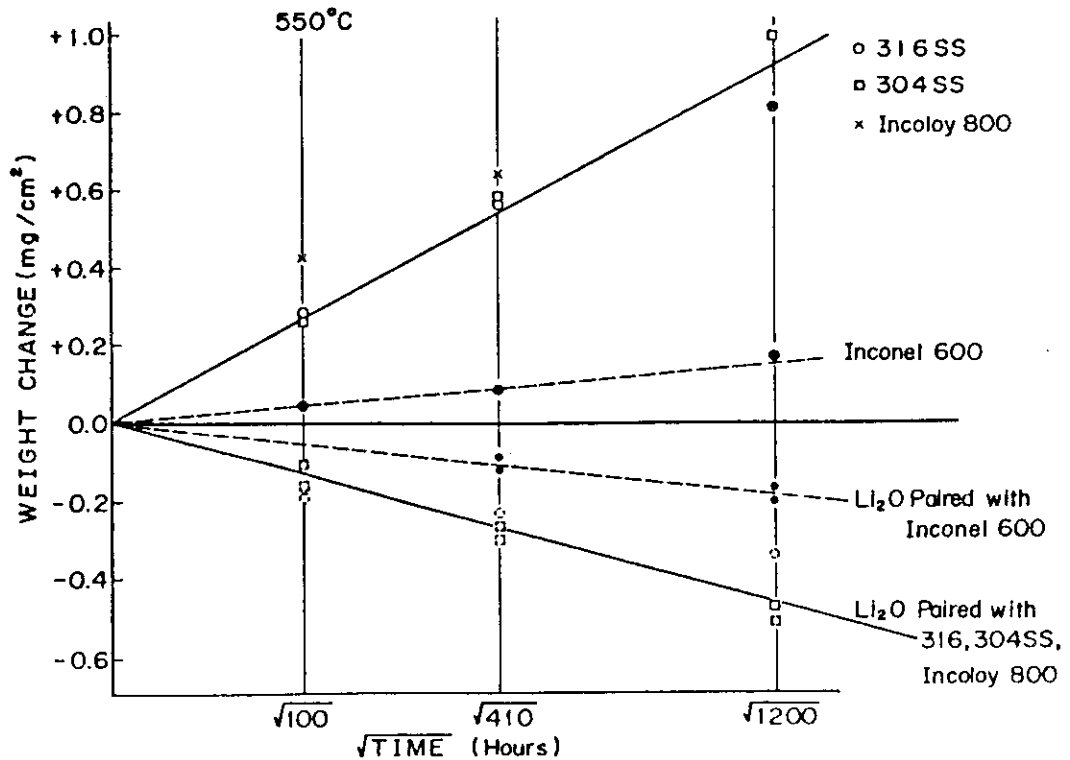


Fig. 5 Temperature dependence of weight change of the alloy and the sintered Li_2O discs at 823 K.

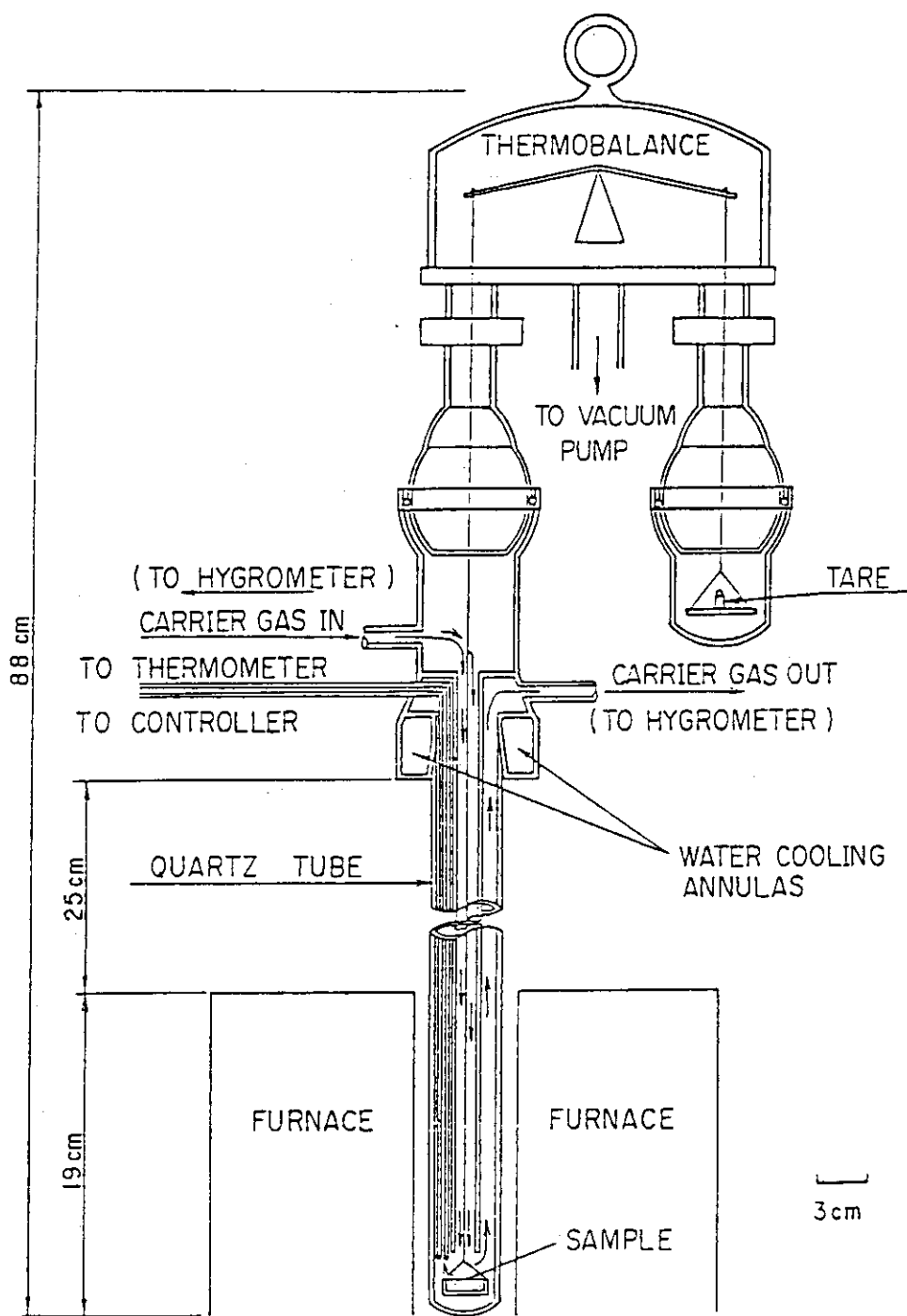


Fig. 6 Outline of the apparatus measuring the weight change of Li_2O

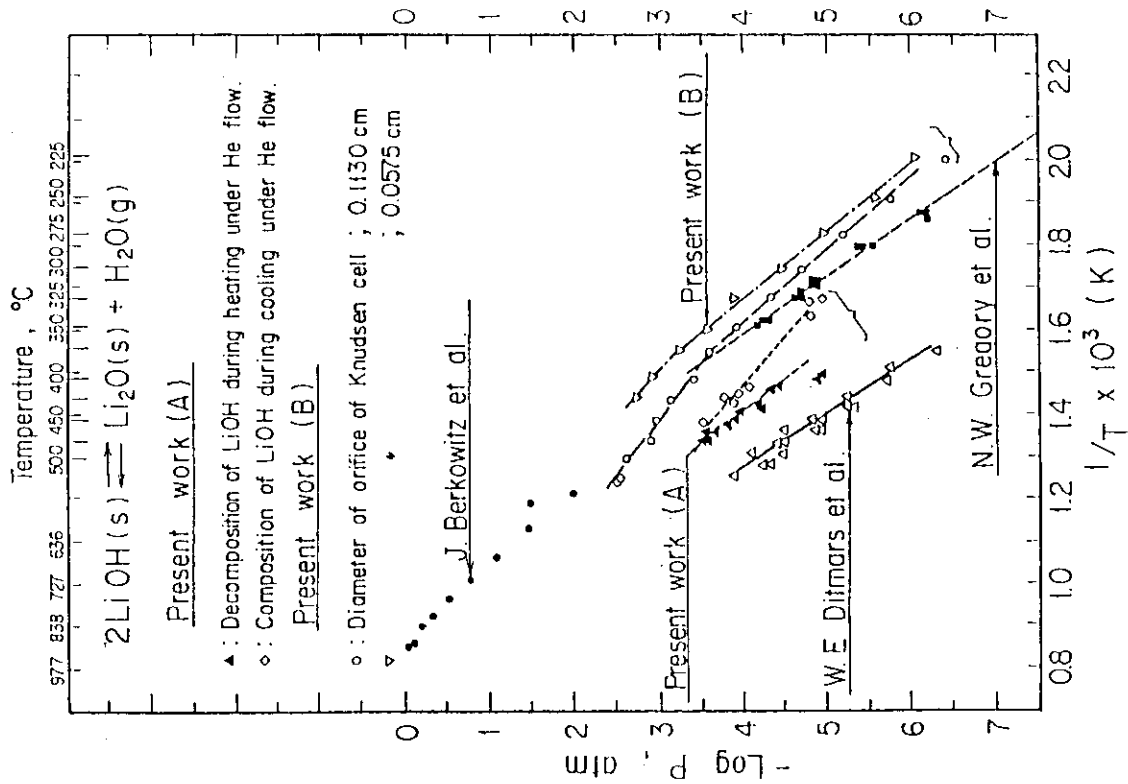


Fig. 7 The equilibrium pressures of water vapor above LiOH and Li₂O

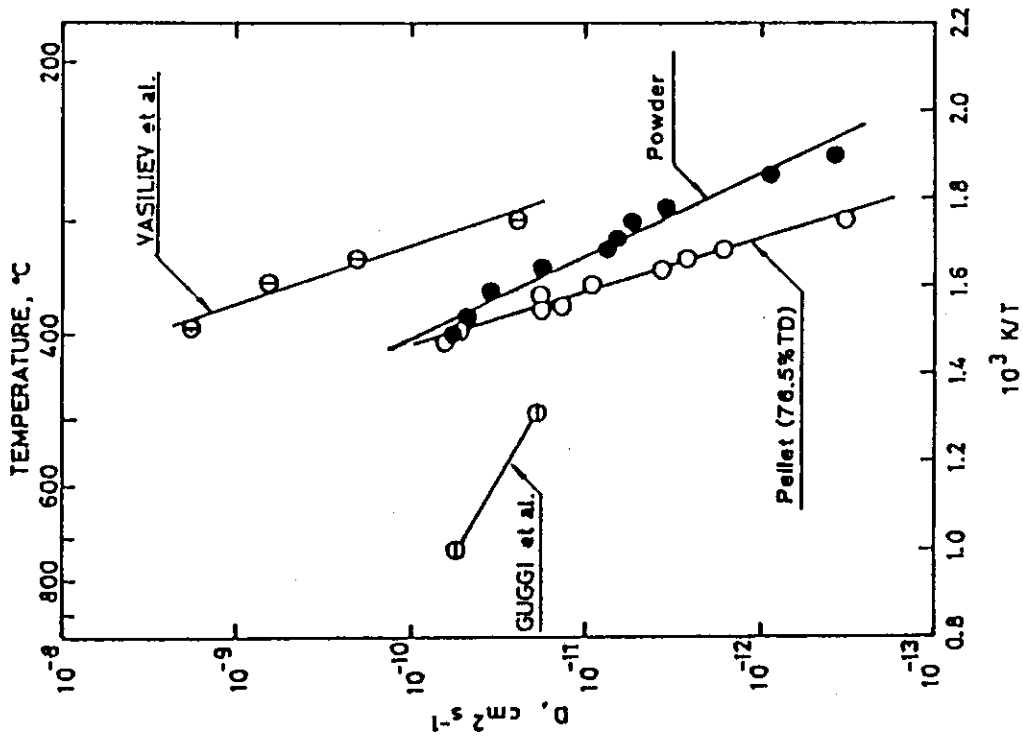


Fig. 8 Diffusion coefficient for tritium produced in Li₂O plotted as a function of temperature

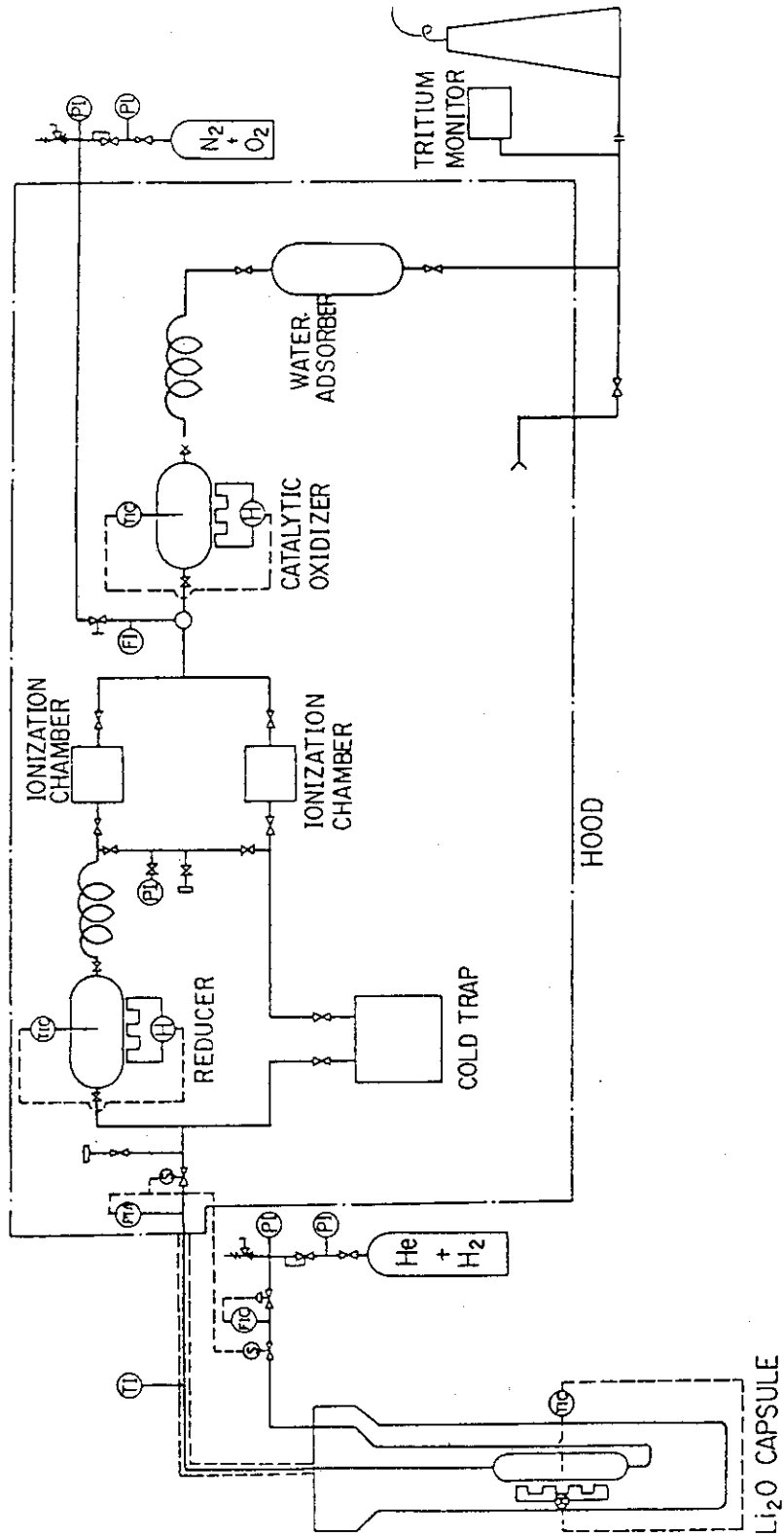


Fig. 9 FLOW DIAGRAM OF VOM-15H IN-PILE TRITIUM RELEASE EXPERIMENT

7. ELECTROMAGNETIC ENGINEERING

7.1 Development of Analysis Methods and Computer Codes for Eddy Current

7.1.1 Lumped constant circuit method

(1) RING-I

This code is for determining transient current distribution on a vacuum vessel of tokamak device which has no electric insulation in the toroidal direction. The vacuum vessel is treated as many toroidal conducting rings connected electrically with their mutual inductance. The current distribution (except saddlelike current) on the vacuum vessel is determined from the currents of these rings by solving the circuit equations. By this method, the current distribution of a vacuum vessel with arbitrary cross section can be obtained. The ring model of vacuum vessel is shown in Fig. 1 and the circuit equations can be expressed as follows.

$$V_k = \frac{d\phi_k}{dt} = \sum (M_{kj} \dot{I}_j + \dot{M}_{kj} I_j) \quad (1)$$

$$\phi_k = \sum M_{kj} I_j \quad (2)$$

$$\phi_k = \int V_k dt \quad (3)$$

$$V_k + R_k I_k = 0 \quad (4)$$

And the symbols in above equations are as follows.

- M_{kk} ; self inductance of ring k
- M_{kj} ; mutual inductance (k and j)
- I_k ; current of ring k
- R_k ; resistance of ring k
- V_k ; one-turn voltage of ring k
- ϕ_k ; linkage flux of ring k

(2) RING-II

This code is for easily evaluating the shell effect for passive control in the case of vertical plasma displacement. This function is added to RING-I. The vertical plasma displacement is expressed by using a dipole current model which is shown in Fig. 2 as follow.

$$\Delta S = 2a_p \delta Z \quad (5)$$

$$\frac{dI_d}{dt} = \frac{I_p}{\pi a_p^2} \frac{\Delta S}{\delta t} = \frac{2I_p}{\pi a_p} \frac{\delta Z}{\delta t} \quad (6)$$

(Uniform plasma current I_p is assumed)

where

a_p ; plasma minor radius

δZ ; vertical displacement

δt ; spent time for δZ

ΔS ; area of shadow

I_d ; dipole current

(3) TOKAMAK CIRCUIT⁽¹⁾

In this method, the MHD equilibrium theory is taken into the framework of circuit equations. By this method, it is possible to carry out the simulation of the horizontal plasma position, plasma cross section, poloidal magnetic field and the current in the plasma channel and tokamak components through all phase of the discharge: current build-up, flat top and shut down phase. For course it's easy to calculate the induced eddy current at the plasma disruption phase.

This simulation is useful both in the analysis of plasma behavior and in the design of the feedback system of the plasma current, position and shape. The magnetic flux functions and equations describing the plasma motion and shape are derived from the MHD equilibrium theory⁽²⁾. A model of plasma and vacuum vessel is shown in Fig. 3. The flux function can be easily expressed by currents in the components. For example, the flux function ψ_p by plasma is given by

$$\psi_p = R_p \mu_0 I_p \left(\ln \frac{8R_p}{r_u} - 2 + \frac{R_p - R_u}{r_u} \cos \omega \right) - \frac{\mu_0 I_p}{2} \left[1 - \ln \frac{8R_p}{r_u} - \frac{r_p^2}{r_u^2} \left(\Lambda_1 + \frac{1}{2} \right) \right] r_u \cos \omega \quad (7)$$

(in the first order approximation of the expansion in the inverse aspect ratio)

where

I_p ; plasma current

$$\Lambda_1 = \beta_p + \ell_i / 2 - 1$$

β_p ; poloidal β

ℓ_i ; internal inductance

An equation which governs the plasma motion can be readily derived from the flux function following the procedure given by V.S. Mukhovatov and V.D. Shafranov⁽²⁾.

$$\frac{\mu_0 I_p}{2} \left(\ln \frac{8R_p}{r_p} + \Lambda_1 - \frac{1}{2} \right) + 2\pi R_p B_z = 0 \quad (8)$$

Similarly, the equation describing the shape of plasma is

$$\delta + \frac{3r^3}{4R_p^2} \left(\ln \frac{8R_p}{r_p} - \frac{5}{4} - \frac{\Lambda_1}{3} \right) - \frac{r^3}{R_p^2} \Lambda_1 - \frac{r^3}{R_p^2} \left(\ln \frac{8R_p}{r_p} - \frac{1}{2} + \Lambda_1 \right) n = 0 \quad (9)$$

where

B_z ; vertical field

$$n ; n\text{-index} \quad n = - \left[\frac{R}{B_z} \frac{\partial B_z}{\partial R} \right]_{R=R_p}$$

while, i_u is set as the current on the vacuum vessel with circular cross section.

$$i_u = i_{u_0} + i_{u_1} \cos \omega + i_{u_2} \cos 2\omega = \frac{I_{u_0}}{2\pi r_u} + \frac{I_{u_1}}{2r_u} \cos \omega + \frac{I_{u_2}}{r_u} \cos 2\omega$$

i_{u_0} ; uniform current density

i_{u_1} ; dipole current density

i_{u_2} ; quadrupole current density

A further study⁽³⁾ in TOKAMAK CIRCUIT enables us to consider the saddlelike current if the saddlelike current have been obtained beforehand.

Similary, the flux functions due to poloidal field coils can be derived.

7.1.2 Distributed constant circuit method

The computer codes of EDDY series have a common theory (method). This method for analyzing the eddy current in thin conductors is named 'Finite Element Circuit Method'. The thin conductor is divided into finite elements and the current potential on each element is defined. Electromagnetic coupling constants between current potentials at respective nodes are calculated by energy integral. The circuit equations are calculated by eigen value analysis. The method is easily applicable to conductor of any shape, especially the vacuum vessel, with no limitation by the aspect ratio and the uniform resistance. For example, the bellows of vacuum vessel are assumed to be anisotropic conductive plate.

In order to calculate the eddy current on the periodically symmetric torus with arbitrary shape, EDDYTORS and EDDYACT were developed⁽⁴⁾. The conductive torus is assumed to be made of infinite thin plate with equivalent surface conductivity to the actual torus. Plasma motion can be simulated by employing the dipole current model in Fig. 2, i.e., MHD equilibrium model as described in TOKAMAK CIRCUIT. Here, the bellows of vacuum vessel is also assumed to be unisotropic conductive plate.

Among EDDY-series computer codes the following EDDYMULT and EDDYARBT are the most advanced.

i) EDDYMULT⁽⁵⁾

To the demands from a numerical design and control analysis of plasma position, current and its shape, intensive efforts of numerical and analytical eddy current studies have been made in JT-60 project.

Current analysis in JT-60 multi-torus system has been made using the numerical code EDDYMULT which was newly developed at JAERI. Taking into account of the mutual coupling between a vacuum vessel, toroidal coils, support plates and a central column, the eigen functions of eddy current defined in the entire multi-torus system are obtained by the method of modal analysis⁽⁷⁾.

In order to confirm the validity of EDDYMULT the model experiments were carried out in a simplified torus plate model illustrated in Fig. 4. The torus consists of rigid and bellows sections each of which is made of copper. Radial distributions of toroidal eddy current along a middle line of rigid section are shown in Fig. 5. The numerical results are in good agreement with the experimental values.

ii) EDDYARBT⁽⁶⁾

The numerical method for analyzing transient eddy currents on thin conductors with arbitrary connections and shapes was developed. The eddy currents are described by current functions and discretized in the usual manner of the finite element method. This code is effectively applied to a torus system comprising multicomponents by analysing simultaneously eddy current distributions on individual components. In particular this method is efficient to analyze the eddy currents on complicated conductor structures. The EDDYARBT has been applied to a electromagnetic design of fusion reactors (FER, commercial reactor and INTOR-J) having belljar-type cryostat, shield, blanket and first wall.

References

- (1) Y. Suzuki, et al.: Japan J. Phys. 16 (1977) 2232
- (2) V.S. Mukhovatov, V.D. Shafranov: Nucler Fusion 11, 665, (1971)
- (3) H. Ninomiya, Y. Suzuki: JAERI-M 7710 (1978)
- (4) A. Kameari, Y. Suzuki: JAERI-M 7120 (1977)
- (5) Y. Nakamura, T. Ozeki: JAERI-M 9612 (1981)
- (6) A. Kameari: Journal of Computational Physics 42, 124-140 (1981)
- (7) Y. Nakamura, T. Ozeki: 12th Symp. on Fusion Technology, Jülich, 13~17 Sept. 1982.

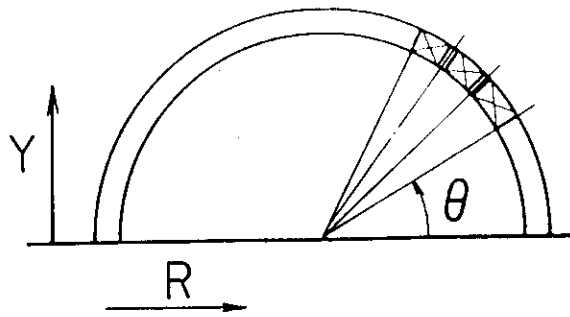


Fig. 1 Ring model of vacuum vessel

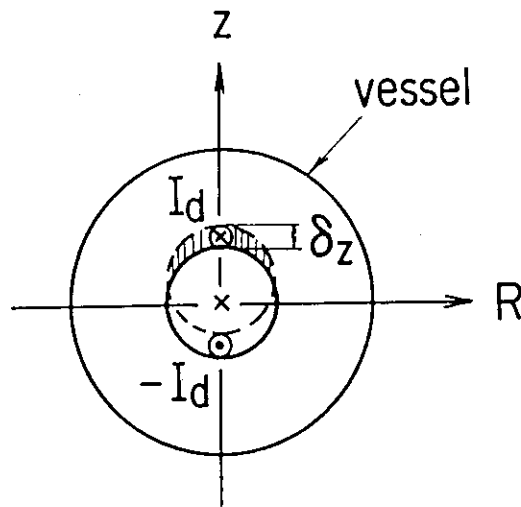


Fig. 2 Dipole current model

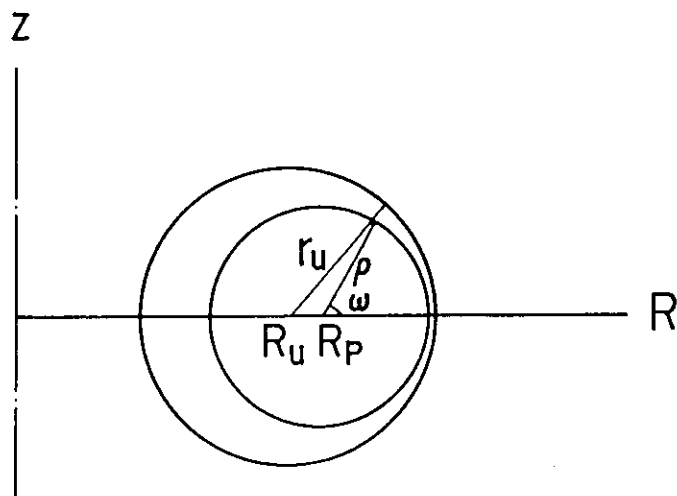


Fig. 3 Model of plasma and vacuum vessel

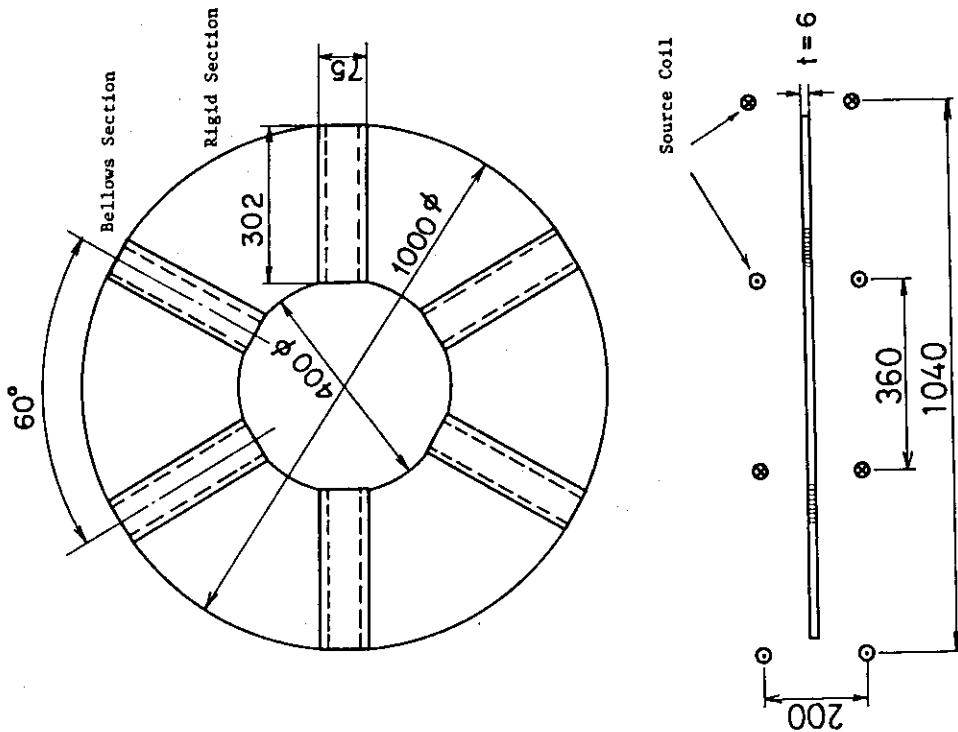


Fig. 4 Schematic view of torus model

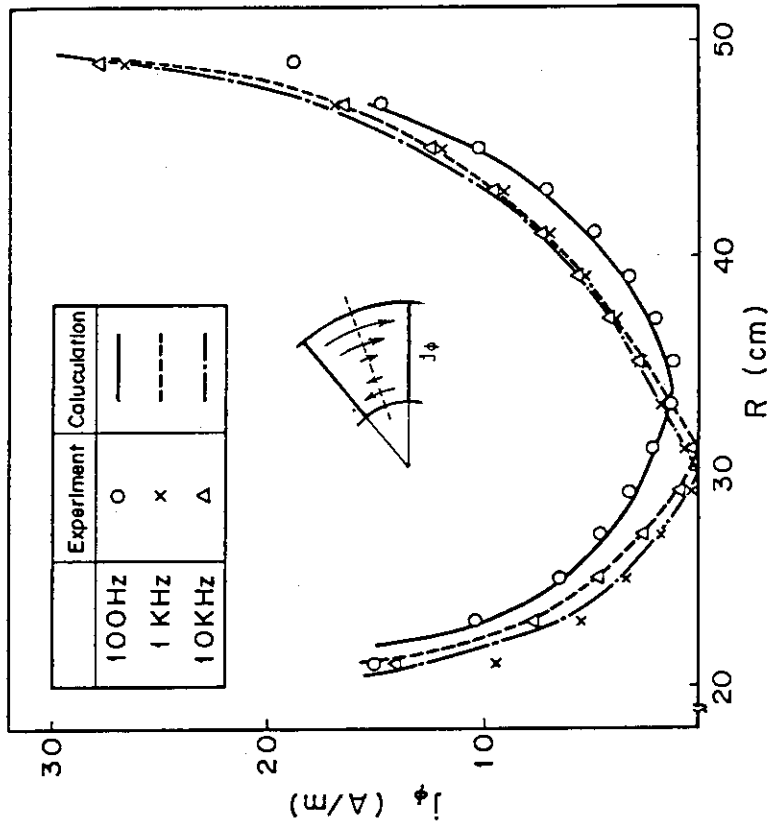


Fig. 5 Radial distributions of eddy current in ϕ direction

7.2 Experiments on Magnetomechanical Behavior of Toroidal Coils and Vacuum Vessel

7.2.1 Objectives

Among many engineering problems relating to the technology of Tokamak type fusion reactor, an achievement of viable structural design of its first wall is indispensable with regard to a protection of the first wall against a plasma disruption, a deterioration of fracture strength by neutron irradiation and sputtering and erosion by plasma particles.

The plasma disruption accident is the most crucial problem to the viable design of the tokamak type reactor among the three at the present time when an effective way to prevent it has not been demonstrated yet.

The experiment to be performed in the near future is closely related to the plasma disruption accident and dynamic deformation of the first wall due to electromagnetic stress is measured to verify the theoretical analysis based on the FEM code.

7.2.2 Contents

(1) Experiment

The experimental devices consist of an 8 coil full torus and a vacuum vessel, which are shown in Fig. 1. The vacuum vessel has four electrical cuts in one case to generate a saddle shaped eddy current and has no cut in other case to generate a loop current. A toroidal field at the axis is about 0.2 Tesla. 10 turn wires are set at the center of the vacuum vessel to simulate the plasma current change. The current is supplied from the 18 kJ condenser bank with the maximum peak current of around 2×10^5 A and a pulse width of about 200 μ sec (Fig. 2).

The dynamic deformation is measured with use of a displacement bar and shielded strain gages.

(2) Numerical analysis

The computer code already available such as SAP is used to analyse the experimental results. And the experimental results are also analysed

by a new FEM code of which originality resides in an application of Kantrovich method.

7.2.3 Goals

The followings are revealed through the present theoretical and experimental investigation.

- (1) A validity of the computer code
- (2) An experimental technique for dynamic deformation measurement under transient magnetic field
- (3) Key features of structural design of the first wall

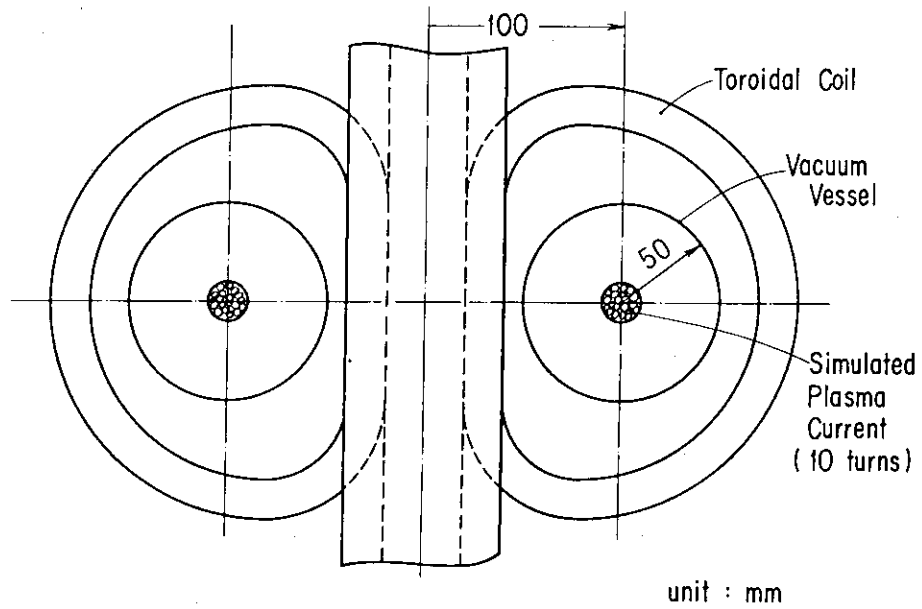


Fig.1(a) Elevated view of the experimental device

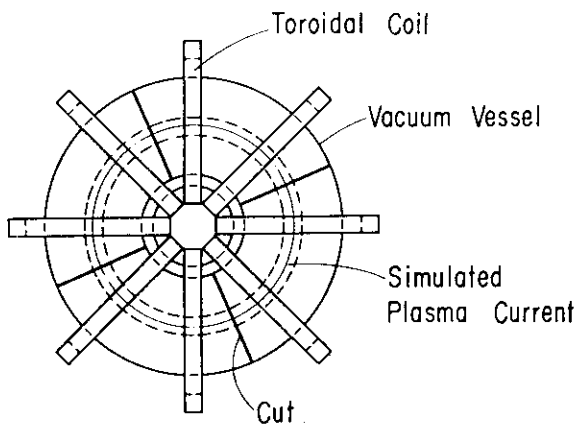


Fig.1(b) Top view of the experimental device

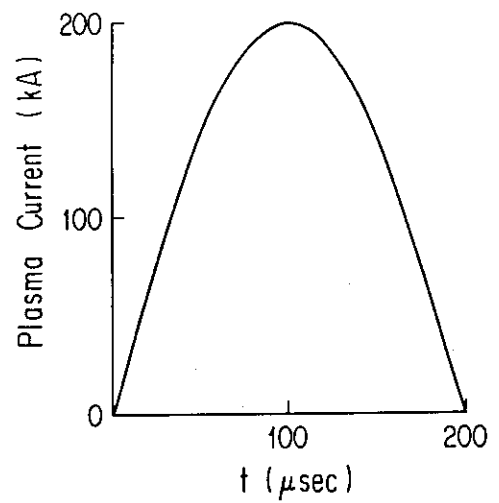


Fig.2 Current shape generated from the condenser bank

8. THERMOMECHANICAL ENGINEERING

Surface heat flux testing of first wall materials is planned. A 30 kW electron beam system will be included in the surface heat flux test facility. On the other hand a test stand with a plasma generator has been completed and experiments, first of all thermal cycle tests of a divertor plate, will soon start.

8.1 Surface Heat Flux Test Facility

Surface heat flux on component materials surrounding a plasma and its duration time largely depend on the plasma operation. Ranges of heat flux and pulse length covering JT-60, FER and INTOR are shown in Fig. 1. The capabilities of the test facility planned are depicted in Fig. 2. Objectives and specifications of the test facility are as follows.

Objectives

Thermal-hydraulic and thermomechanical testing of various candidate first wall materials (and components) with emphasis on surface heat load and heat load transient (such as during plasma disruption) effects.

Specifications

Vacuum System

- Vacuum chamber diameter 1.0 m
- Vacuum chamber length 1.5 m
- Pumping system Turbomolecular pumps & cryopumps
- Base pressure $\leq 10^{-5}$ Torr

Electron Beam System

- Max. power on target 30 kW
- Beam diameter ≤ 1 cm
- Scan rate Very fast
- Max. scan length on target ± 8 cm
(x-y plane)

Diagnostics IR camera, thermocouples, etc.

Heat Removal System

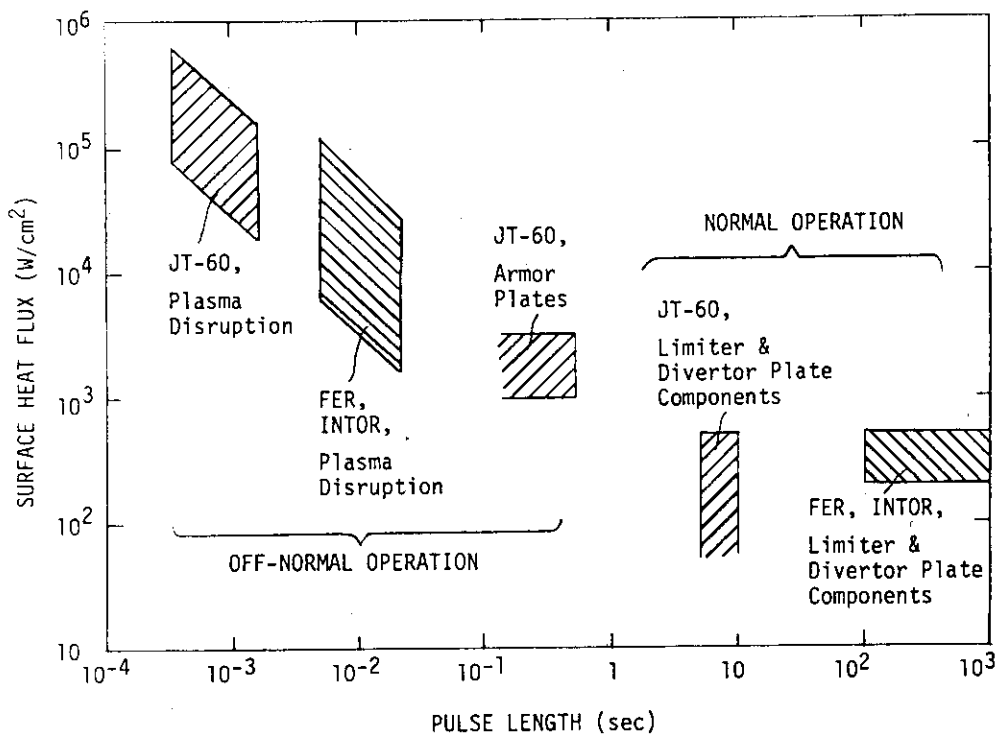


Fig. 1 Estimated surface heat flux vs. pulse length on various first wall components of JT-60 and FER (INTOR)

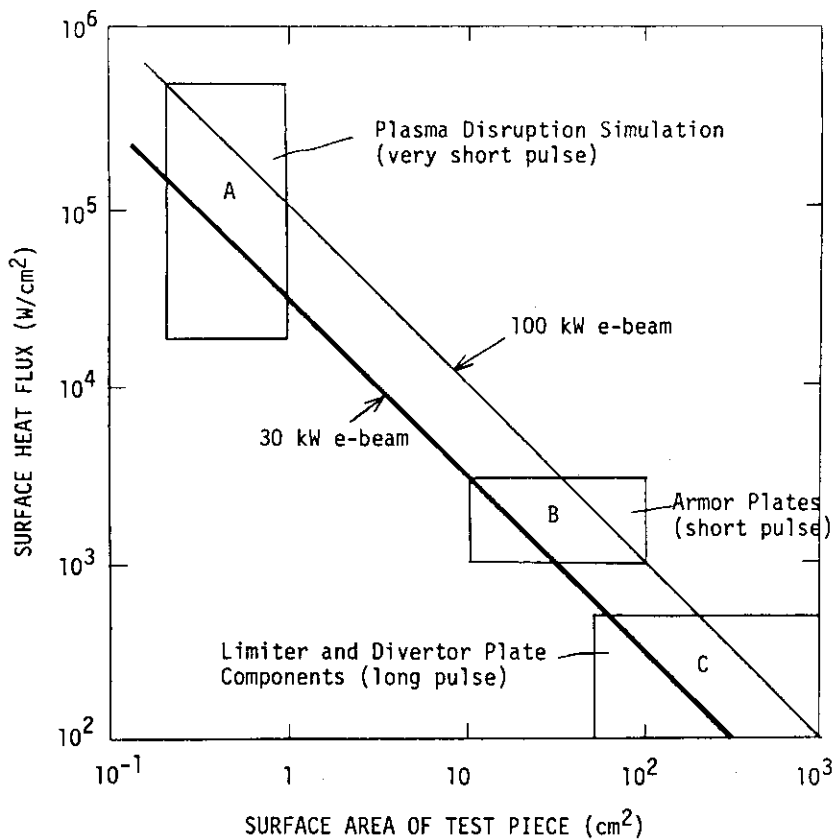


Fig. 2 Composite surface heat flux operating map

8.2 Thermal Cycle Test of A Composite Divertor Plate

A thermal cycle test of a divertor plate is prepared. The wall is made of a composite solid of Cu and W. A question has been raised whether such a composite solid can endure to thermal cycles or not.

In this test, a brazed test piece of 5 cm in diameter is set up in a plasma flow conduit of 9 cm in diameter. It is heated by an Ar plasma as shown in Fig. 1. The other side of the test piece is cooled by an impinging jet of water.

Figures 2 and 3 are photographs of the plasma generator and the plasma flow conduits, respectively. The performance of the Ar plasma is

Ar gas pressure	10 atm (guage) max.
Ar gas flow rate	$1.6 - 20 \times 10^{-2}$ kg/s
mean temperature of plasma	2500 - 8000 °K
power source	240 kW.

An average heat load of 2 MW/m^2 has been obtained over a test piece surface of 20 cm^2 in area. The plasma is discharged automatically in repeated pulses.

Photographs of the test pieces are shown in Figs. 4 and 5. Cu and W of the composite solid was brazed by two methods; by the silver-brazing and by the nichro-brazing

High heat flux removal tests are being conducted; and the thermal cycle test will be started in November 1982.

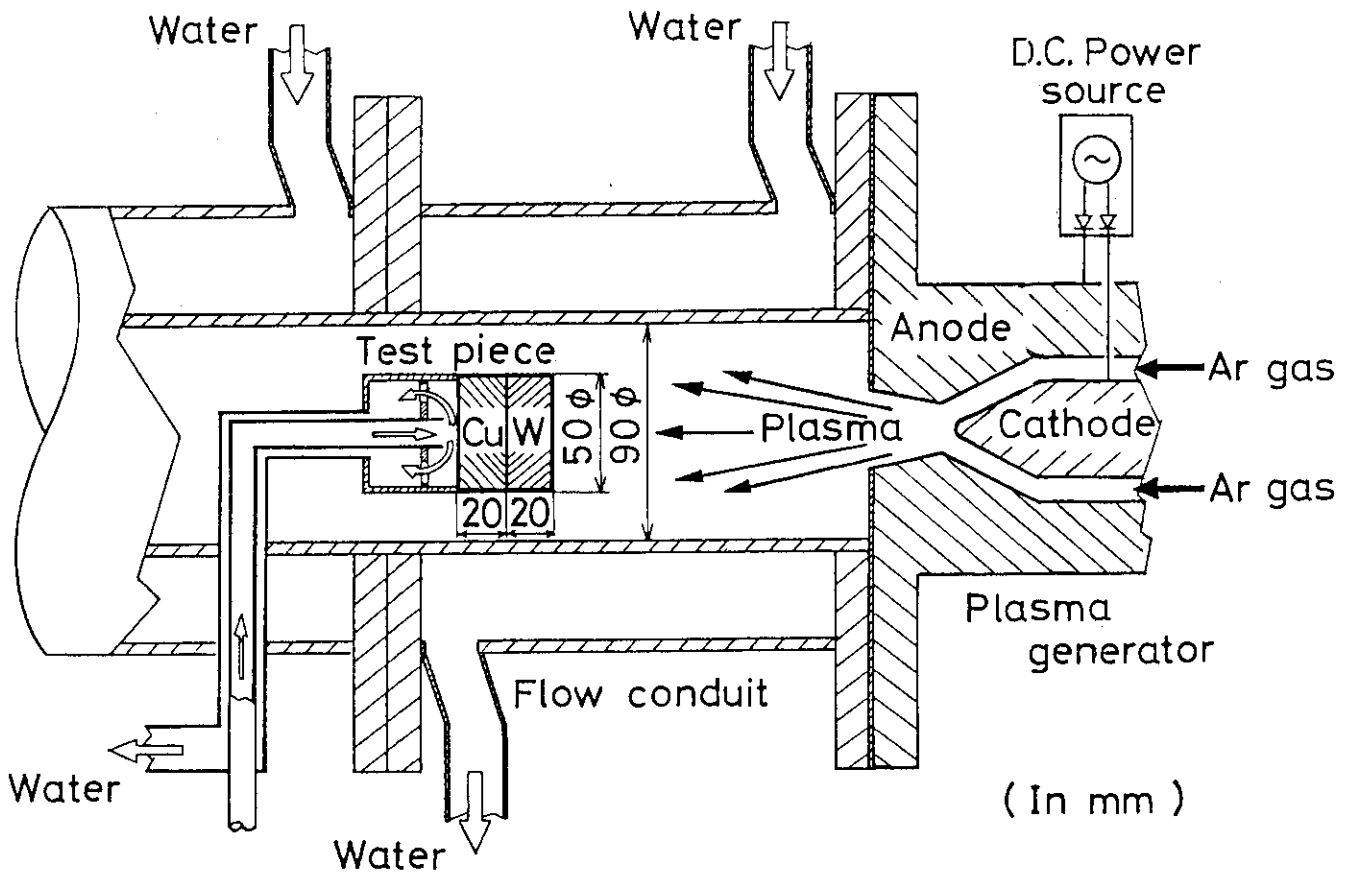


Fig. 1 Experimental apparatus

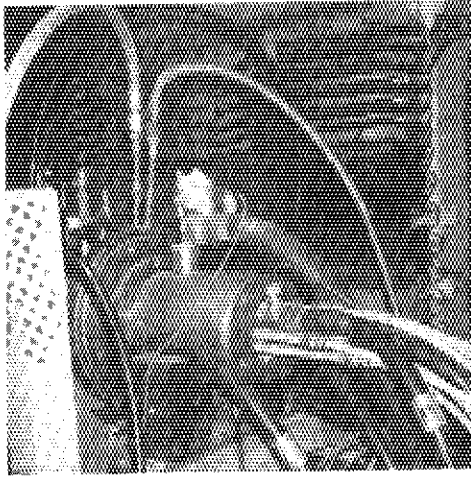


Fig. 2 Plasma generator

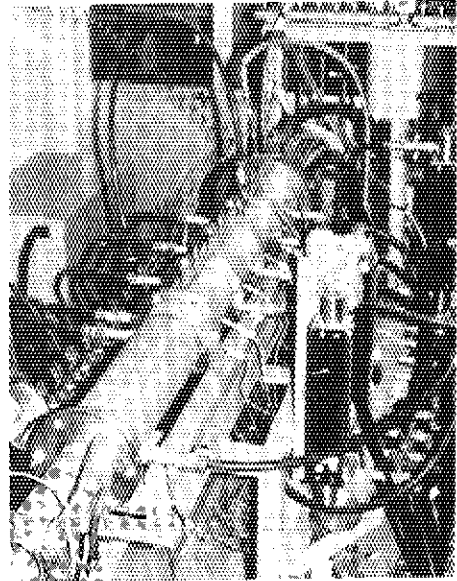


Fig. 3 Plasma flow conduits

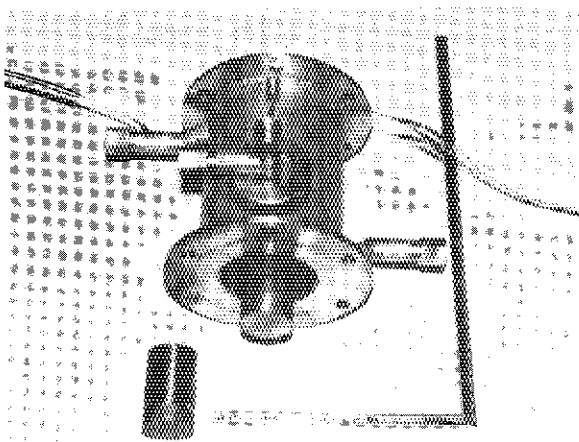


Fig. 4 Test piece set up in a flow conduit

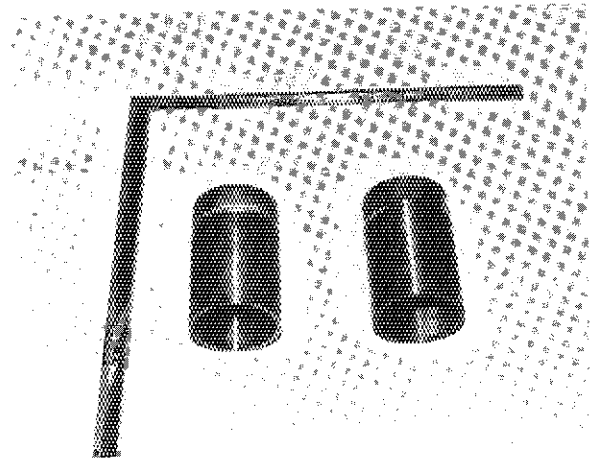
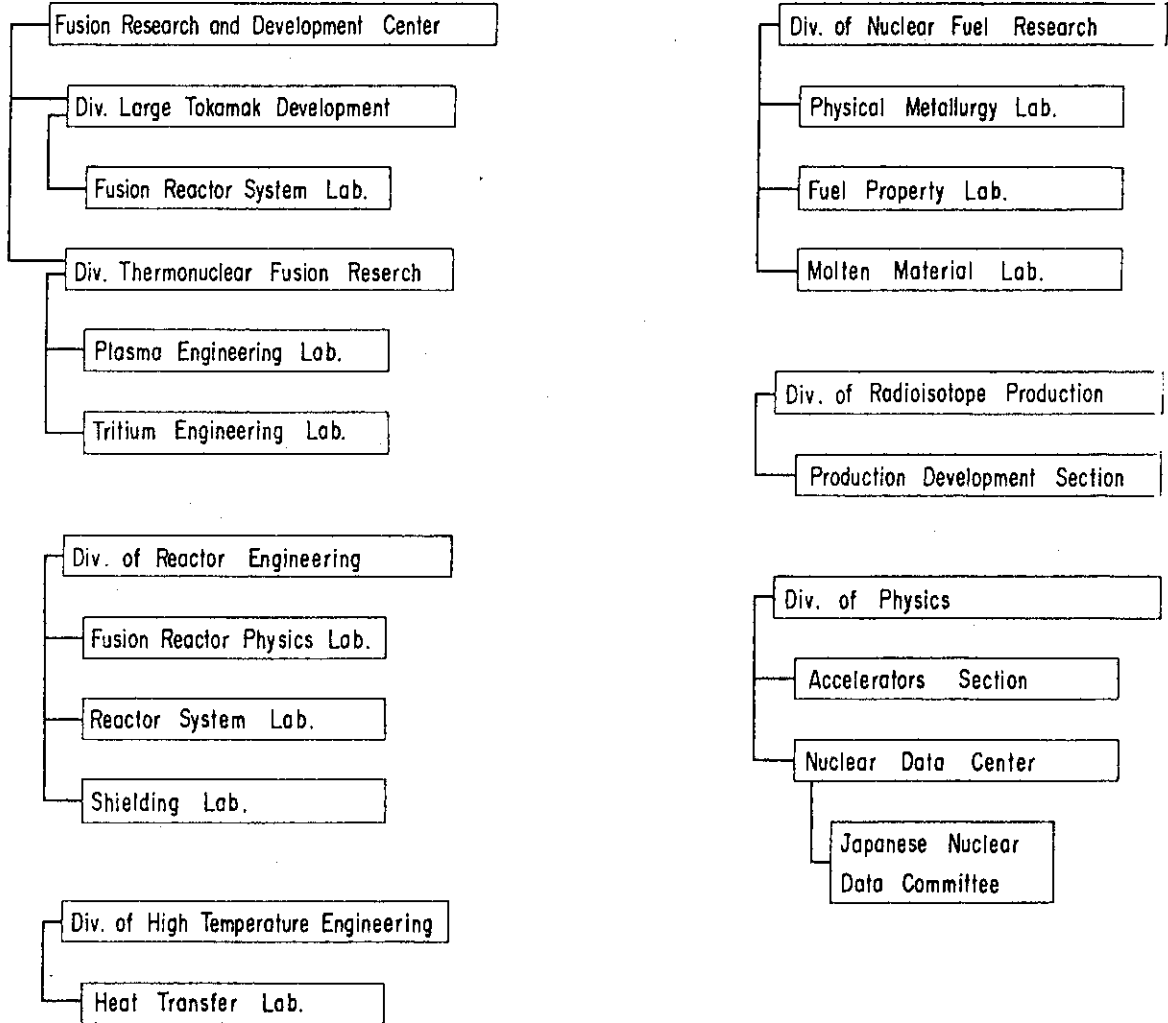


Fig. 5 Test pieces

Appendix (View graph presented)

RELATED DIVISIONS FOR FUSION BLANKET RESEARCH AND DEVELOPMENT AT JAERI



III. Outline of FER Blanket Concept

The outline of FER blanket concept is introduced. The reference blanket design is given in Section 3.1 followed by two alternatives in 3.2. Tritium breeding ratio for the reference design is discussed in Section 3.3, thermal and mechanical design in Section 3.4 and the effect of vertical position stabilization measures on the tritium breeding ratio is discussed in Section 3.5.

3.1 Reference Blanket Design

Design philosophy for FER blanket is summarized in Table 3.1. Key features of the reference blanket configuration are described in Table 3.2. The overview of the outer blanket and its cross sectional view are shown in Figs. 3.1 and 3.2, respectively.

3.2 Alternative Blanket Design

The key features of the reference and alternative blanket designs are compared in Table 3.3. Since the alternative A design has tritium breeding blanket only in the outboard portion, the tritium breeding ratio is 0.69. Key features of alternative blankets are summarized in Tables 3.4 and 3.5 and are shown in Figs. 3.3 ~ 3.12. The alternative A design is similar to the reference one except for the employment of Pb multiplier. The alternative B design contains Li_2O pellets in tank type blanket vessel separated by cooling channels. Heavy water is used to cool lead blocks to increase tritium breeding ratio.

3.3 Tritium Breeding Ratio for the Reference Blanket

Tritium breeding ratio (T) calculated with one-dimensional (1D), two-dimensional (2D) and three-dimensional (3D) models are summarized in Table 3.6.

From the results of 1D calculations, T is evaluated to be in the range of 1.05~1.08. For the model without the NBI port, 2D and 3D calculation give T of 1.053 and 1.037, respectively. The small difference between the 2D and 3D results is mostly due to the difference in the modelling of the outboard blanket.

Since the NBI port exist only in the 2 out of 7 sectors of the blanket, while the 3D calculation assumes an NBI port for each sector, the actual T is evaluated to be,

$$\frac{2}{7} \times 1.002 + \frac{5}{7} \times 1.038 = 1.028 \quad .$$

3.4 Thermal and Mechanical Design

Thermal and mechanical design has been conducted based on 1D or 2D finite element method analyses. The thickness of the first wall and the blanket wall facing the plasma side is made as thin as possible so as to obtain tritium breeding ratio greater than 1.0.

Two types of the first wall are designed. One is the integral type with the blanket wall and the other is the separated type from the blanket wall.

The blanket wall is designed as to endure the pressure of purge gas in tube-in-shell type or to endure the pressure of coolant in tank type. The pressure and temperature of the coolant are held at low level.

The temperature in Li_2O region is controlled with helium gap.

The life time of the blanket is dependent on the erosion and melting rate of the first wall.

3.5 Shell Effect Enhancement

The shell structure made of electric conductor shown in Figs. 3.12 and 3.13 is proposed as a mean to stabilize the vertical motion of the elongated plasma. The change in tritium breeding ratio caused by the introduction of such a shell structure is evaluated by 1D and 2D neutronics calculation for various type of shell structure made of Cu, Be and Pb. As a result, the one employing the combination of Pb and Cu is shown to give the largest tritium breeding ratio. (Fig.3.14) Further optimization is in progress.

Table 3.1 Design Philosophy of FER Blanket

- o Tritium generation for fuel self-sustaining
- o In-situ, continuous tritium recovery
- o Non electricity generation
- o Adequate life time
- o Simple structure

Table 3.2 Key Features of Reference Blanket Configuration

- o Tube-in-Shell Type — Poloidal Axis for Coolant Tube
(simplest structure) Breeder : Li_2O small pebble form
Neutron Multiplier : none
Neutron Moderator : none
- o Integrated First Wall
Tube-Panel Type — Toroidal Axis for Coolant Tube
- o Low Temperature Coolant — H_2O : $60/100^\circ\text{C}$
- o Helium Gap and Coolant Tube Arrangements for
Temperature Control — $400^\circ\text{C} \sim 1000^\circ\text{C}$
(Nominal $450 \sim 700^\circ\text{C}$)
- o Helium Gas Purging for Continuous Recovery of Generated Tritium

Table 3.3 Comparison of Reference and Alternative Blanket Designs

	Reference	Alternative A	Alternative B
•Blanket type	Tube in shell	Tube in shell	Tank
•Number of modules	63 (3 modules/sector)	60 (3+2 modules/sector)	70 (3+2 modules/sector)
•Number of sector	21	12	14
•Thickness			
Inboard (cm)	40	-	40
Outboard (cm)	50	50	50
•Structure			
Material	316 SS	316 SS	304 SS
Max. Temp. (°C)	250	350	350
•Coolant			
Pressure (MPa)	H ₂ O 1.5	H ₂ O 0.5	D ₂ O (in Pb), H ₂ O (in Li ₂ O) 1
Velocity (m/sec)	1.4	2.0	0.2
Inlet/Outlet temp. (°C)	60/100	50/70	50/100
Tube dia. in Li ₂ O	100.D./8I.D.	100.D./8I.D.	
•Breeder			
Material	Li ₂ O	Li ₂ O	Li ₂ O
Multiplier	-	Pb (5 cm)	Pb (5 cm)
Mini./Max. Temp. (°C)	400/1000 (nominal 450/750)	400/1000	400/900
Temp. control	Gap with helium	Gap with helium	Gap with helium
Purge gas	Helium	Helium	Helium
•Tritium Breeding Ratio at beginning of life	1.03	0.69	1.09

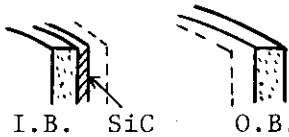

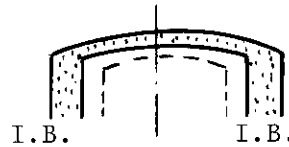
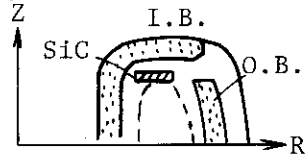
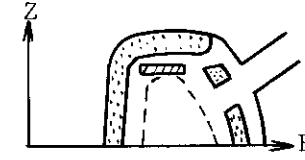
Table 3.4 Alternative Blanket A

• Blanket	: Tube in Shell
• First wall	: Integral with blanket wall, panel of rectangular cross section tubes with groove. (Fig. 3.3)
• Multiplier	: Pb (5 cm), both sides cooling (Fig. 3.4)
• Blanket wall	: Partition plate with coolant channel to cool lead and to sustain the purge gas pressure.
• Temp. Control in Li_2O	: Helium gas with spacer ring (Fig. 3.5)
• Evaluation	: thermal stress, mechanical stress by helium purge gas, electro-magnetic force (Fig. 3.6)
• Sector of blanket/shield	: Fig. 3.7

Table 3.5 Alternative Blanket B

• Blanket	: Tank type (Fig. 3.8)
• First wall	: Separated from blanket wall, SiC armor brazed to Al. (Fig. 3.9)
• Multiplier	: Pb (5 × 5 cm square pillar) All sides cooling (Fig. 3.10)
• Blanket wall	: Ribbed panel to sustain the coolant pressure (1 MPa) (Fig. 3.8)
• Evaluation	: thermal stress, mechanical stress by coolant pressure
• Sector of blanket/shield	: Fig. 3.11

Table 3.6 Comparison of Calculated Tritium Breeding Rate of the Reference Blanket

Calculational Model	Inboard Blanket			Outboard Blanket			Total T
	T _{6in}	T _{7in}	T _{in}	T _{6out}	T _{7out}	T _{out}	
1D  I.B. SiC O.B.	—	—	0.286	—	—	0.733	1.02
1D  I.B. O.B.	—	—	0.355	—	—	0.728	1.08
1D  I.B. I.B.	—	—	—	—	—	—	1.05
2D  Z I.B. SiC O.B. R	0.353	0.100	0.453	0.388	0.213	0.600	1.053
2D  Z I.B. R	0.308	0.096	0.404	0.186	0.080	0.266	0.670
3D w/o NBI Port	0.353	0.100	0.453	0.392	0.191	0.583	1.037
3D with NBI Port	0.361	0.101	0.462	0.361	0.180	0.542	1.002

1D : one-dimensional calculation by ANISN

2D : two-dimensional calculation by DOT-3.5

3D : three-dimensional calculation by MORSE-I

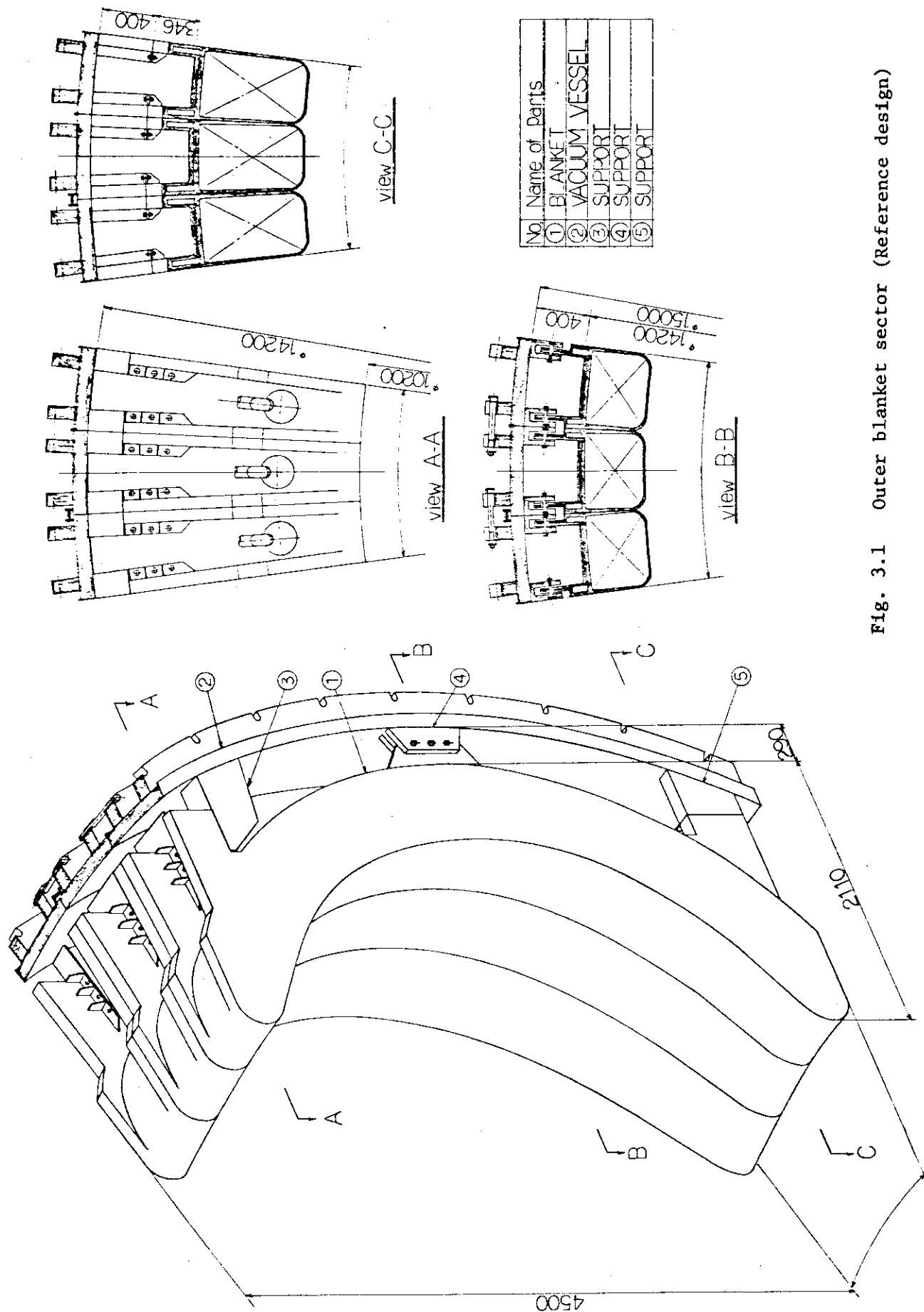


Fig. 3.1 Outer blanket sector (Reference design)

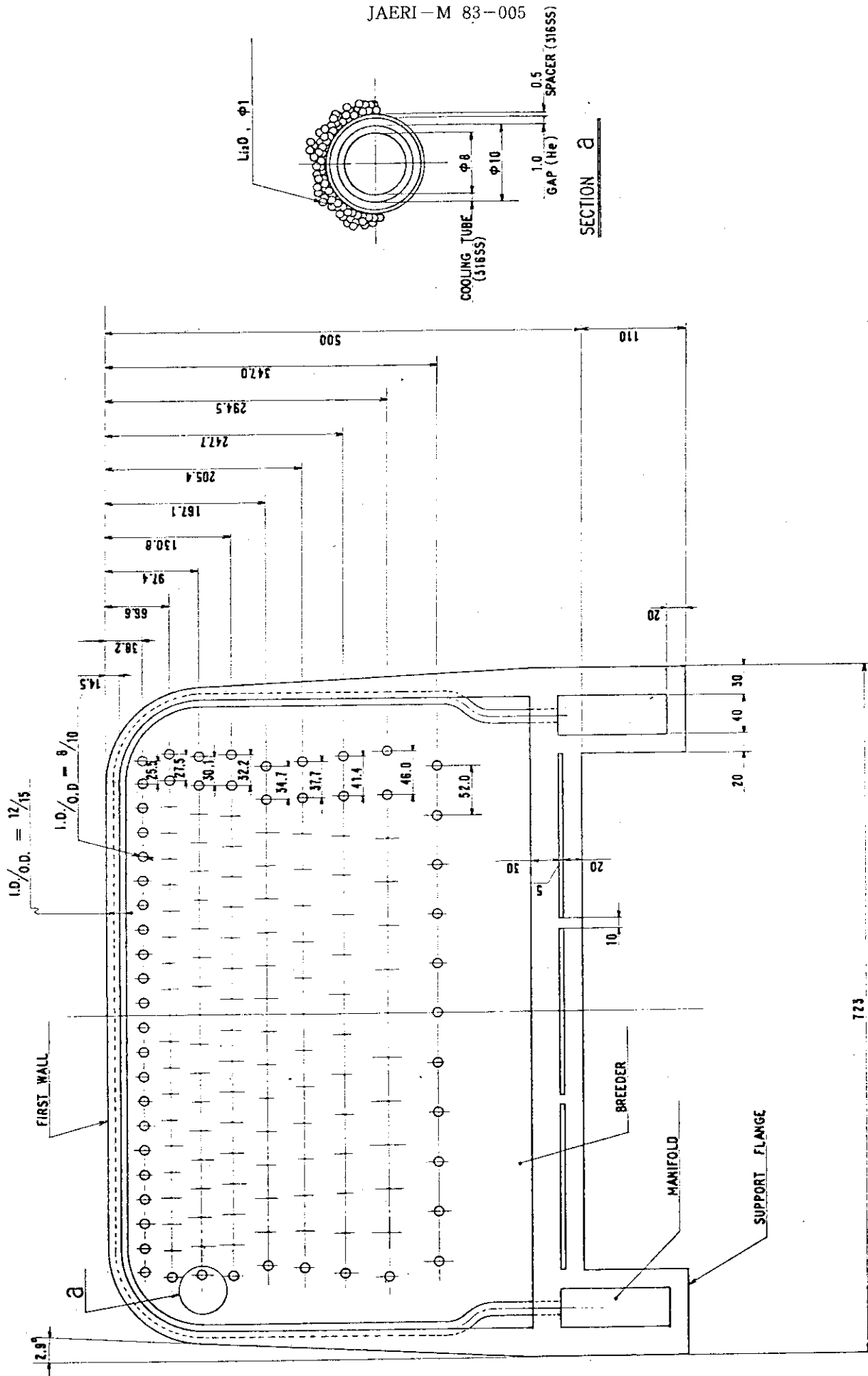


Fig. 3.2 Cross-sectional view of outer blanket at the midplane

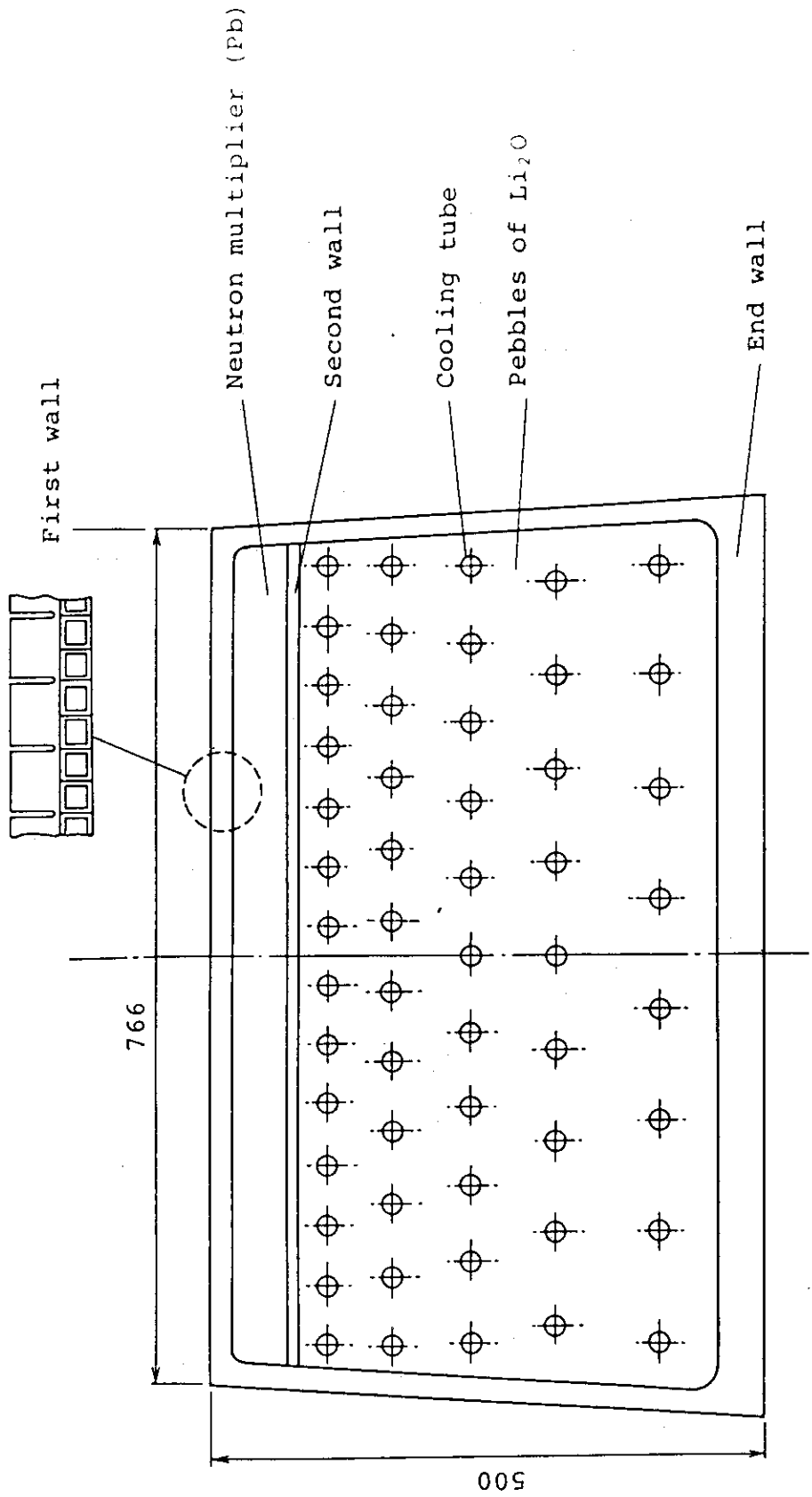


Fig. 3.3 Cross-sectional view of alternative blanket A

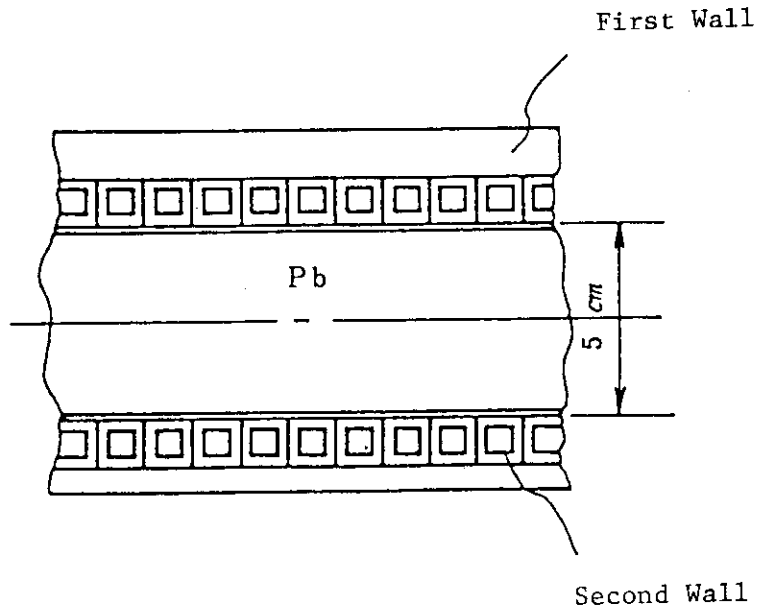


Fig. 3.4 Lead multiplier zone of alternative blanket A

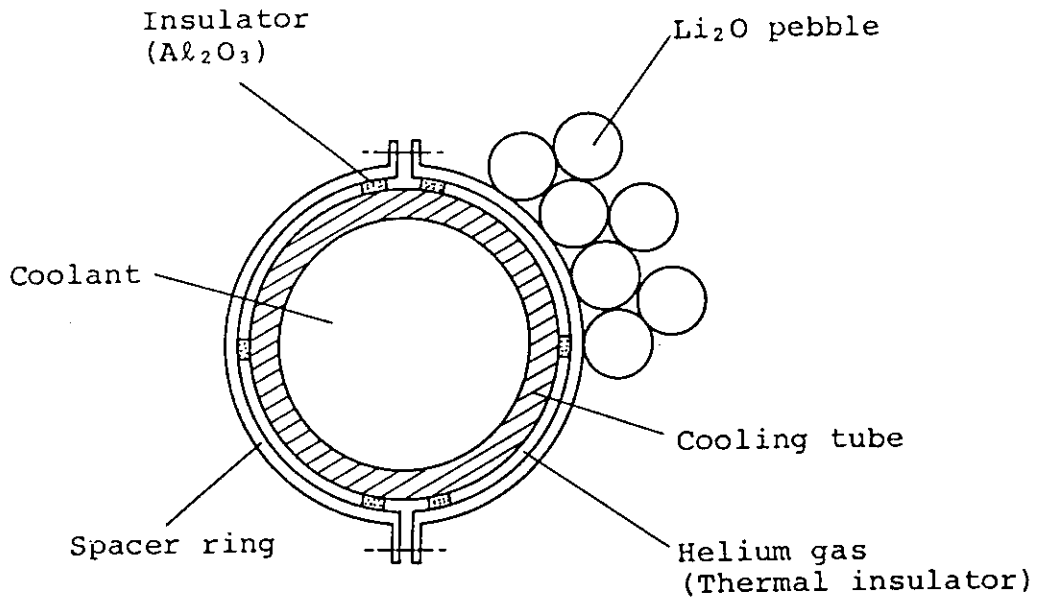
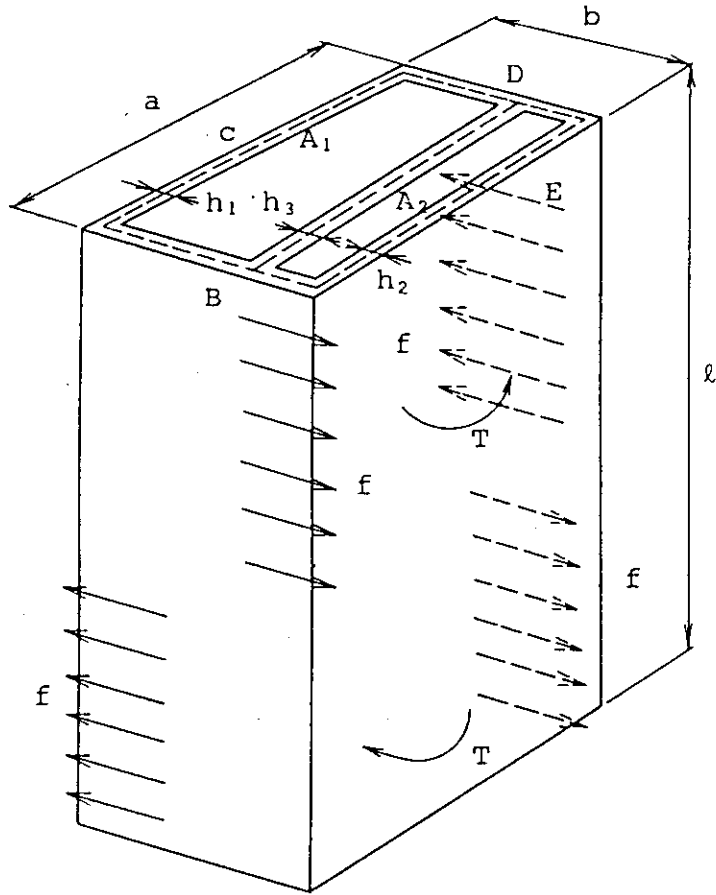


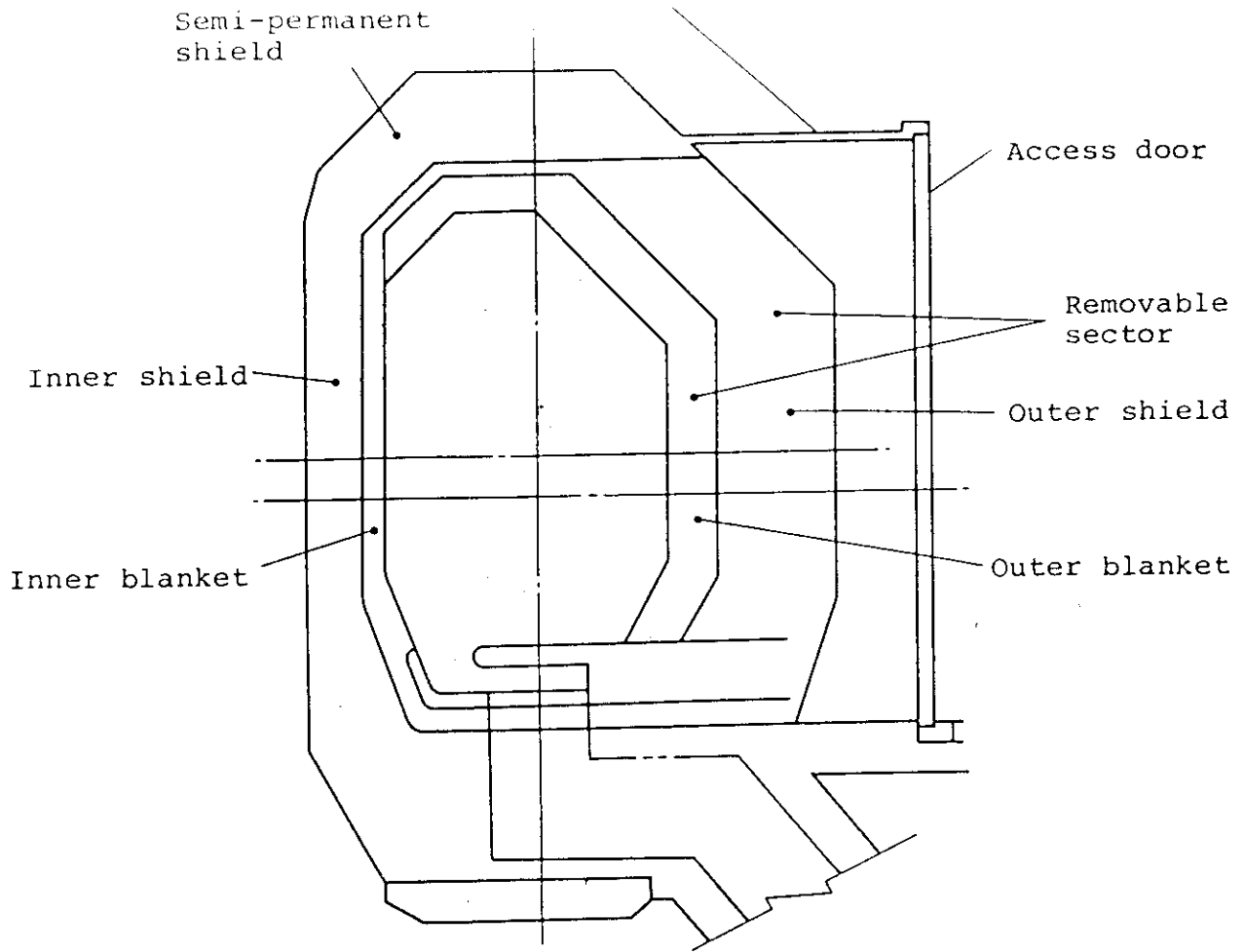
Fig. 3.5 Cooling tube structure of alternative blanket A



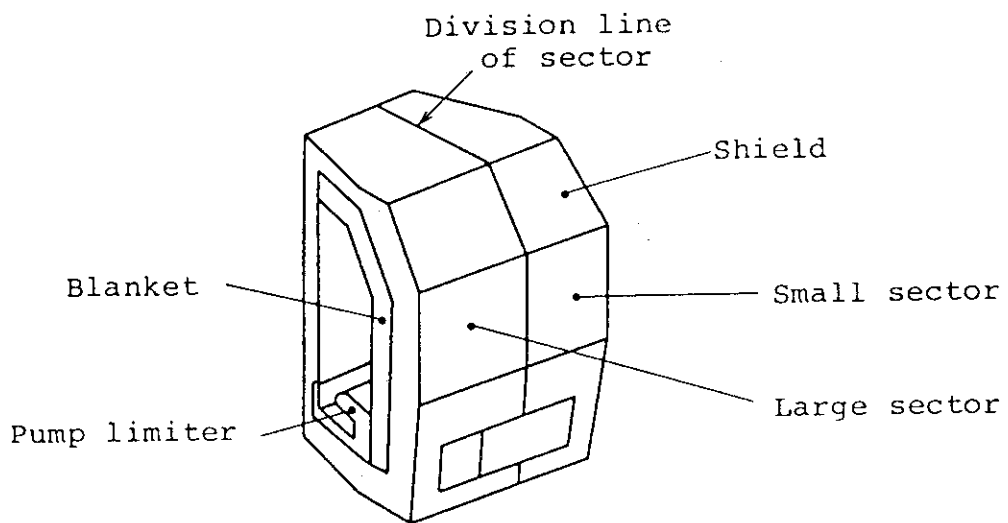
l : effective length of blanket

Fig. 3.6 Electro magnetic force on blanket shell (blanket A)

Blanket
access port



(a) Cross section of blanket/shield



(b) Removable torus sector

Fig. 3.7 Schematic of blanket/shield concept (blanket A)

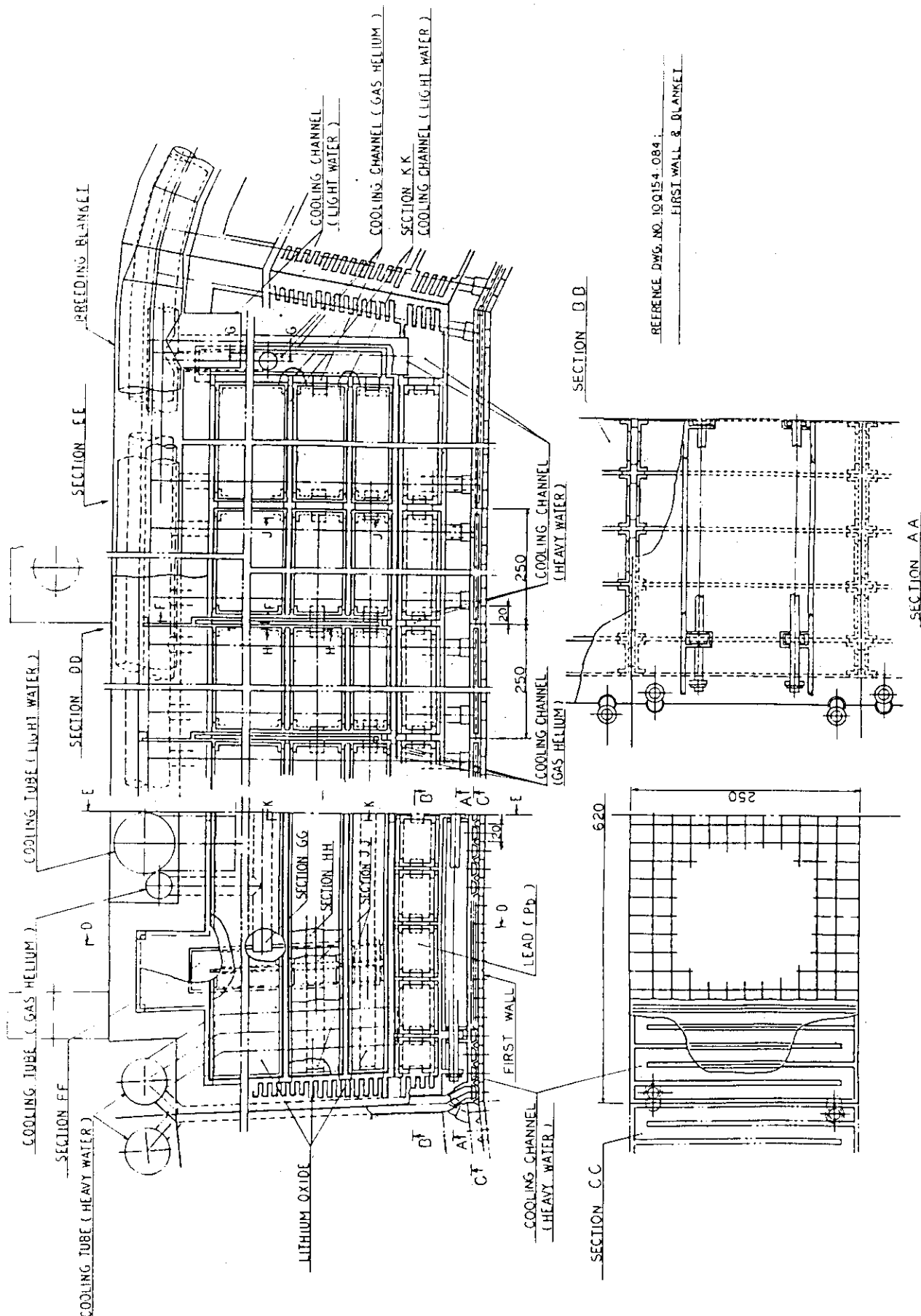


Fig. 3.8 Cross-sectional view of alternative blanket B

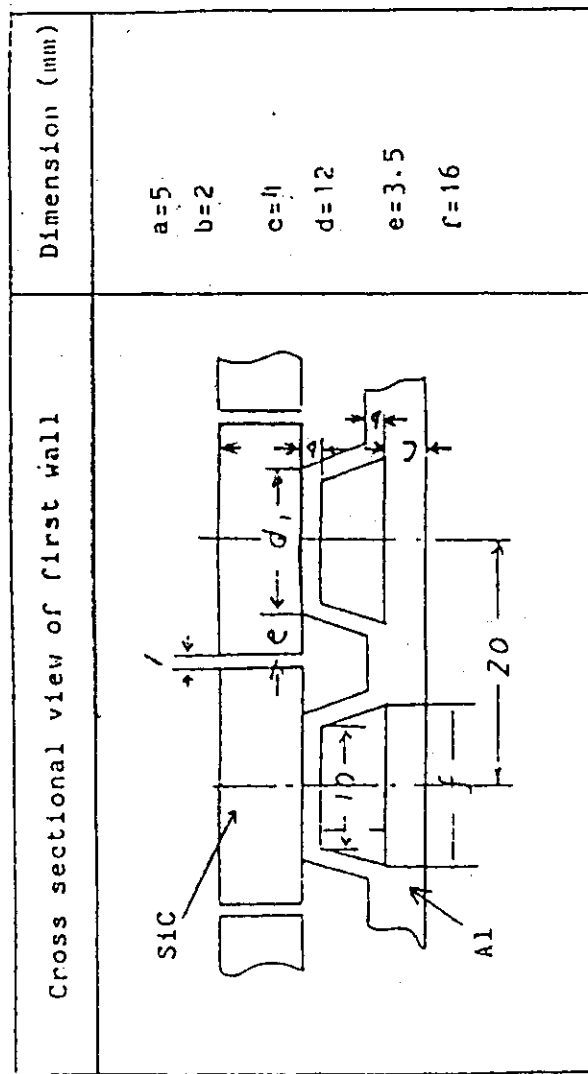


Fig. 3.9 Cross-sectional view of the first wall (blanket B)

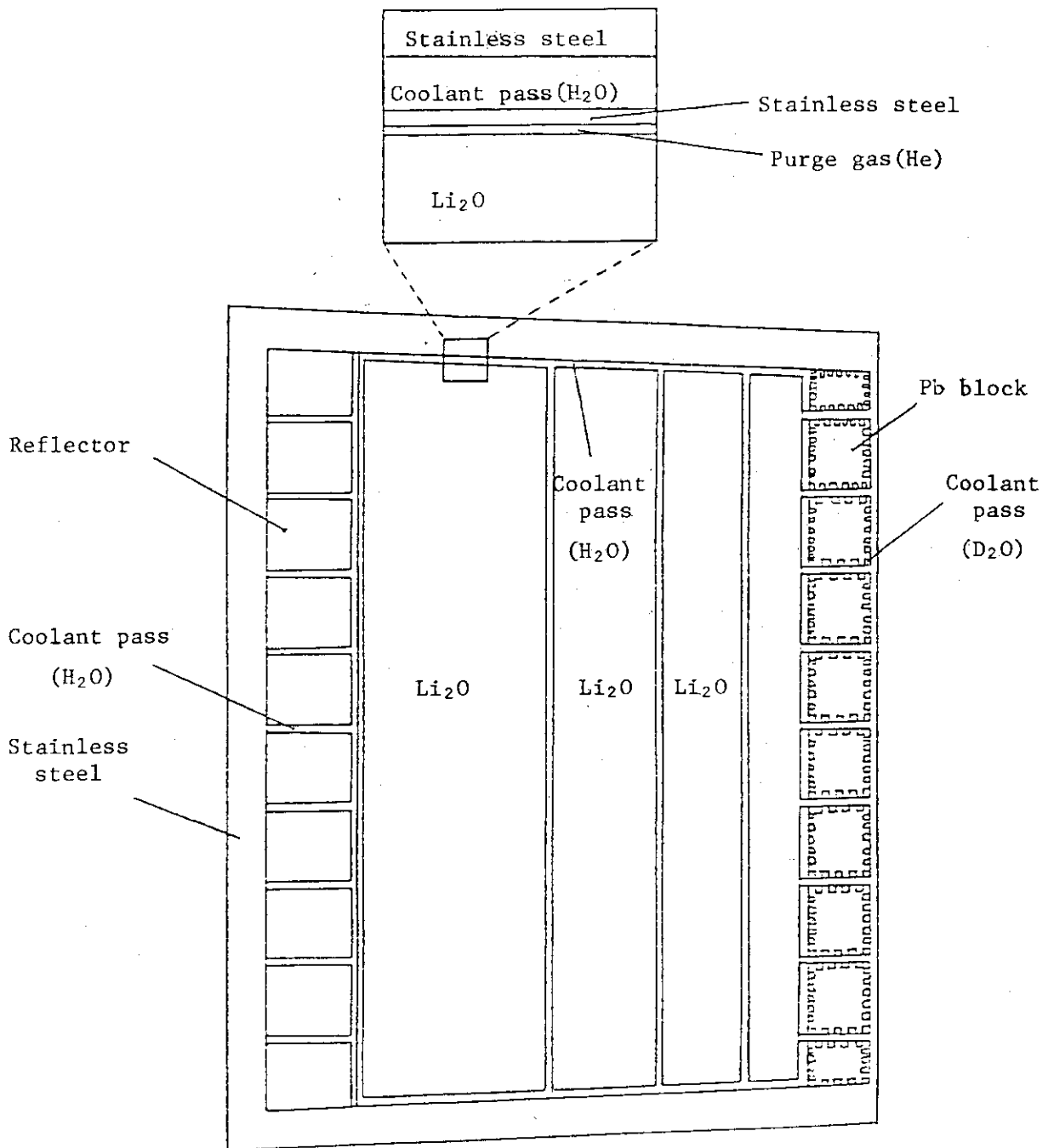


Fig. 3.10 Schematic of alternative blanket B

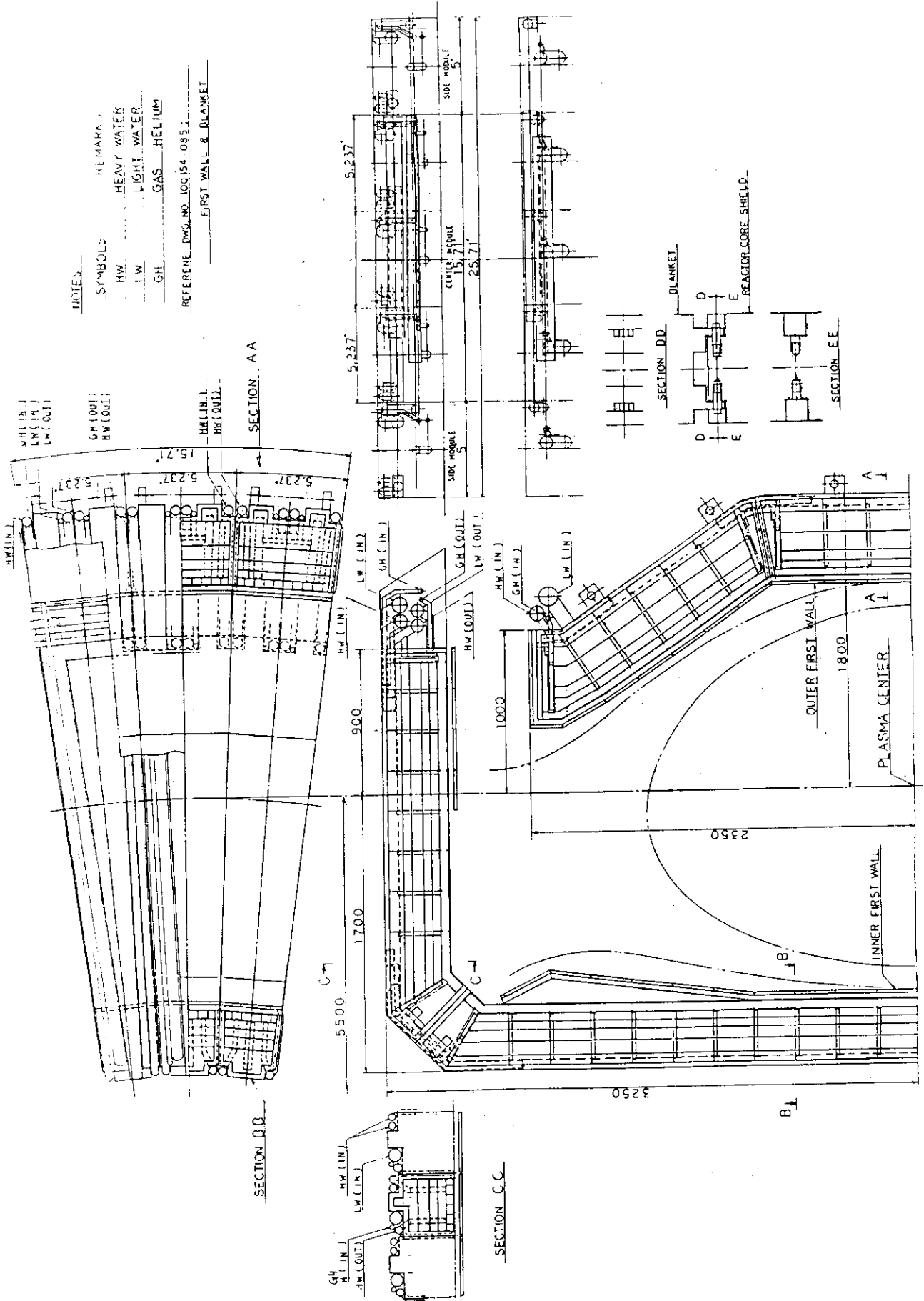


Fig. 3.11 Blanket sector of alternative blanket B

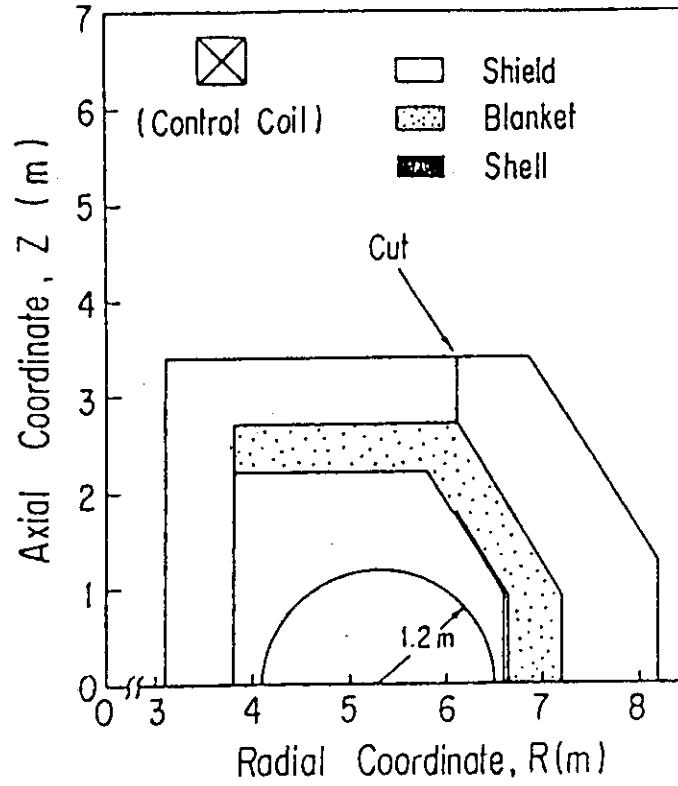
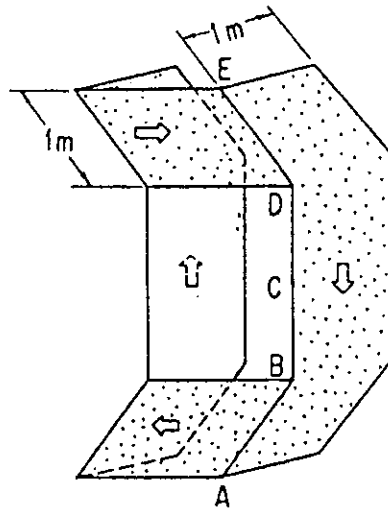


Fig. 3.12 Vertical cross-sectional view of inductive components in blanket and shield



A (5.8^m, -1.6^m), B (6.6^m, -0.3^m)
 C (6.6^m, 0.6^m), D (6.6^m, 1.5^m)
 E (5.8^m, 2.8^m)
 ⇔ : Current Flow

Fig. 3.13 Structure of rectangular shell

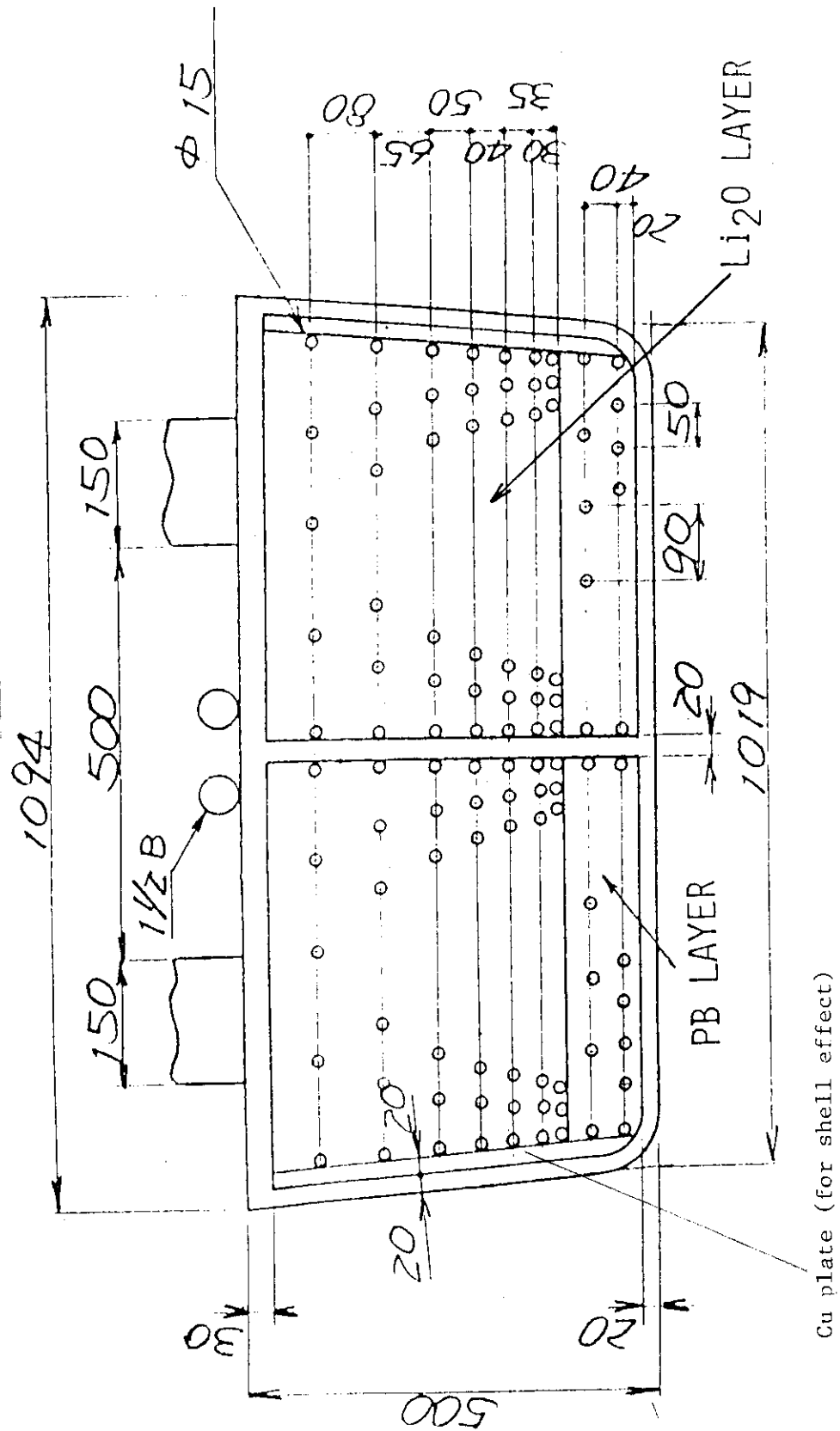


Fig. 3.14 Blanket design with shell effect considerations

IV. Neutronics Design of FER Blanket/Shield

Subjects of this presentation are as follows:

1. Requirements for neutronic design of FER
2. Tritium breeding ratio (TBR) calculations
3. TBR parametric survey
4. Inboard shield considerations
5. Outboard shield considerations
6. Penetration shield considerations
7. Neutronics considerations of the Swimming Pool-type Tokamak Reactor (SPTR)

1. Neutronics Requirements

Table 4.1 Major Requirements for FER Neutronics Design

- Net TBR greater than 1.05
(Local TBR greater than 1.15)
- Sufficient shielding for superconducting magnets (SCM)

Cu-dpa rate	$< 5 \times 10^{-5}$ dpa/yr*
SC fast neutron fluence	$< 2 \times 10^{18}$ n·cm ⁻² /10 yr*
Nuclear heating rate	$< 10^{-3}$ W·cm ⁻³ *
Epoxy absorbed dose	$< 3 \times 10^9$ rad/10 yr*
Total nuclear heating rate	< 10 kW*
- * Values being re-evaluated
- Sufficient shielding for personnel access after shutdown, 2.5 mrem outside the outboard shield one day after shutdown

2. TBR calculations

○ Computational Method

GICX40 Library ----- $^{42}\text{n-21Y}$ from ENDF/B-3, 4

1D --- ANISN

2D --- DOT-3.5 DOT-DOMINO-MORSE

3D --- MORSE-I

Induced activity ----- THIDA code system

○ Computational Model

Fig. 4.1 ----- 2D Model

Fig. 4.2 ----- 3D Model

○ TBR results ----- Table 4.2

If $^{7}\text{Li}(n,n'\alpha)t$ cross section evaluated by P.G. Young is used,

T decreases by ~3%.

3. TBR Parametric Survey

Use of multiplier (s)	Pb, Be	-----	Fig. 4.3
Reduced 1st wall thickness		-----	Fig. 4.4
Pb + (Pb + Li ₂ O) mixed zone		-----	Fig. 4.5
Pb + (Be + Li ₂ O) mixed zone		-----	Fig. 4.6
(Be + Li ₂ O) mixed zone			
1st wall and/or blanket coolant		----->	He, D ₂ O, H ₂ O
Blanket thickness		-----	Fig. 4.7
⁶ Li enrichment (Pb-multiplier)		-----	Fig. 4.8
⁶ Li enrichment (Be-multiplier)		-----	Fig. 4.9
Pb thickness		-----	Fig. 4.10
Be thickness		-----	Fig. 4.11
Be volume fraction	Pb + (Be + Li ₂ O)	-----	Fig. 4.12

Relation of TBR and Blanket Complexity (Cost) ----- Fig. 4.13

Recommended actions in case the TBR of reference blanket becomes lower than 1.0

	estimated increase
(1) Change 1st wall coolant H ₂ O → D ₂ O	~ 3%
(2) Employ Pb or Be multiplier	~ 3%
(3) Multiplier + ⁶ Li enrichment	~13%
(4) Mix Be pebbles with 30% enriched Li ₂ O pebbles	
with 5 % Be -----	~10%
with 50% Be -----	~30%

4. Inboard Shield Consideration

When inboard breeding blanket with 40 cm thickness is employed and more than 20 cm is required for the SCM helium vessel and cryostat, only about 40 cm remains for the inboard shield. Inboard blanket materials should be chosen with high TBR as the first priority. Considering the structural strength required in the inboard shield and its heat removal, stainless steel cooled by water seems to be the reasonable choice as the major constituents of the inboard shield. Addition of ^{10}B in some form, the use of W or Mo will be considered only if further improvement in the shielding capability is required.

5. Outboard Shield Considerations

As regards the shielding of the outboard region of a tokamak reactor, its objective is to allow personnel access at the reactor shutdown. If personnel access is made to be permissible, radiation damage to the reactor components will be held sufficiently below the allowable level.

To reduce the shutdown dose outside the shield, first of all the attenuation of 14 MeV neutron flux must be accomplished to reduce the products of the (n,p) reactions such as ^{58}Co and ^{54}Mn . Stainless steel (or iron) is an excellent attenuator of the 14 MeV neutron flux and should be used up to ~90% of the volume fraction of the outboard shield. Secondly, low energy neutrons penetrating through the shield must also be reduced to decrease the troublesome (n, γ) reaction products such as ^{59}Fe , ^{60}Co and ^{51}Cr . Neutron moderation by water and its absorption by ^{10}B is one of the best combination to reduce low energy neutrons. The material arrangement of SS90B4C shield proposed in Fig. 4.14 is believed to be near the optimum for reducing shutdown dose.

6. Penetration Shield Considerations

Classification of Penetrations in a Tokamak Reactor

- A. Thru blanket and shield ----- NBI port, rf duct, diagnostic port,
- B. Thru blanket ----- divertor/limiter gap, blanket
module gap, cooling pipe
- C. Thru shield ----- Exhaust duct, cooling pipe
Shield sector gap
Space taken by bellows

D. Gaps between blanket, shield and TFC

Most problematic ----- Class A-type

○ NBI port streaming effect study ----- Fig. 4.15

DOT - DOMINO - MORSE

DOT (R - Z) with and w/o NBI port

DOT (R - θ) with and w/o NBI port

Fig. 4.16 ~ 4.19

Comparison of results

Table 4.3

7. Neutronics consideration of SPTR



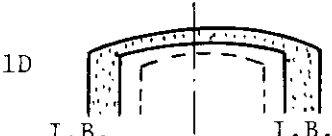
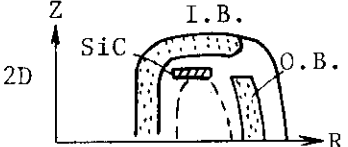
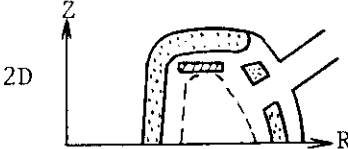
Merits

1. Penetration shieldings greatly simplified
NBI ports, rf ducts, diagnostic ports,
evacuation ducts, cooling pipes
2. Non existence of shield sector gaps, gaps between shield and TFC
3. Relaxation of shielding requirements by the wall and roof of the reactor room.
4. Reduction of solid radwaste
- (5. Increase the feasibility of repair and maintenance)

Problems and evaluations

1. No increase in inboard shield thickness
2. Tritium leakage into pool water ----- tolerable
3. Additional hydraulic pressure ----- tolerable
4. Corrosion problems ----- tolerable
5. Heat loss to pool water ----- thermal insulation required

Table 4.2 Comparison of Calculated Tritium Breeding Rate of the Reference Blanket

Calculational Model	Inboard Blanket			Outboard Blanket			Total T
	T _{6in}	T _{7in}	T _{in}	T _{6out}	T _{7out}	T _{out}	
1D 	—	—	0.286	—	—	0.733	1.02
1D 	—	—	0.355	—	—	0.728	1.08
1D 	—	—	—	—	—	—	1.05
2D 	0.353	0.100	0.453	0.388	0.213	0.600	1.053
2D 	0.308	0.096	0.404	0.186	0.080	0.266	0.670
3D w/o NBI Port	0.353	0.100	0.453	0.392	0.191	0.583	1.037
3D with NBI Port	0.361	0.101	0.462	0.361	0.180	0.542	1.002

1D : one-dimensional calculation by ANISN

2D : two-dimensional calculation by DOT-3.5

3D : three-dimensional calculation by MORSE-I

Table 4.3 Neutron and Gamma-Ray Fluxes Around NBI Port
(unit in neutrons or gamma ray. $\text{cm}^{-2} \cdot \text{s}^{-1}$)

Calculation code		DOT-3.5			MORSE (fsd)
Geometry		R-Z		R- θ	General
NBI port shape		Without port	Toroidal slit	Vertical slit	Cylindrical duct
At NBI beam line (R=865 cm) (Z=180 cm)	ϕ_n (14 MeV)	—	1.8×10^{13}	1.5×10^{13}	1.3×10^{13} (0.011)
	ϕ_n (>0.1 MeV)	—	4.1×10^{13}	4.9×10^{13}	6.6×10^{13} (0.010)
	ϕ_n (total)	—	5.6×10^{13}	6.4×10^{13}	9.3×10^{13} (0.011)
	ϕ_γ (total)	—	1.5×10^{13}	2.5×10^{13}	4.2×10^{13} (0.044)
At water between NBI and SCM (R=863 cm) (Z=180 cm)	ϕ_n (14 MeV)	3.8×10^7	2.4×10^{10}	9.4×10^{10}	2.0×10^{10} (0.075)
	ϕ_n (>0.1 MeV)	8.2×10^7	2.3×10^{11}	5.4×10^{11}	3.9×10^{10} (0.166)
	ϕ_n (total)	1.5×10^8	1.1×10^{12}	2.2×10^{12}	3.9×10^{10} (0.166)
	ϕ_γ (total)	3.1×10^{10}	1.6×10^{12}	5.6×10^{12}	2.0×10^{12} (0.280)
At water midplane (R=895 cm) (Z=0 cm)	ϕ_n (14 MeV)	3.8×10^6	4.6×10^7	—	3.6×10^7 (0.973)
	ϕ_n (>0.1 MeV)	9.3×10^7	7.0×10^8	—	9.1×10^7 (0.564)
	ϕ_n (total)	2.7×10^8	1.8×10^{10}	—	9.1×10^7 (0.564)
	ϕ_γ (total)	2.4×10^{10}	1.5×10^{11}	—	1.2×10^{11} (0.198)
At SCM front surface (R=860 cm) (Z=180 cm)	ϕ_n (14 MeV)	1.2×10^6	—	2.3×10^8	3.6×10^7 (0.118)
	ϕ_n (>0.1 MeV)	5.5×10^8	—	3.8×10^{10}	4.9×10^7 (0.119)
	ϕ_n (total)	1.1×10^9	—	7.0×10^{10}	9.5×10^7 (0.119)
	ϕ_γ (total)	2.3×10^8	—	7.0×10^9	9.5×10^8 (0.163)
At SCM midpoint (R=922 cm) (Z=215 cm)	ϕ_n (14 MeV)	7.0×10^2	—	2.8×10^7	2.4×10^7 (0.350)
	ϕ_n (>0.1 MeV)	5.8×10^6	—	1.3×10^{10}	3.3×10^7 (0.266)
	ϕ_n (total)	1.8×10^7	—	3.2×10^{10}	3.3×10^7 (0.266)
	ϕ_γ (total)	1.3×10^6	—	2.6×10^9	9.9×10^{10} (0.288)

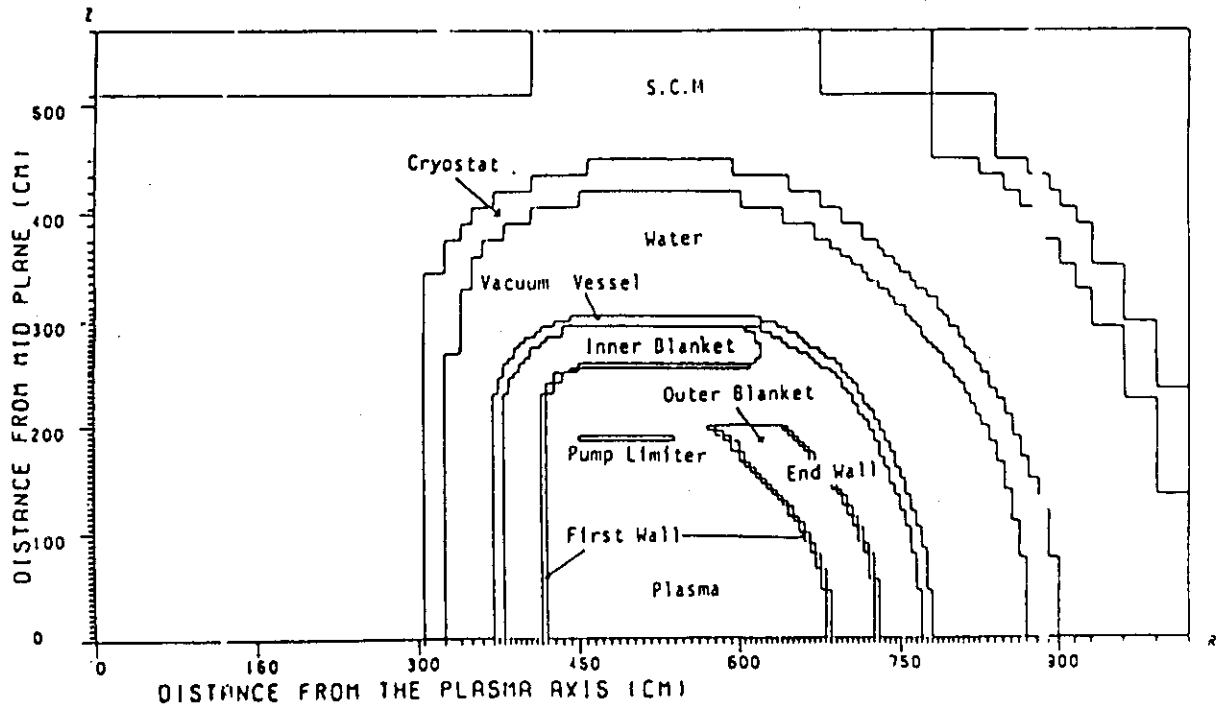
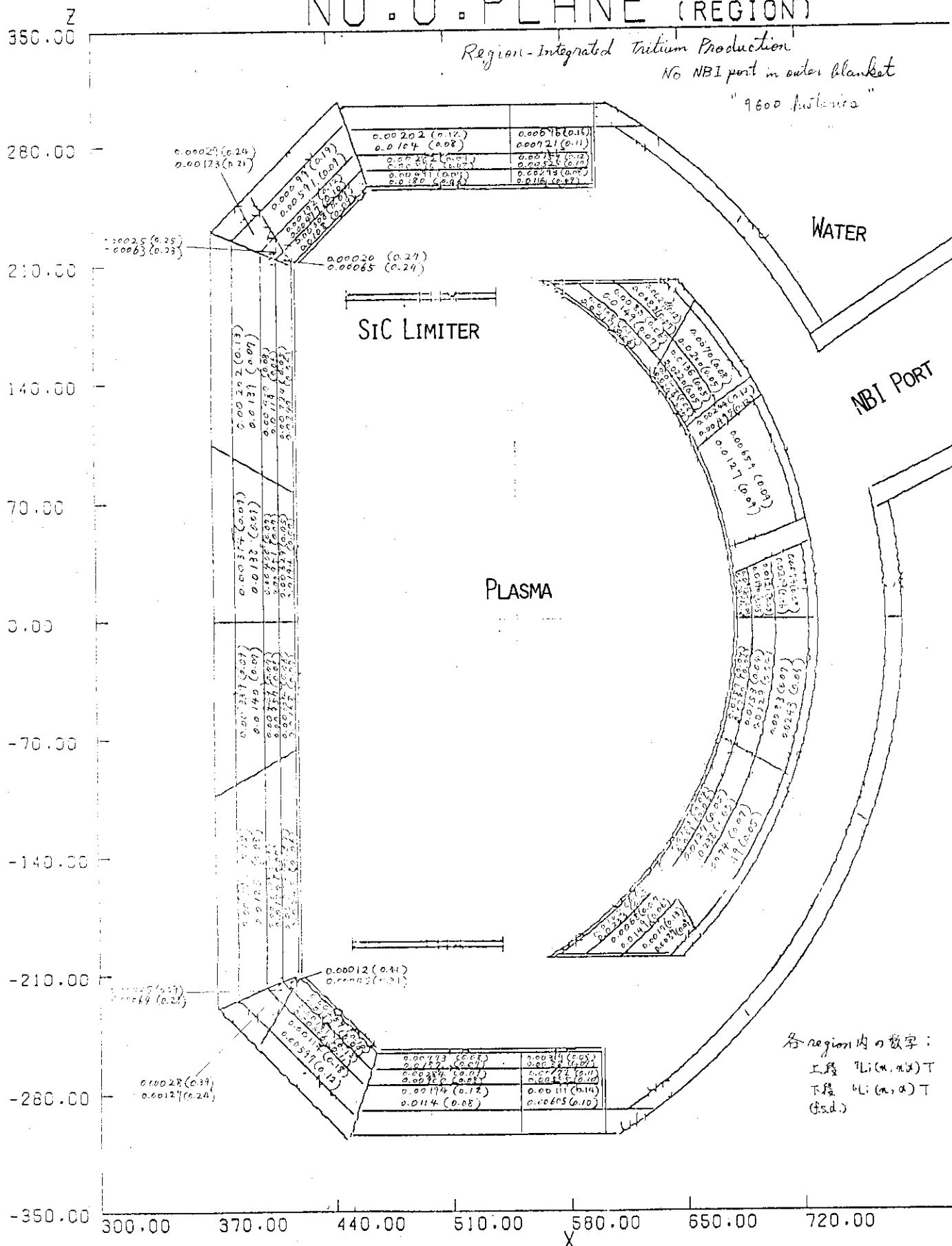


Fig. 4.1 Two-dimensional model of FER (SPTR alternative)

NO.0 PLANE (REGION)

Region-Integrated Tritium Production
 NO NBI port in outer blanket
 "9600 Austenite"



各region内の数字:
 上段 ${}^6\text{Li}(n, \alpha)\text{T}$
 下段 ${}^6\text{Li}(n, \alpha)\text{T}$
 (f.s.d.)

Fig. 4.2 Three-dimensional model of FER (SPTR alternative)

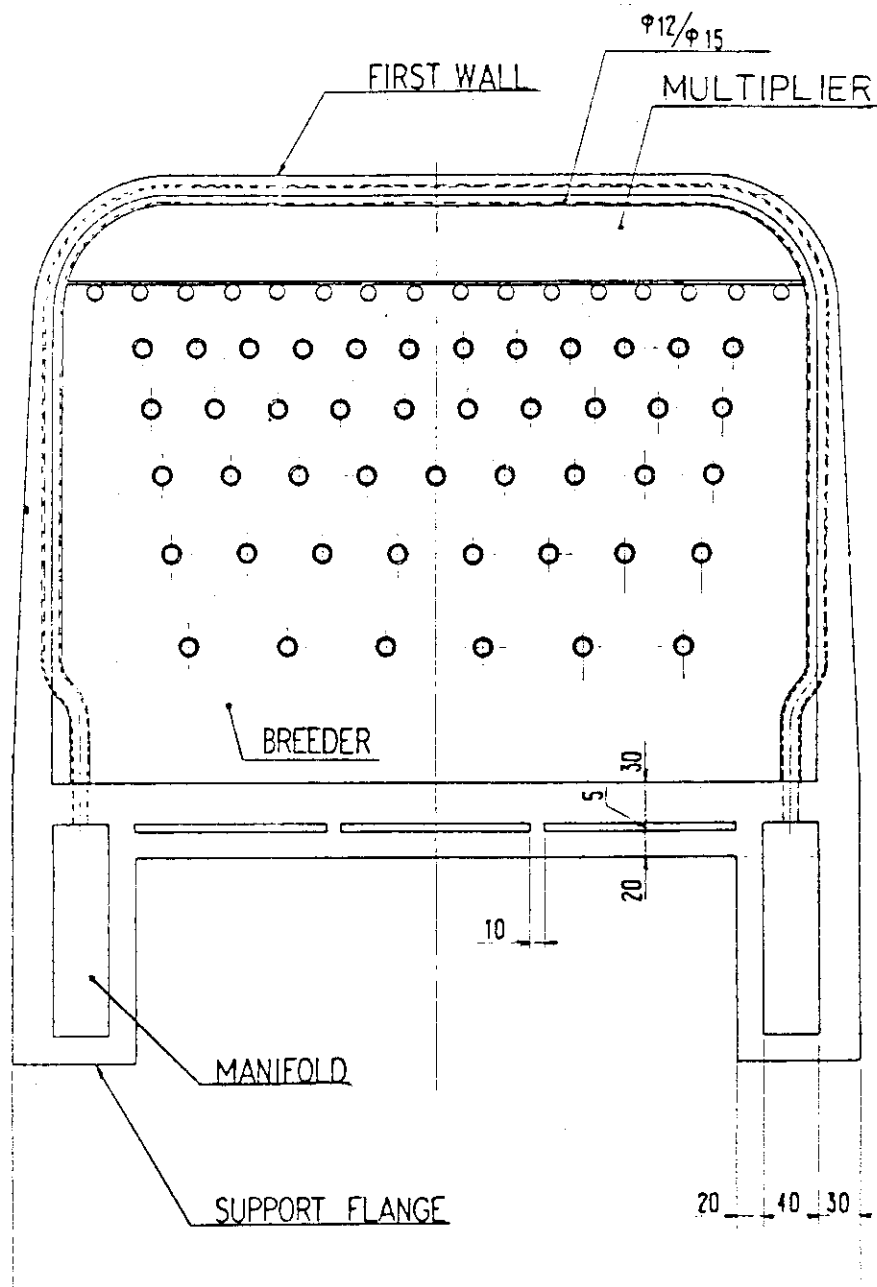
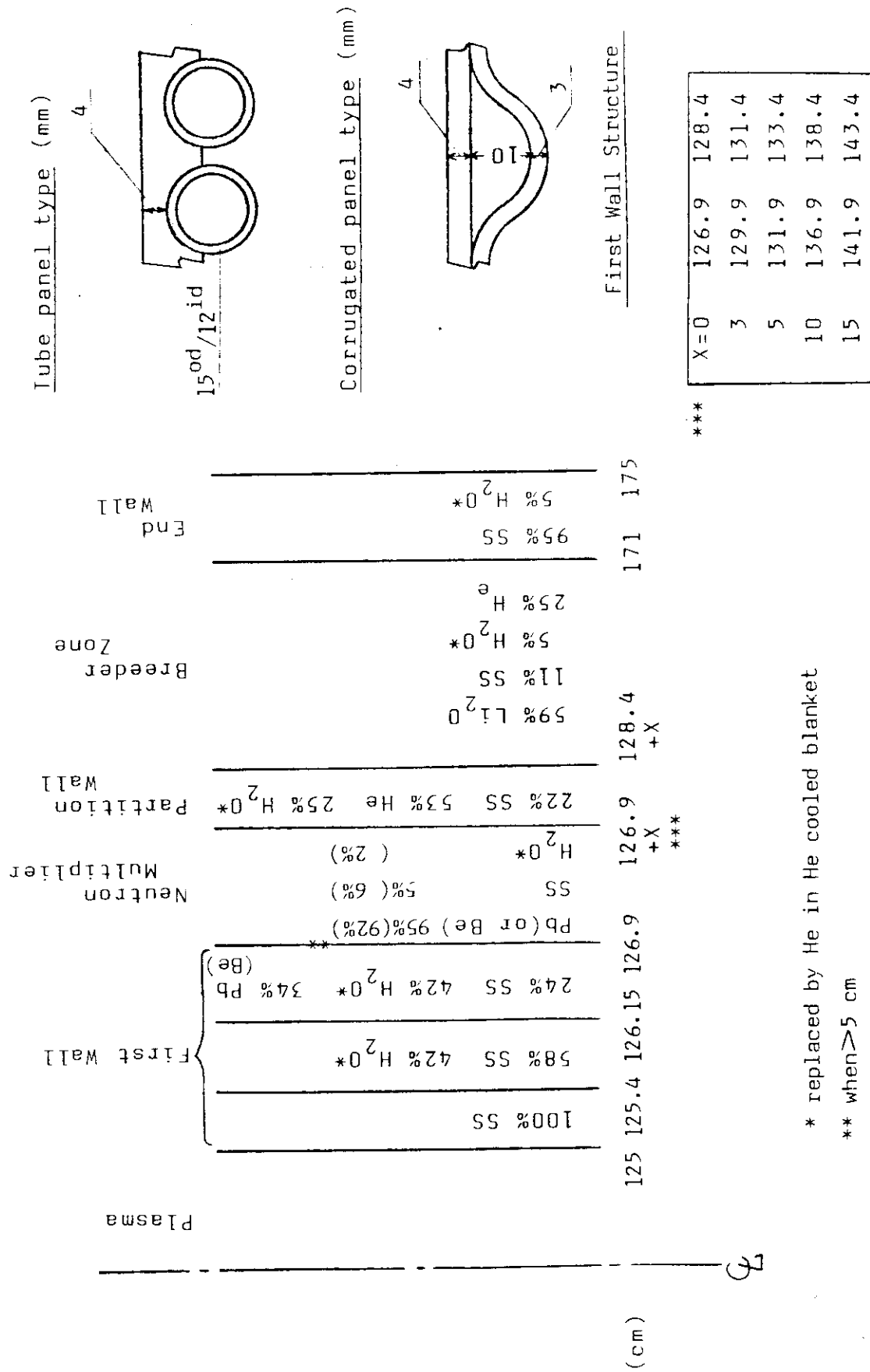


Fig. 4.3 Tube in shell type blanket with multiplier



* replaced by He in He cooled blanket
** when > 5 cm

Fig. 4.4 Geometrical Model for ANISN Calculation

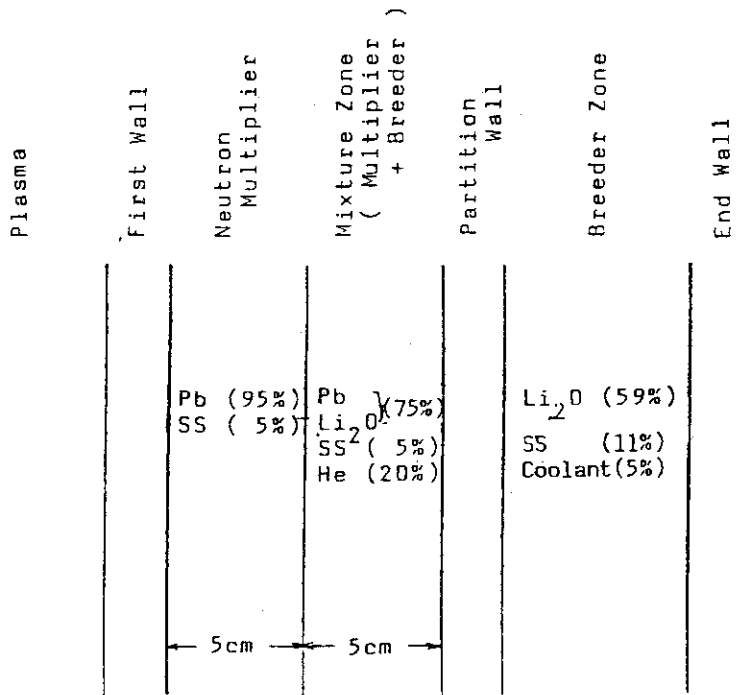


Fig. 4.5 Blanket Concept of Pb-Li₂O Mixed Zone

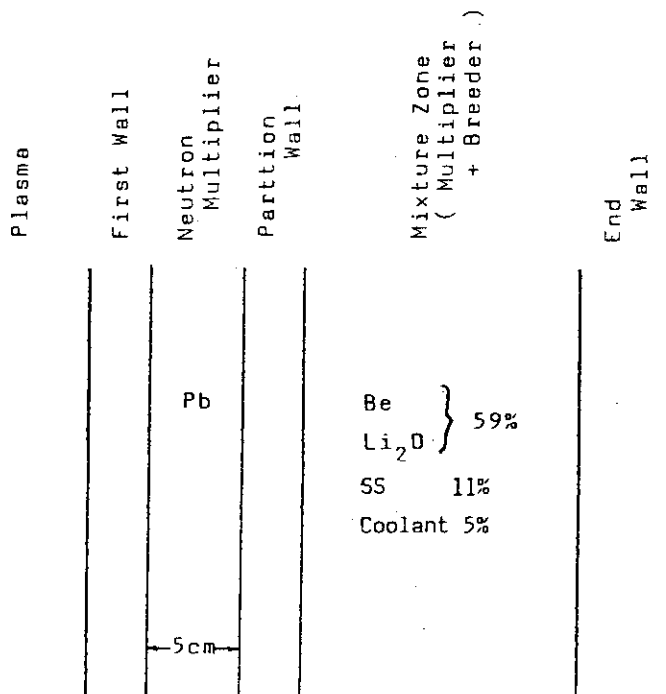


Fig. 4.6 Blanket Concept of Be-Li₂O Mixed Zone

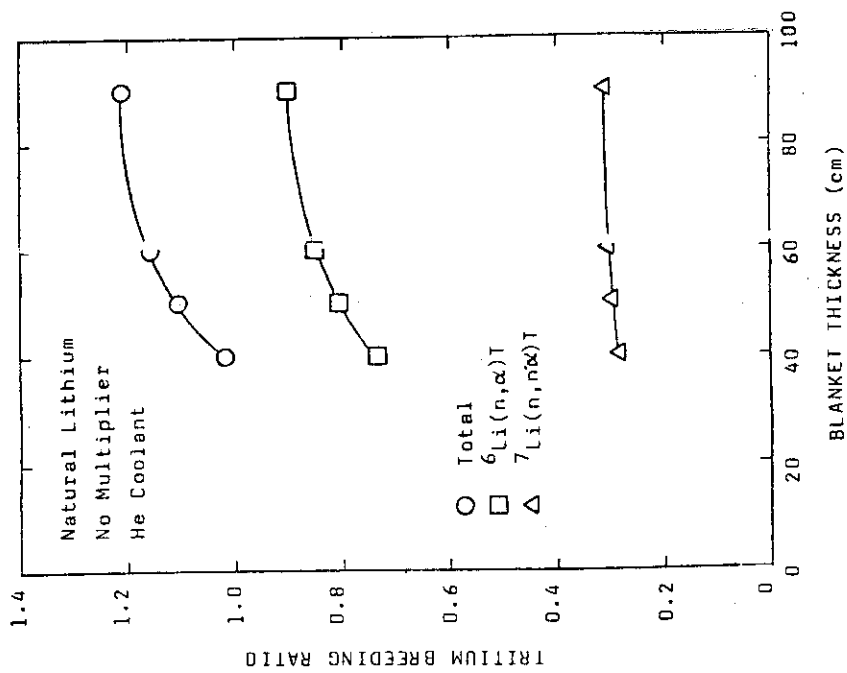


Fig.4.7 Effect of Blanket Thickness on Tritium Breeding

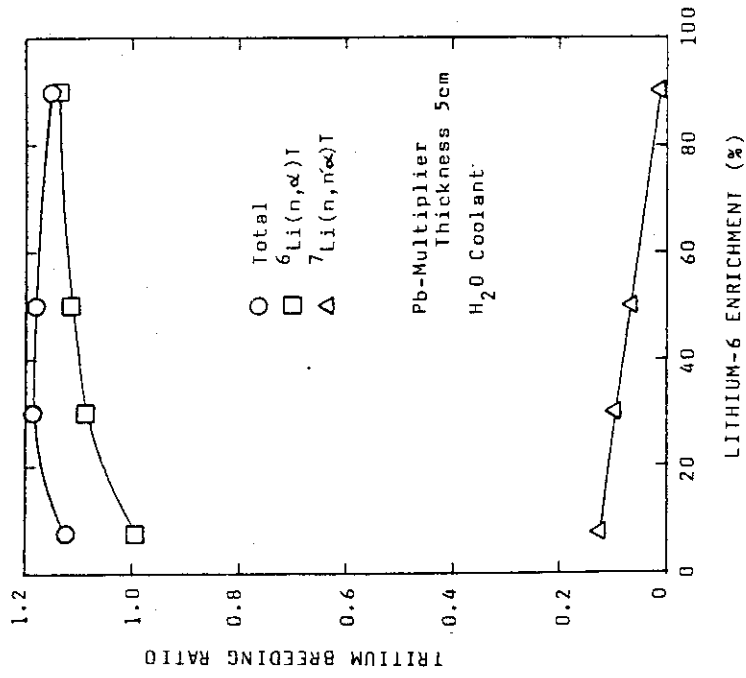


Fig.4.8 Effect of ${}^6\text{Li}$ Enrichment on Tritium Breeding

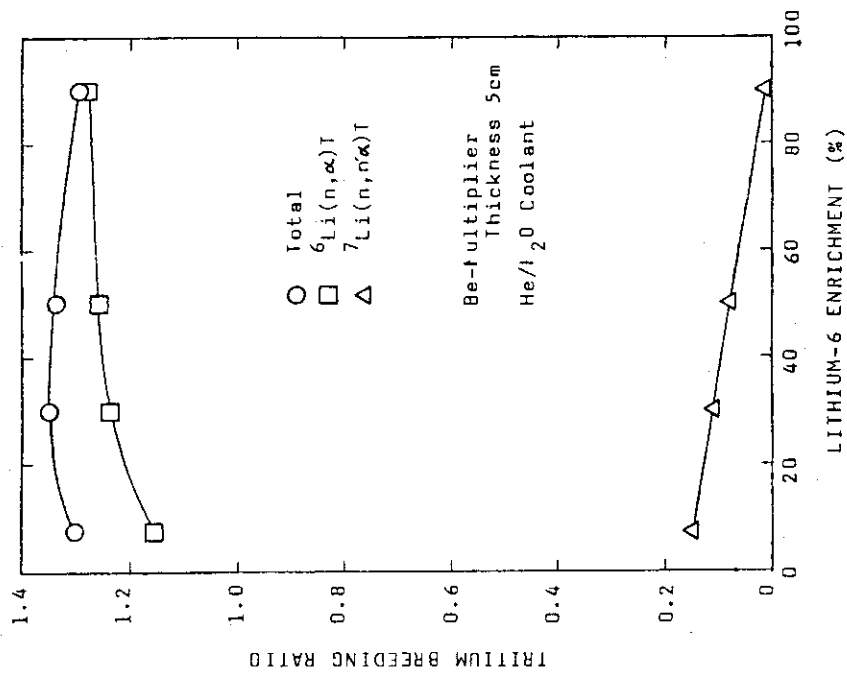


Fig. 4.9 Effect of ⁶Li Enrichment on Tritium Breeding

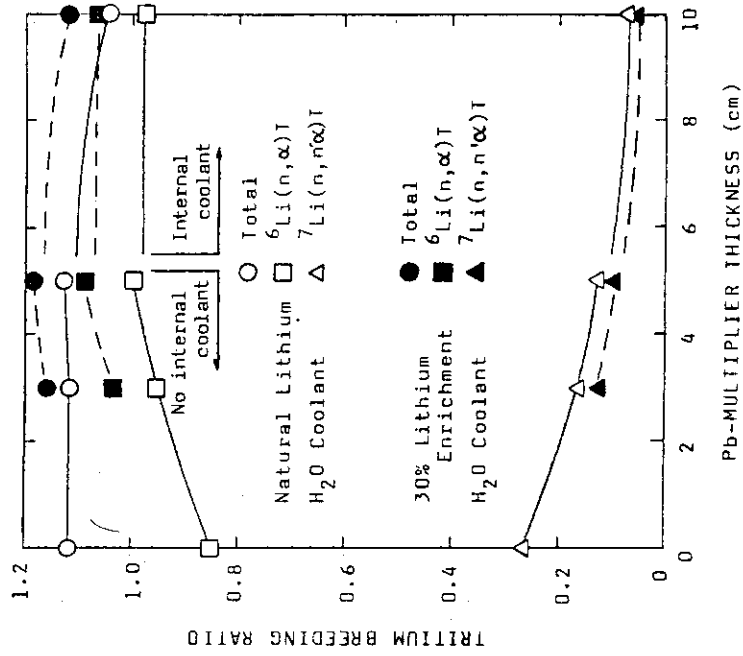


Fig. 4.10 Effect of Pb Multiplier Thickness on Tritium Breeding

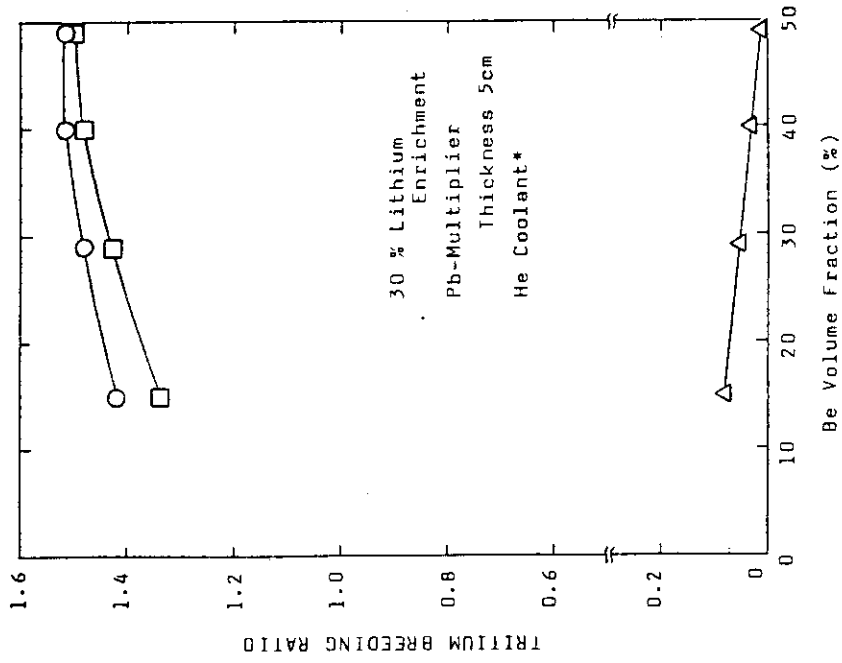


Fig. 4.12 Effect of Be Volume Fraction on Iritium Breeding

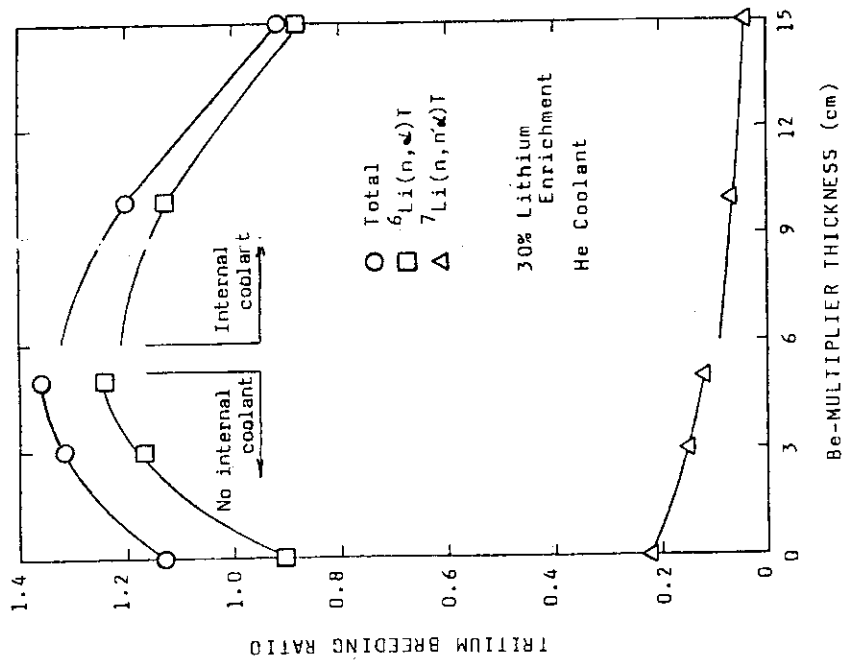


Fig. 4.11 Effect of Be Multiplier Thickness on Iritium Breeding

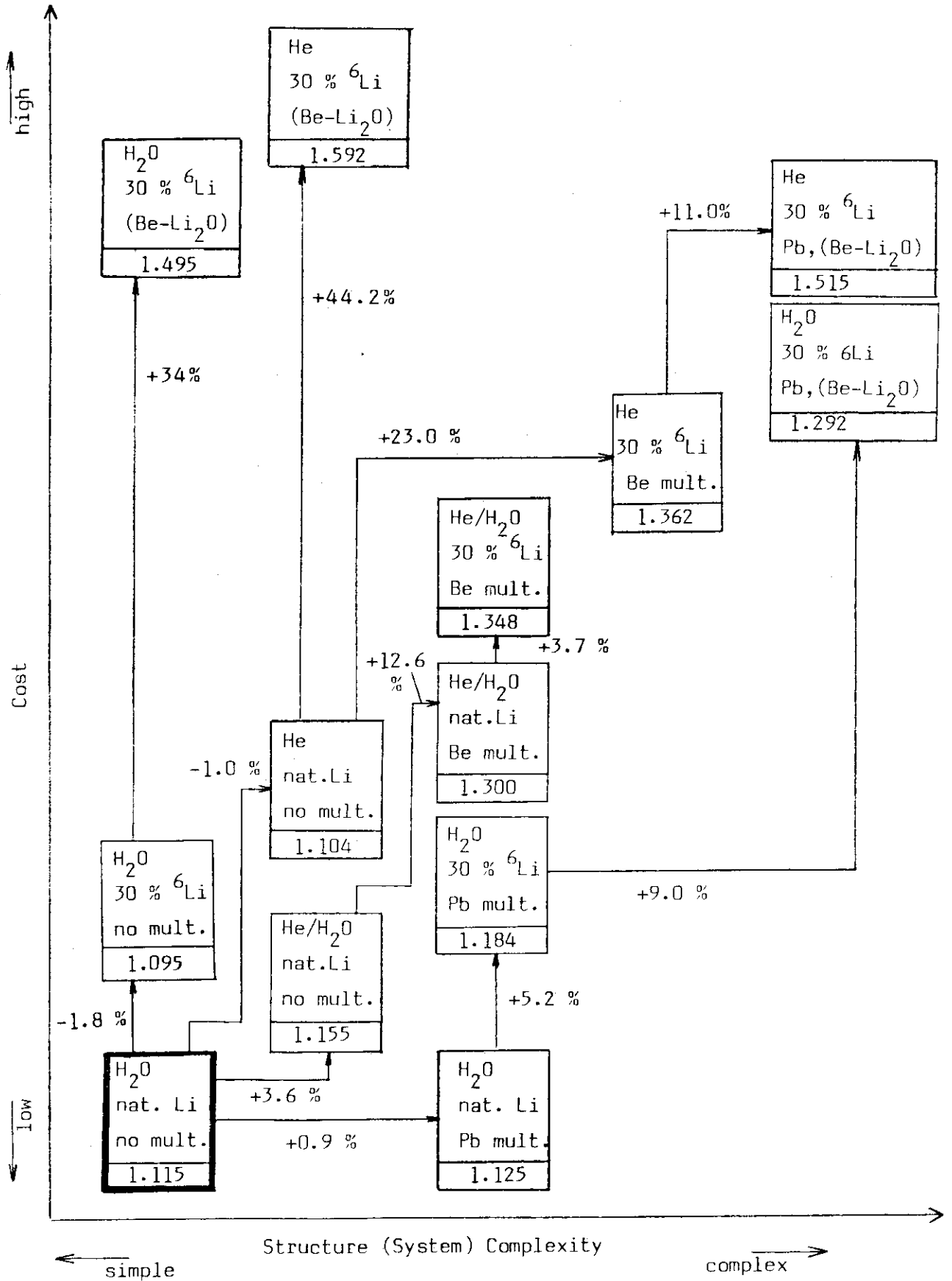


Fig. 4.13 Relation of TBR Improvement with Structure Complexity and Cost

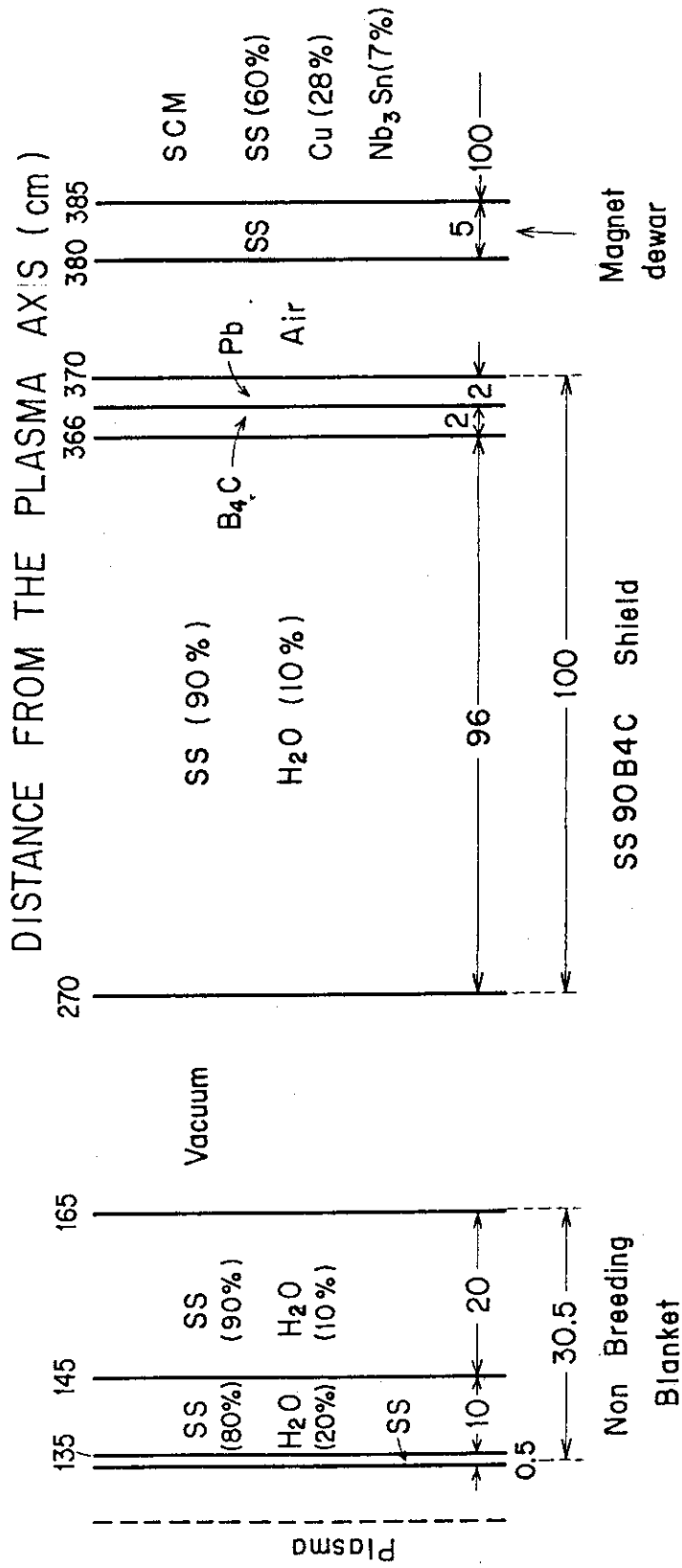


Fig. 4.14 Material arrangement of non-breeding blanket and the SS90B4C shield

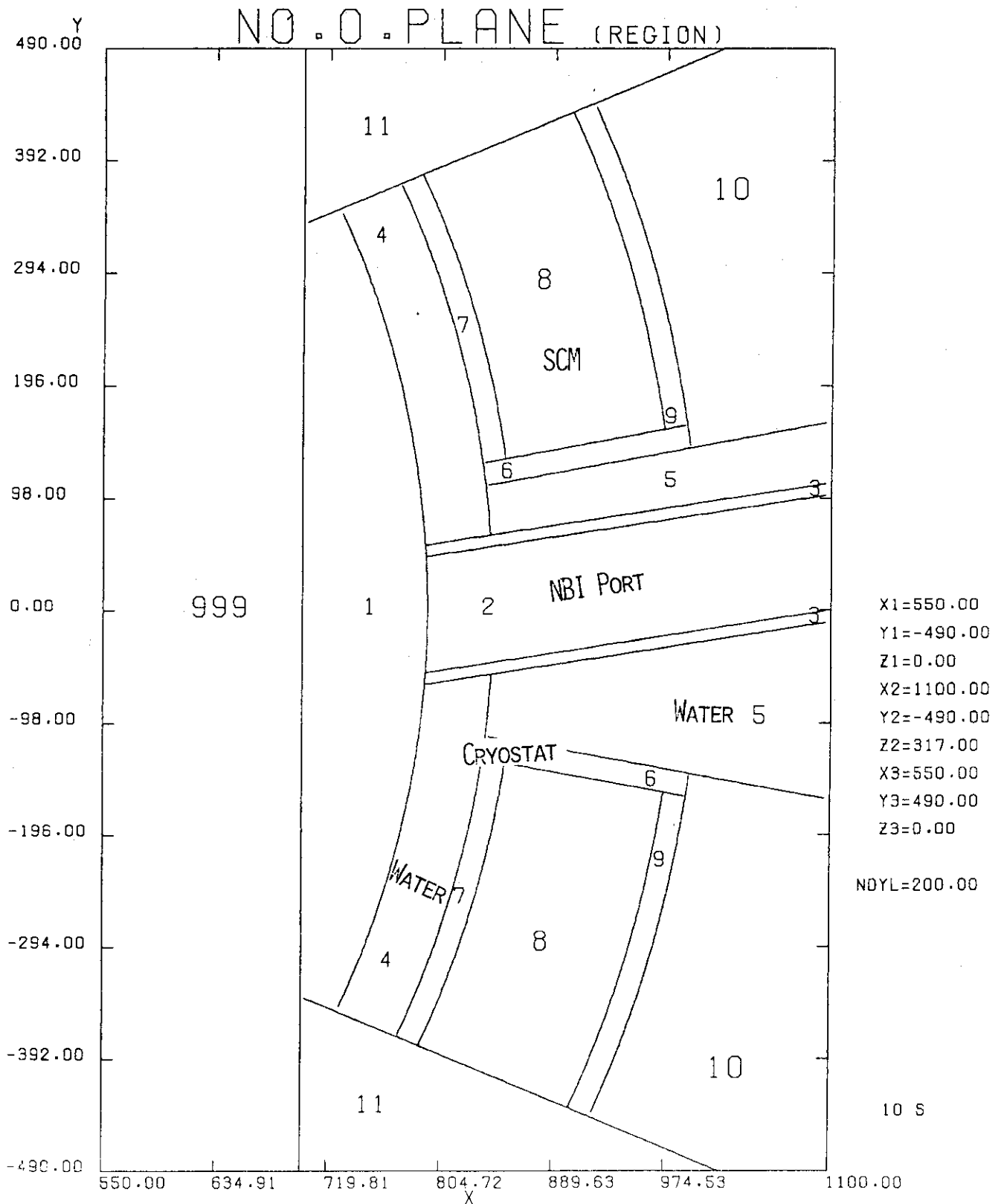


Fig. 4.15 Three dimensional model of the NBI port and the TFC (SPTR alternative)

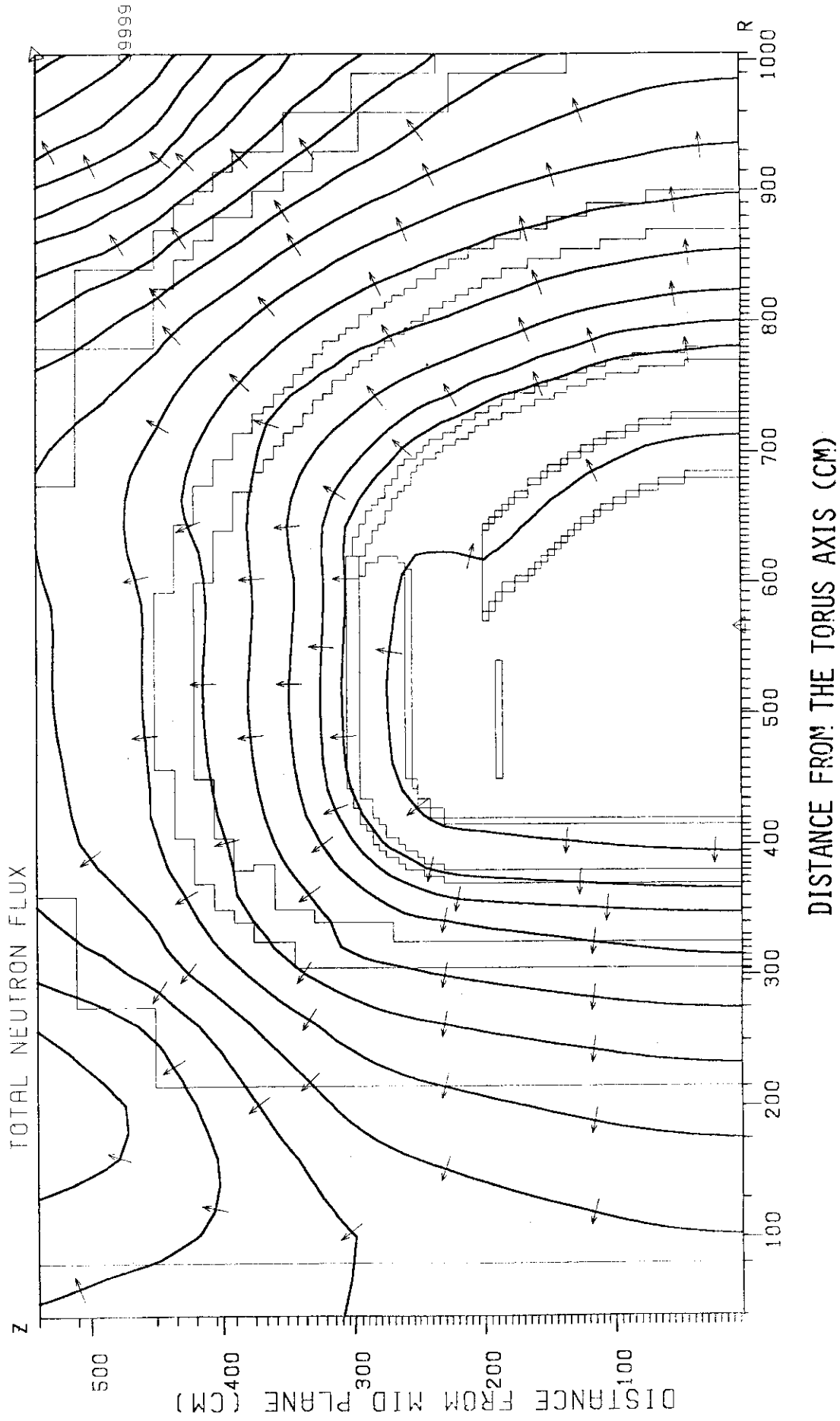


Fig. 4.16 Total neutron flux distribution in SPTR without NBI port (R-Z model)

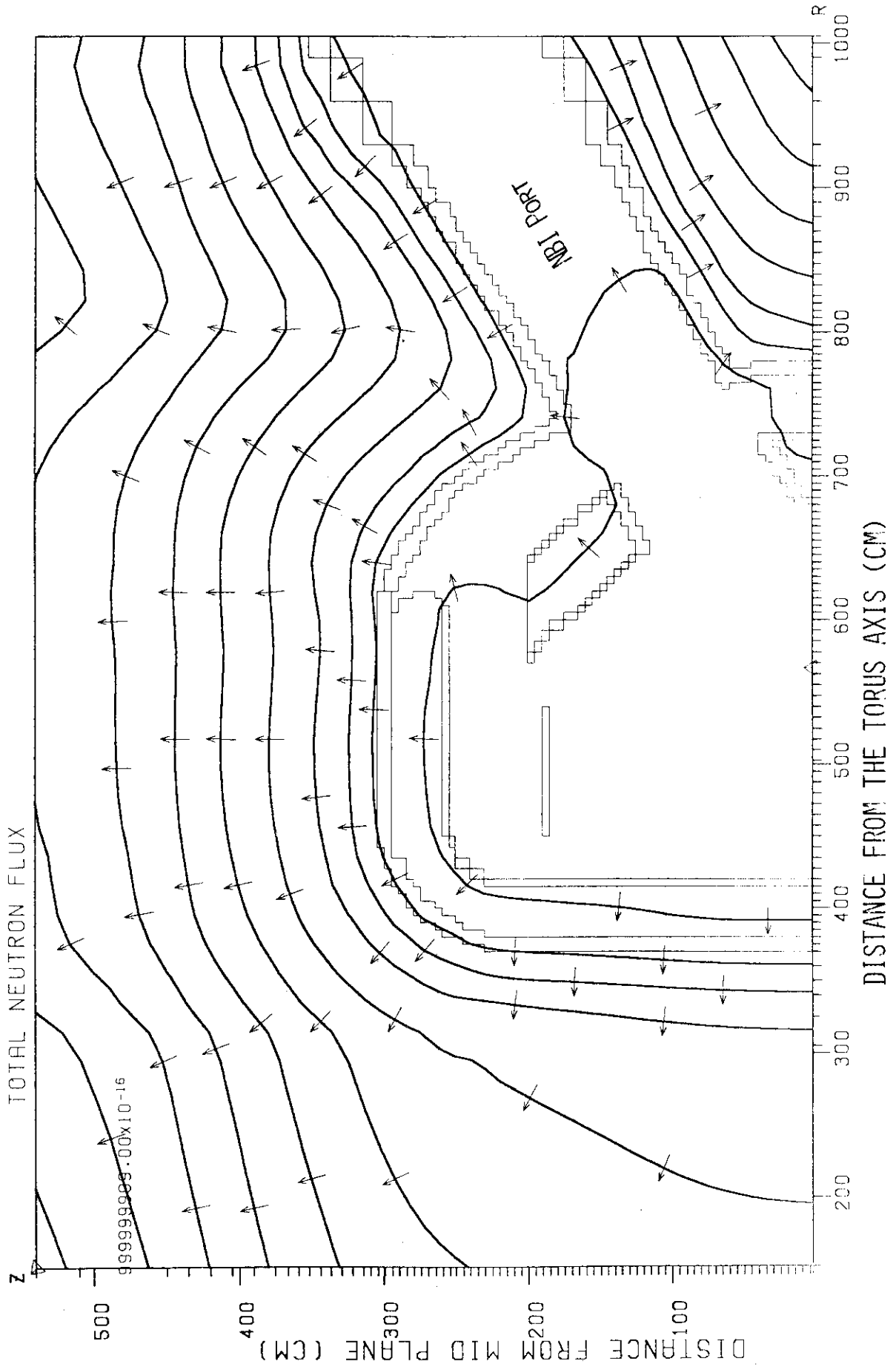


Fig. 4.17 Total neutron flux distribution in SPTR with NBI port (R-Z model)

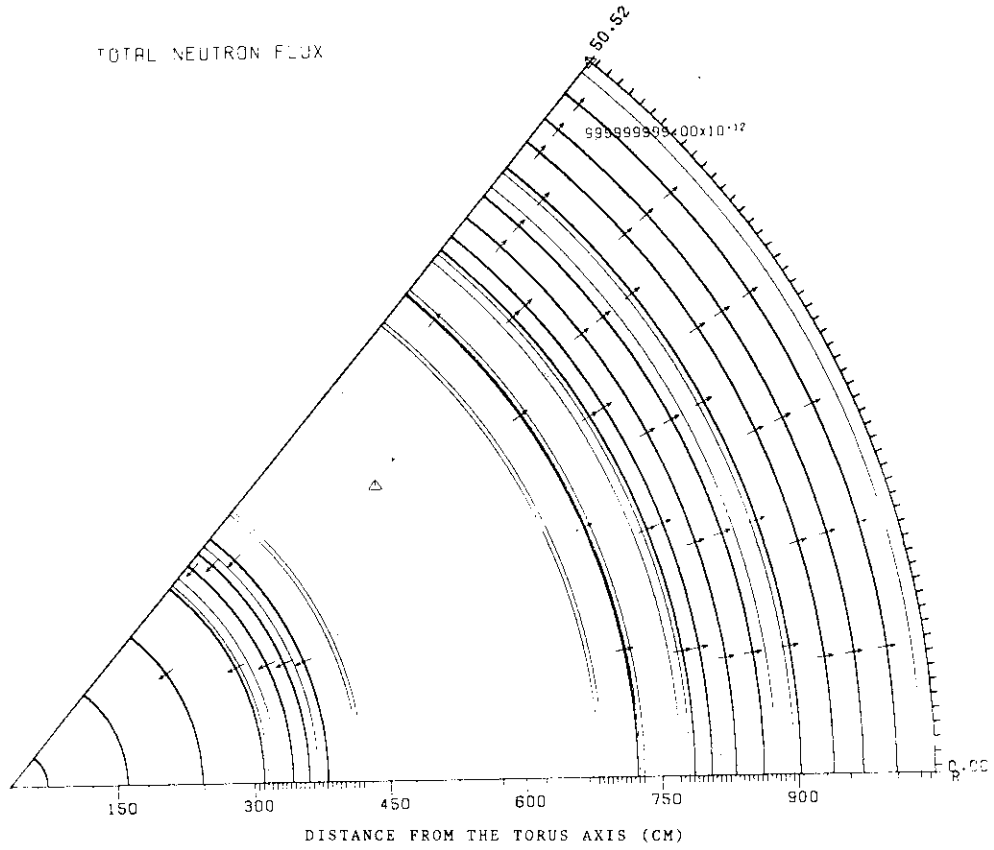


Fig.4.18 Total neutron flux distribution in SPTR without NBI port (R-θ model)

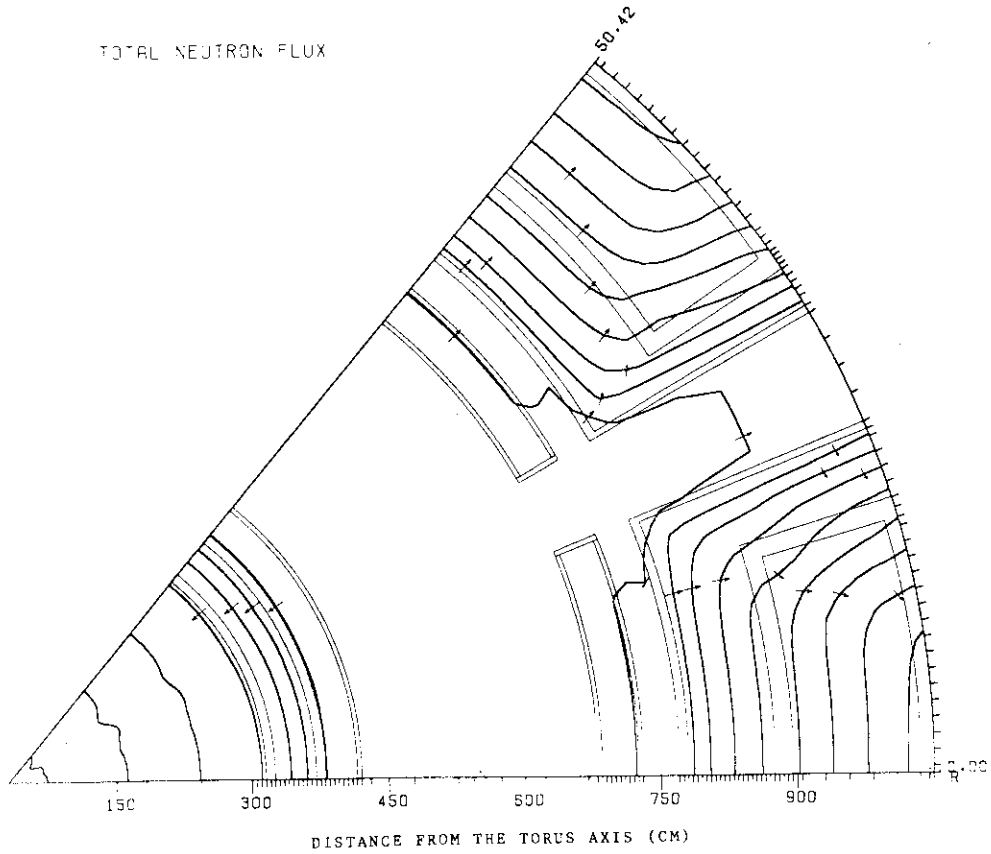


Fig.4.19 Total neutron flux distribution in SPTR with NBI port (R-θ model)

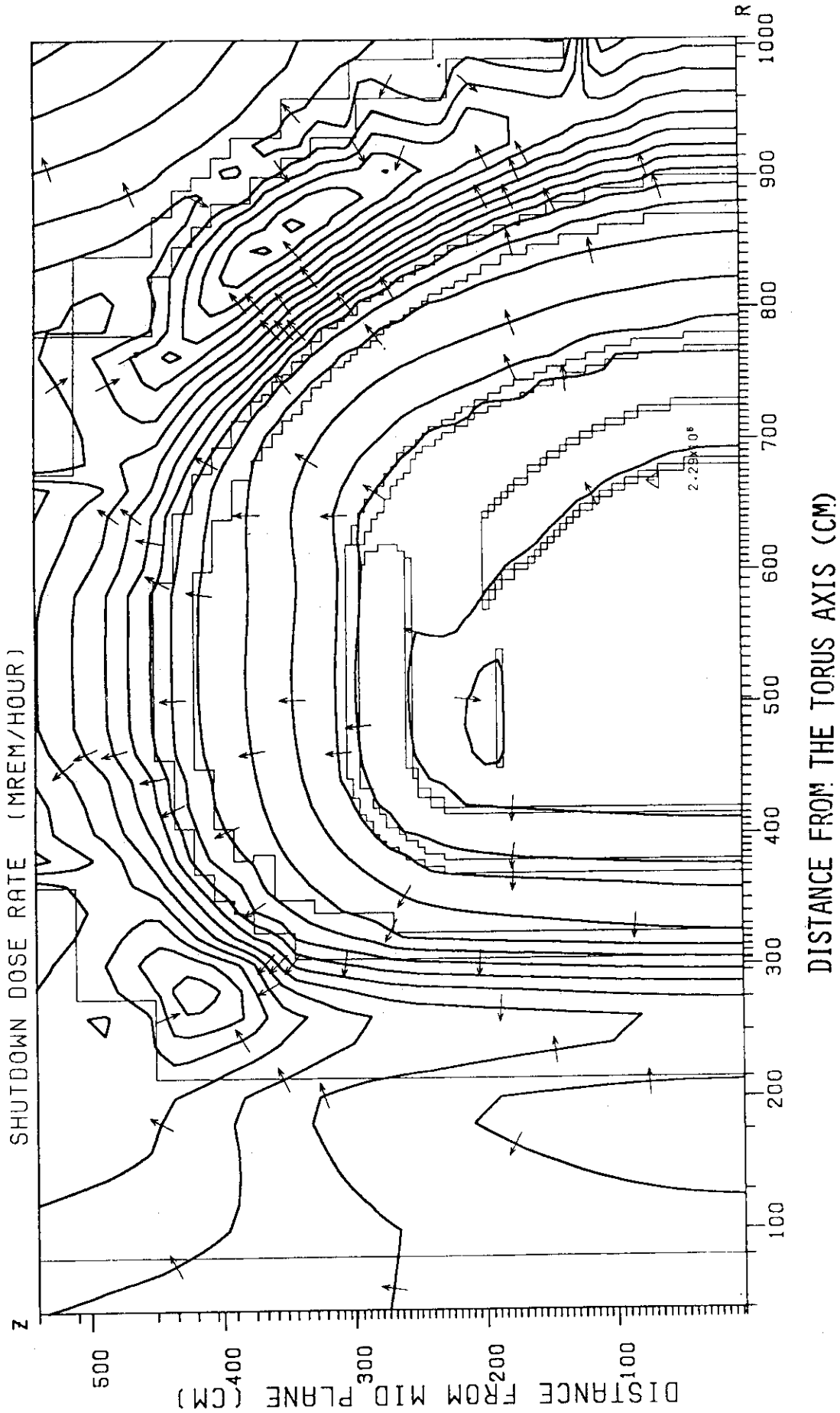


Fig. 4.20 Shutdown dose rate distribution in SPTR without NBI port (R-Z model)

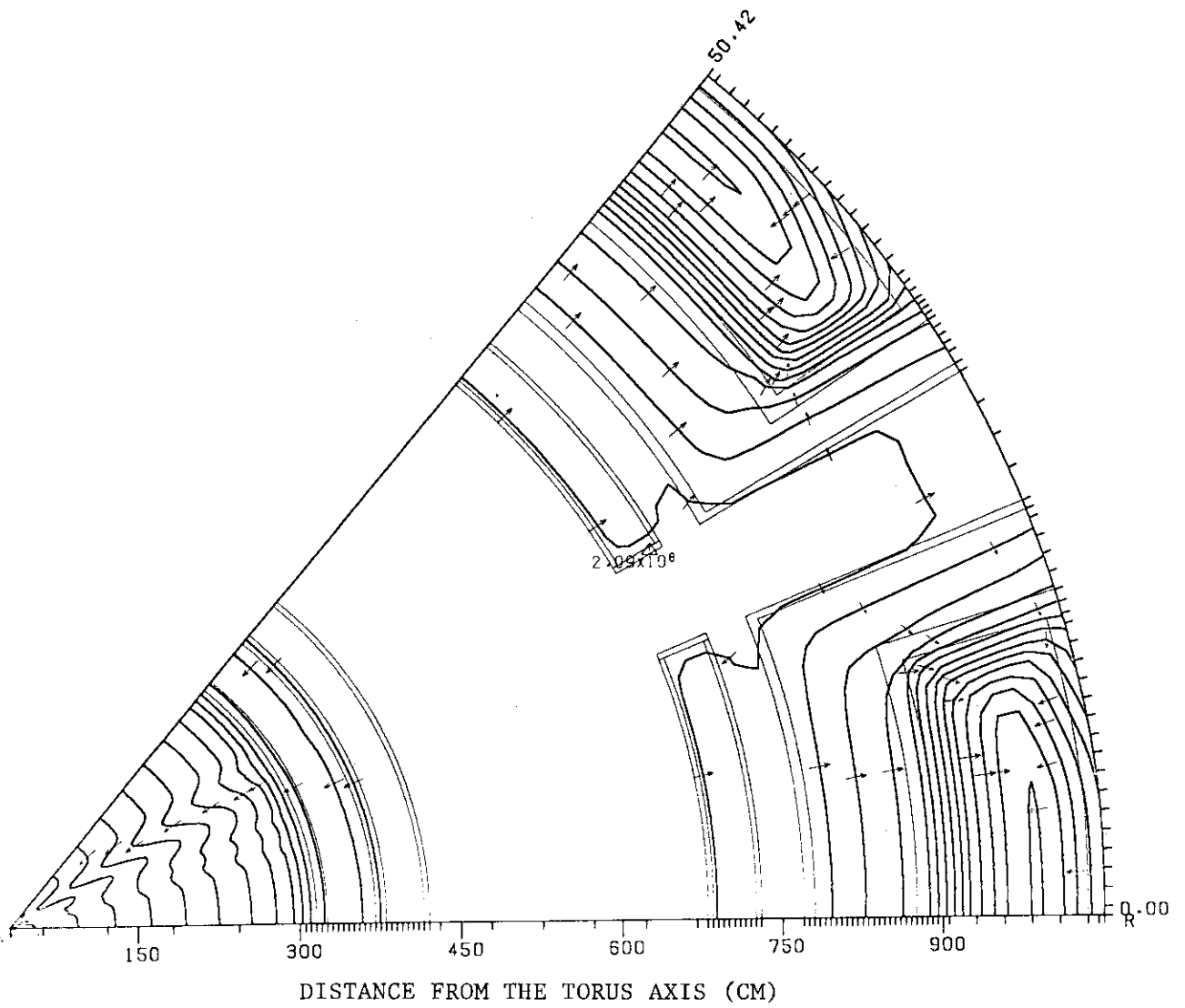


Fig. 4.21 Shutdown dose rate distribution in SPTR with NBI port
(R- θ model)

V. Thermo-mechanical Design of the FER Blanket

Considerations for Design of FER Blanket

Mission of fusion Experimental Reactor is integral test of technologies concerned with future fusion reactors. Tritium production technology by incorporating a tritium breeding blanket is one of the missions. Since annual tritium consumption rate of about 3 Kg-T₂ is anticipated for FER operation, tritium availability from existing sources is questionable. So tritium breeding ratio (TBR) of greater than unity is required for self-sustaining of reactor fuel.

The solid breeding material is preferable because it offers the advantages of engineering design simplicity and relatively low stored chemical energy. Lithium oxide (Li₂O) was selected because of its relatively high thermal conductivity and good tritium breeding capacity.

From the economical and safety points of view, tritium generated in the blanket is continuously removed by a low pressure helium purge stream. For this purpose, temperature of the breeder must be maintained above 400°C to facilitate tritium release and to reduce tritium inventory in the breeder.

Electricity production is not planned because it places difficult constraints on material and configuration of the blanket. The blanket is cooled by low temperature water coolant.

Type 316 stainless steel is selected as the structural material because it provides adequate radiation damage resistance and an allowable design stress intensity under the anticipated operating conditions.

Blanket vessel must be designed to endure electromagnetic force during plasma disruption in addition to internal pressure and thermal stress. Baking system for outgassing blanket surfaces must be considered related to the torus vacuum system.

Blanket Configuration

Major design parameters of tritium breeding blanket are shown in Table 1. The type of the blanket is tube-in-shell that consists of a box-like container and coolant tubes for removing thermal energy generated in the breeder region.

Figure 1 shows the bird's-eye-view of the outboard sector. Tritium breeding blanket is provided in almost all part around plasma except NBI, RF and vacuum ducts. It consists of outboard and inboard blankets.

Coolant tube in the breeder region have a poloidal axis for the structural simplicity, that means it will have less number of welding parts than the structure using coolant tubes with a toroidal axis.

The outboard blanket vessel is supported at three levels that are upper, middle and lower levels. The weight of a blanket is mainly supported by one support structure. The others support horizontal movements during replacement and so on, and they are

loose fittings considering the thermal expansion of the blanket vessel.

The number of blanket modules is 63, and three of the modules form into a sector which is moved as a unit at replacement.

Figure 2 shows the cross-sectional view of the outboard blanket. First wall is integrated to the blanket wall from the viewpoint of obtaining relatively high tritium breeding performance and avoiding the complexity of its own support system. The first wall is a bare tube-panel type that the plate with circular coolant tubes brazed to it. The minimum thickness of the first wall is decided for 10 years of lifetime considering erosions by physical sputtering and plasma disruption. The wall thickness of the outboard and inboard blankets are 7.5 mm and 8.5 mm, respectively at the beginning of life, and 5 mm and 4 mm, respectively at the end of life.

Coolant tubes have a toroidal axis considering reinforcement of the blanket vessel. The coolant of the first wall also cools the blanket side wall, and manifold collecting the coolant is provided in the support flange.

The depth of outboard blanket is 500 mm, and the width is about 720 mm which is designed for blanket vessel to endure the internal pressure of 0.1 MPa of helium purge gas.

The basic concepts of the inboard blanket design are the same as those of the outboard blanket. Blanket depth is 400 mm, and the width is about 370 mm in order to provide the same number of blanket modules as outboard blanket.

Natural Li_2O is used as the breeder. Li_2O is formed into small size pebbles because packing in the blanket vessel seems to be easier as compared with pellet or block forms. In addition, small pebbles have less possibility of cracking due to temperature difference in them. The bulk packing fraction of the breeder is 0.7. And estimated net tritium breeding ratio for this design of no neutron multiplier and no moderator is about 1.03 by 3-D Monte Carlo in consideration of penetrations.

Pressurized light water, H_2O , is selected as the coolants of both of the breeder region and the first wall. Its inlet and outlet temperature are 60°C and 100°C , respectively. The outlet temperature is low because of no electricity generation.

The allowable temperature range of the breeder is estimated to be from 400°C to 1000°C from thermochemical consideration of Li_2O . To keep the minimum temperature of the breeder higher than 400°C , a stagnant helium gap is provided around a coolant tube, and to keep the maximum temperature lower than 1000°C . Coolant tubes in the breeder region are properly arranged according to attenuating heating rates. Considering several uncertainties, the blanket is designed to maintain the breeder in the temperature range between 450°C and 700°C under nominal operating condition.

For continuous tritium recovery, helium gas purging is adopted.

Thermal-mechanical Performances

Thermal-hydraulic and mechanical analyses for the blanket module have been carried out, and the performances obtained from these analyses are described below.

(1) Breeder Region

The blanket structure is BOT/NM type and the heat generated in the blanket is removed by the coolant flowing poloidally. The breeder which consists of small pebbles of natural isotopic lithium oxide is packed in the blanket vessel.

A diameter of 1 mm was chosen for the pebbles in order to keep off a remarkable wall effect of coolant tubes on the packing fraction of pebbles.

Breeder temperature is controlled by helium gaps around coolant tubes and proper arrangements of blanket coolant tubes. The breeder temperature is maintained in the range between 450°C and 700°C, at any part of breeder region in nominal operating condition. The effective thermal conductivities are used in the estimation of breeder temperature. Two dimensional effects, coolant tube wall effects and thermal radiation effects are taken into account for coolant tube arrangement. It is considered that the limits of operational temperature range for lithium oxide is 400°C ~ 1000°C, from the viewpoint of continuous tritium recovery. And as a result,

it is obtained that the permissible range of power density variation is 85% ~ 150% of predicted power density.

Pressurized water is used as the coolant for breeder region. The inlet pressure is 1.5 MPa and the inlet and outlet temperatures are 60°C and 100°C, respectively. The pressure losses of the coolant in the blanket module is about 0.3 MPa, and maximum coolant velocity is about 4.5 m/s. These values would not cause severe problems.

(2) First Wall/Blanket Vessel

Some thermal analyses for the first wall have been carried out. Temperature distributions in outboard and inboard first walls during burn were calculated. Surface heat fluxes are 12 W/cm² for both outboard and inboard walls. Volumetric heating rates within outboard first wall structure are 10 W/cc, and within inboard first wall are 7 W/cc. The maximum temperatures of the outboard and inboard first walls are both about 240°C by 2-D calculations. These values are permissible from the viewpoint of structural integrity. The maximum film temperature drops at the surface of first wall coolant tubes are about 30°C for both outboard and inboard cases. Therefore, even local subcooled boiling will not take place on the coolant tube surface.

Temperature response during beam shine-through were also calculated. The surface heat flux during beam shine-through which continues about two seconds is 3 MW/4m² on the inboard wall. The maximum structural temperature after two seconds is about 215°C.

It is considered that the temperature would not cause a severe problem.

Pressure losses and velocity of the first wall coolant were estimated. The pressure loss of the outboard first wall coolant is 0.048 MPa, and of the inboard case is 0.077 MPa. The coolant velocity is about 1.6 m/s. These values are acceptable.

The eroded thickness by physical sputtering and vaporization during major plasma disruptions was evaluated. The thickness of about 2.5 mm is necessary for physical sputtering during reactor life (10 years). The vaporization thickness is predicted to be about 2.0 mm. Therefore eroded thickness for outboard and inboard first wall are 2.5 mm and 4.5 mm, respectively. In this design, the lifetime of the first wall is equal to full reactor life (10 years).

Primary stresses in the blanket vessels have been analyzed with the load of internal pressure of 0.1 MPa by two-dimensional model under plain strain condition. The maximum stress intensity of the outboard blanket is 187 MPa even at the end of reactor life when the minimum wall thickness is 5.0 mm. A value of 127 MPa is obtained at the beginning of life when the minimum wall thickness is 7.5 mm. For the inboard blanket case, these values are 98 MPa and 46 MPa, respectively. The value of $1.5 S_m$ for type 316 stainless steel is 191 MPa by ASME Section III. The evaluation is based on design standards of as-received 316SS, because hot working such as welding will impair the properties of cold-worked material. All of the calculated stress intensities are below this value.

Thermal stress intensity in the first wall was also analyzed. The maximum stress intensity of the outboard first wall at the beginning of reactor life is 357 MPa. And that of the inboard first wall is 370 MPa. At the end of life these values would be reduced due to depletion of the wall. The value of $3 S_m$ for type 316 stainless steel is 382 MPa, and that of $2 S_a$ for 4×10^5 cycles reactor full life is 373 MPa. Therefore, even at the beginning of reactor life, the maximum stress intensity is below these values. Table 2 summarizes the results of these stress analyses.

From these discussions the integrity of the blanket structure was confirmed.

Fabrication of Blanket Structure

Fig. 3 shows the fabrication sequence of blanket structure and vacuum vessel. The material of blanket structure is type 316 Stainless Steel. As shown in this figure, main technologies required for fabrication of blanket are shown below;

- 1) Machining of Heavy-section Stainless Steel
- 2) Cold- or Hot-working of Heavy-section Stainless Steel such as Bending Work
- 3) Joining of First Wall and Cooling Tube
- 4) Welding of Heavy-section Stainless Steel
- 5) Bending of Small-size Cooling Tube
- 6) Welding of Small-size Cooling Tube
- 7) Non-destructive Testing of Stainless Steel Welds

Afore-mentioned technologies, key technologies to the fabrication of blanket, are explained below in accordance with the fabrication sequence.

(1) Machining of Heavy-section Stainless Steel

Heavy-section stainless steel is machined at first to prepare the joining between front wall of blanket (first wall) and cooling tube. This groove machining is carried out by milling machining.

(2) Cold- or Hot-working of Heavy-section Stainless Steel

Heavy-section stainless steel (50 mm thick for outboard blanket and 100 mm thick for inboard blanket) is bent by 90 degrees with hydraulic press of several thousands tons in its capacity.

(3) Joining of First Wall and Cooling Tube

In this blanket design, front wall of the blanket serves as the first wall at the same time. Therefore, cooling tube is joined to the grooved blanket by brazing or some other technique for preventing overheat of first wall.

(4) Welding of Heavy-section Stainless Steel

Heavy-section stainless steel is welded to fabricate the blanket vessel. In this case, full considerations should be paid to select proper welding process. That is to say, welding should be performed at small heat input lest the welds should incur hot cracking and heat affected zone should widen. In this sense, EBW (electron beam welding) is most desirable.

(5) Bending of Small-size Cooling Tube

Small-size cooling tube is bent by cold-bending machine.

(6) Welding of Small-size Cooling Tube

Small-size cooling tube is welded in a limited space by automatic orbital TIG welder. In this case, heat input should be controlled to as small value as possible. Further, tube-to-stub welding is performed by inner bore welding process.

(7) Non-destructive Testing of Stainless Steel Welds

Every welds is examined by non-destructive testing to assure integrity of the welds. Inner bore welds is tested by radioactive isotope of small diameter such as Tm-170.

Table 1 Summary of Design Parameters for Tritium Breeding Blanket

Number of Modules	63
Number of Sectors	21 (3 modules/sector)
First Wall	Integral with Blanket Tube-Panel (bare 316 S.S.)
Thickness (initial)	
Outboard	7.5 mm (sp.;2.5mm)
Inboard	8.5 mm (sp.;2.5mm, disr.;2mm)
Thickness (end of life)	
Outboard	5 mm
Inboard	4 mm
Lifetime	10 years (estimated)
Blanket	Tube-in-Shell Type
Thickness (including F/W)	
Outboard	50 cm
Inboard, Top, Bottom	40 cm
Structure	type 316 stainless steel
Maximum Temperature	<250 °C
Breeder	Li ₂ O (natural lithium)
Form	pebble (1 mm ϕ)
Density	85 %T.D.
Packing Fraction	70 % (bulk)
Min./Max. Temperature	450/700 °C (Nominal) 400/1000 °C (Limits)
Allowable Power Variation	85%~150% of Nominal Power
Temperature Control Method	Helium Gap
	Coolant Tube Arrangements
Coolant	H ₂ O
Inlet/Outlet Temperature	60/100 °C
Inlet Pressure	1.5 MPa
Flow Direction	Poloidal
Tube Diameter	10 mmO.D.
Net Tritium Breeding Ratio	1.03 (3-D Monte Carlo)
Tritium Purge Gas	He (0.1 MPa) 200 Nm ³ /hr

Table 2 Mechanical Performances The evaluations are based on design standards of as-received 316SS, because hot working such as welding will impair the properties of cold-worked material.

Maximum Stress Intensities

	Wall Thickness (mm)	$P_L + P_b$ (Mpa)	$1.5 S_m^*$ (Mpa)	Thermal (Mpa)	$2S_a^*$ (4×10^5 cycles) (Mpa)
Outboard BOL**	7.5	127	191	357	373
EOL**	5.0	187	191	(<357)	373
Inboard BOL	8.5	46	191	370	373
EOL	4.0	98	191	(<370)	373

* Values from ASME Boiler and Pressure Vessel Code, Section III

** BOL : Beginning of Life

EOL : End of Life (10 years)

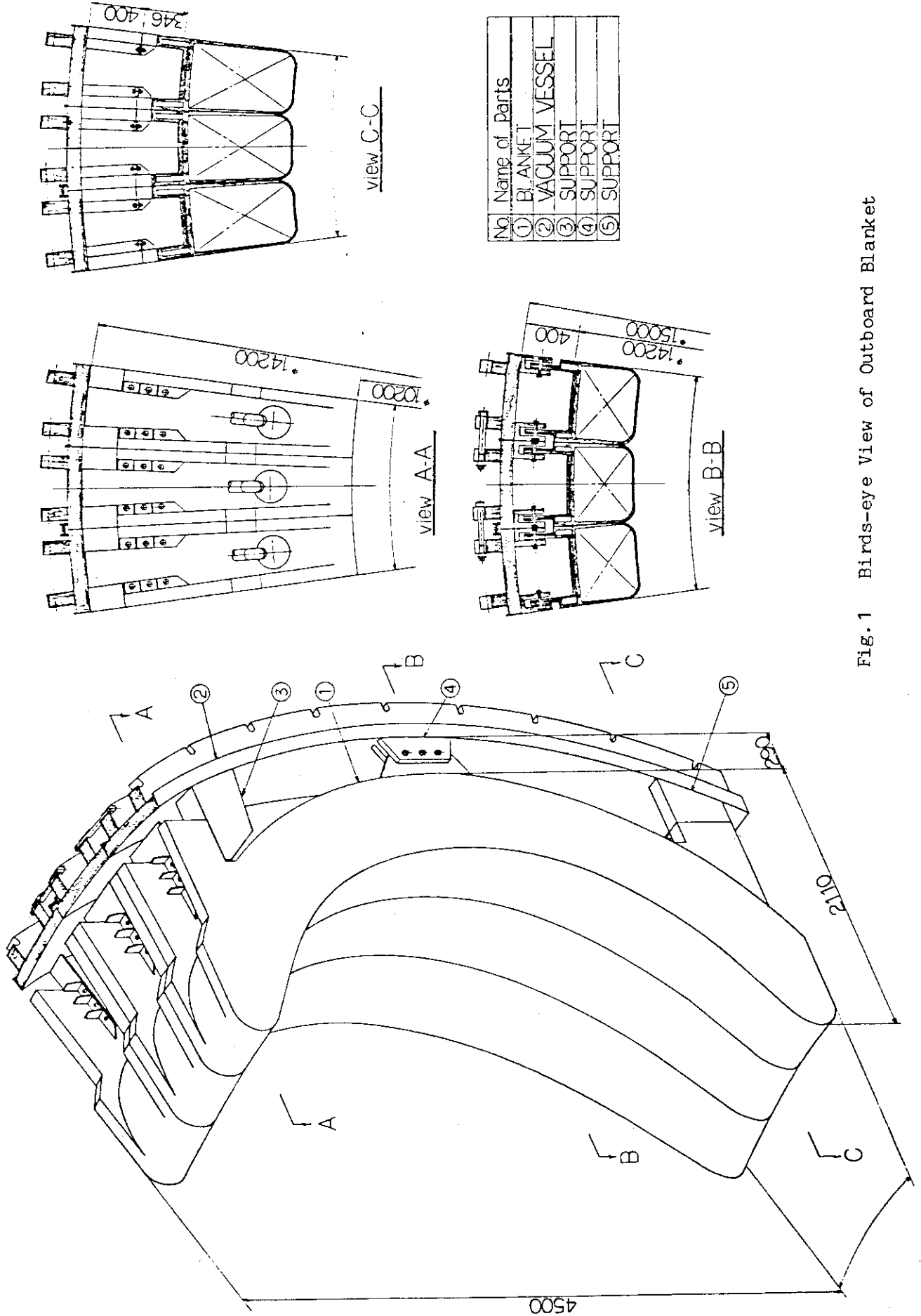


Fig. 1 Birds-eye View of Outboard Blanket

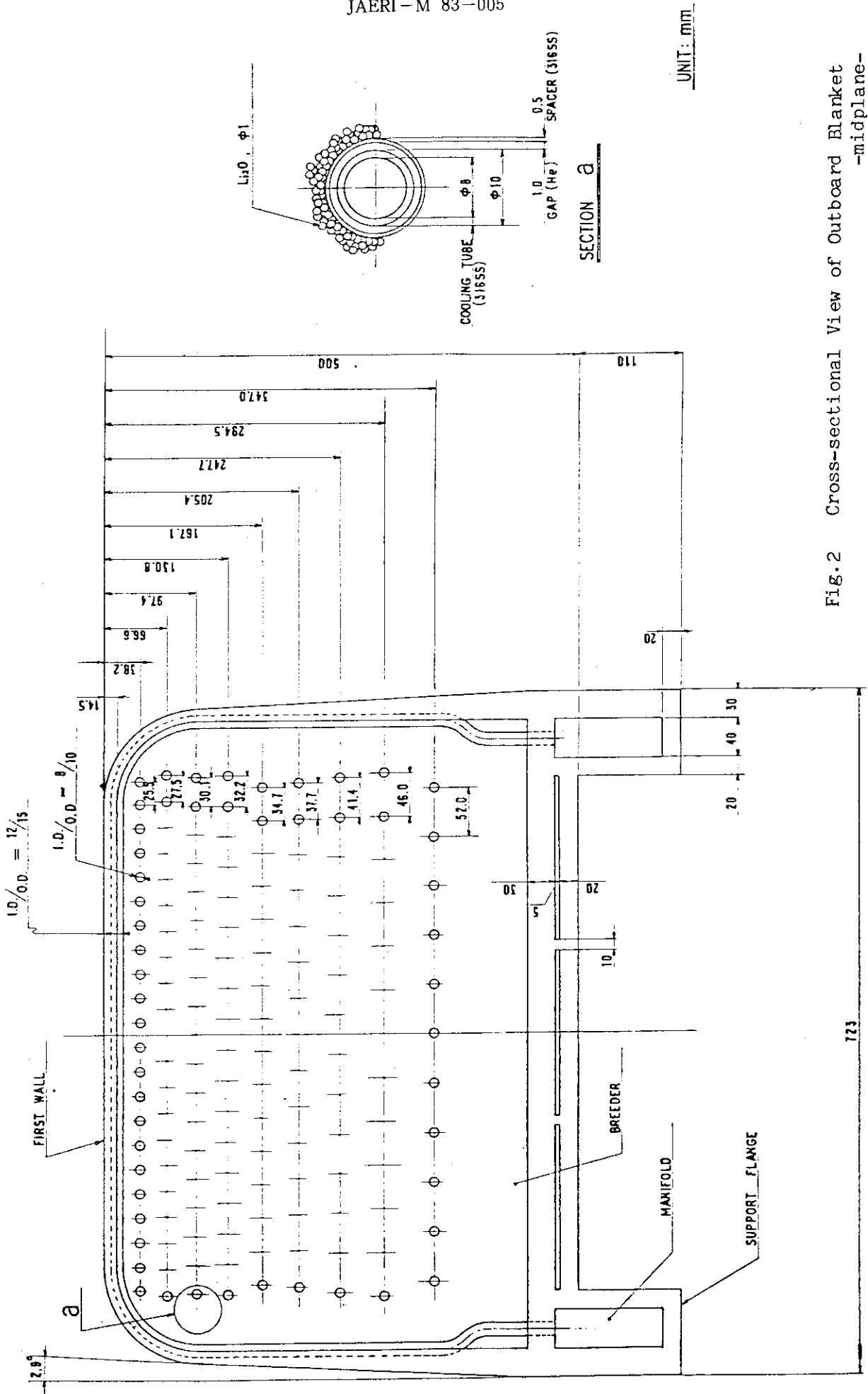


Fig.2 Cross-sectional View of Outboard Blanket -midplane-

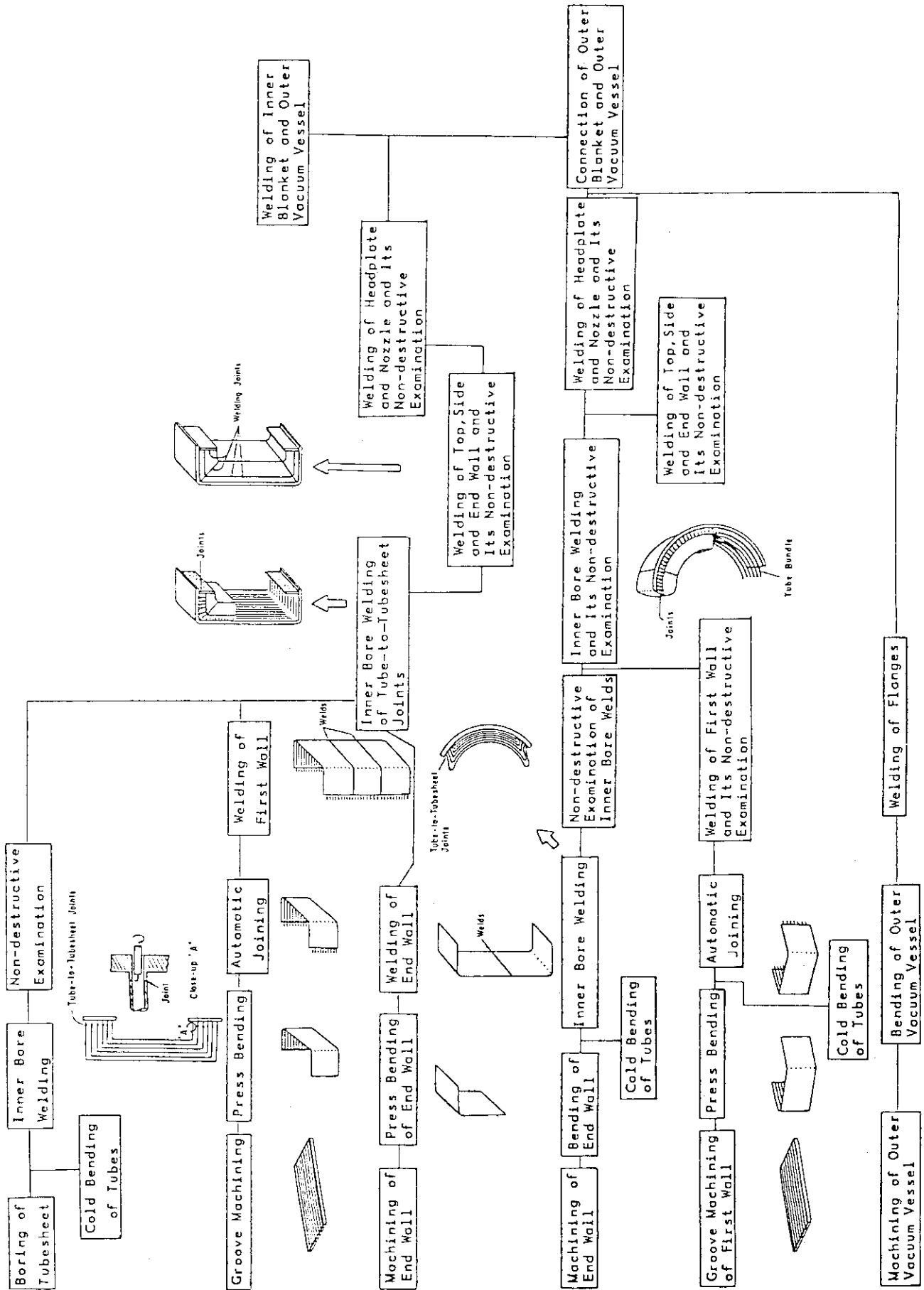


Fig. 3 Fabrication Sequence of Blanket and Vacuum Vessel

Appendix (View graphs presented)

V Thermo-mechanical Design of the FER Blanket

Design Philosophy for the FER Blanket

- o Tritium generation for fuel self-sustaining ($TBR \geq 1.0$)
- o Low tritium inventory (in-situ, continuous tritium recovery)
- o Non electricity generation (low temperature structure)
- o Adequate lifetime (~ 10 years)
- o Simple structure
- o Structure to accommodate to the uncertainties

Appendix

Key Features of Blanket Configuration

- | | |
|--|--|
| oTube-in-Shell Type
(simple structure,
BOT/NM) | Poloidal Axis for Coolant Tube
Breeder : Li_2O small pebble form
Neutron Multiplier : none
Neutron Moderator : none |
| oIntegrated First Wall | Tube-Panel Type
Toroidal Axis for Coolant Tube |
| oLow Temperature Coolant | H_2O : 60 / 100 °C |
| oStructural Material | Type 316 stainless steel |
| oTBR | 1.0 (3-D Monte Carlo) |
| oTemperature Control | Helium Gap
Coolant Tube Arrangements
Nominal : 450 ~ 700 °C
Limits : 400 ~ 1000 °C |
| oHelium Gas Purging for Continuous Recovery of Generated Tritium | |
| oStructure to endure Internal Pressure, Thermal Stress and Electromagnetic Force | |
| oShell Effect for Vertical Plasma Stability | |

Appendix

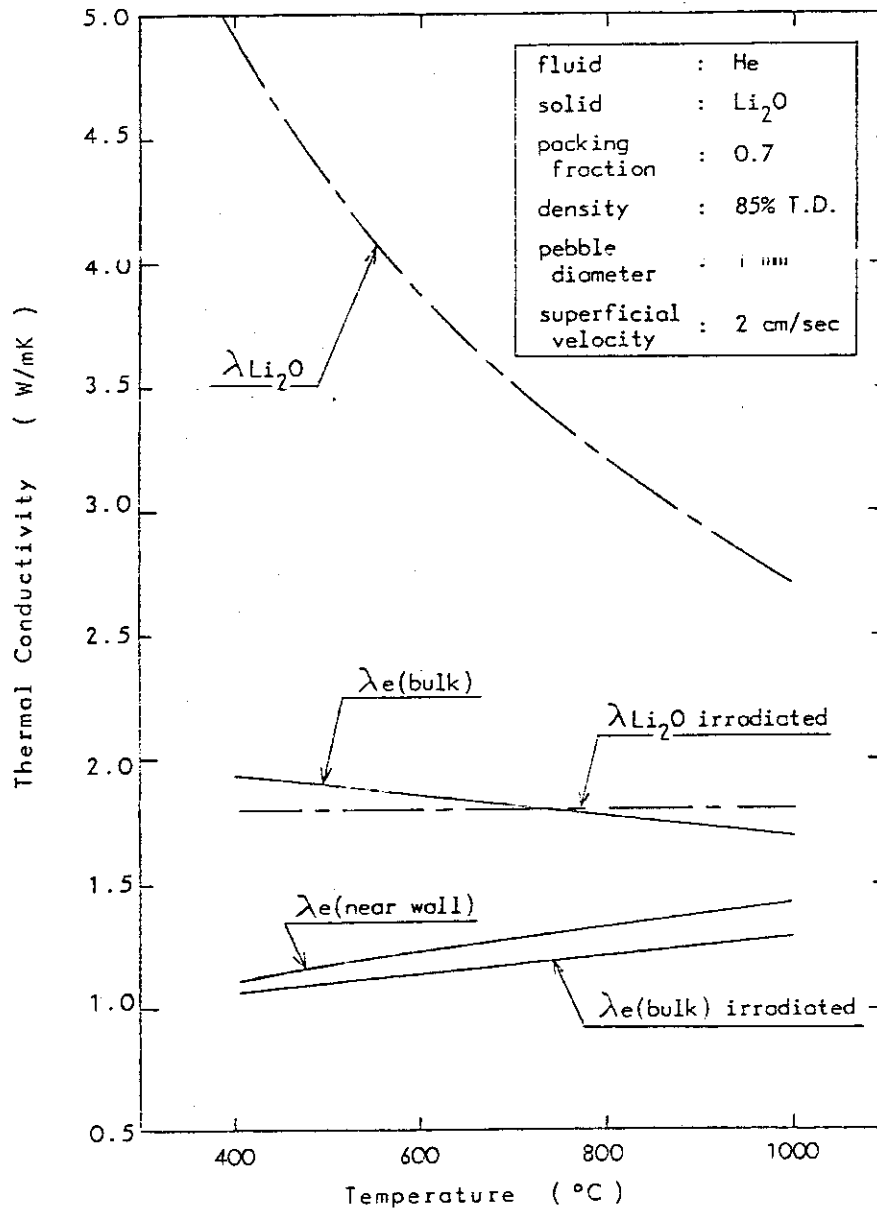
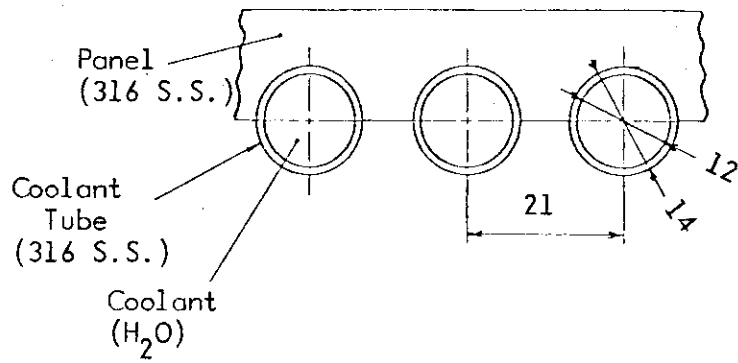


Fig. Effective Thermal Conductivity of Packed Column

Appendix



Concept of First Wall

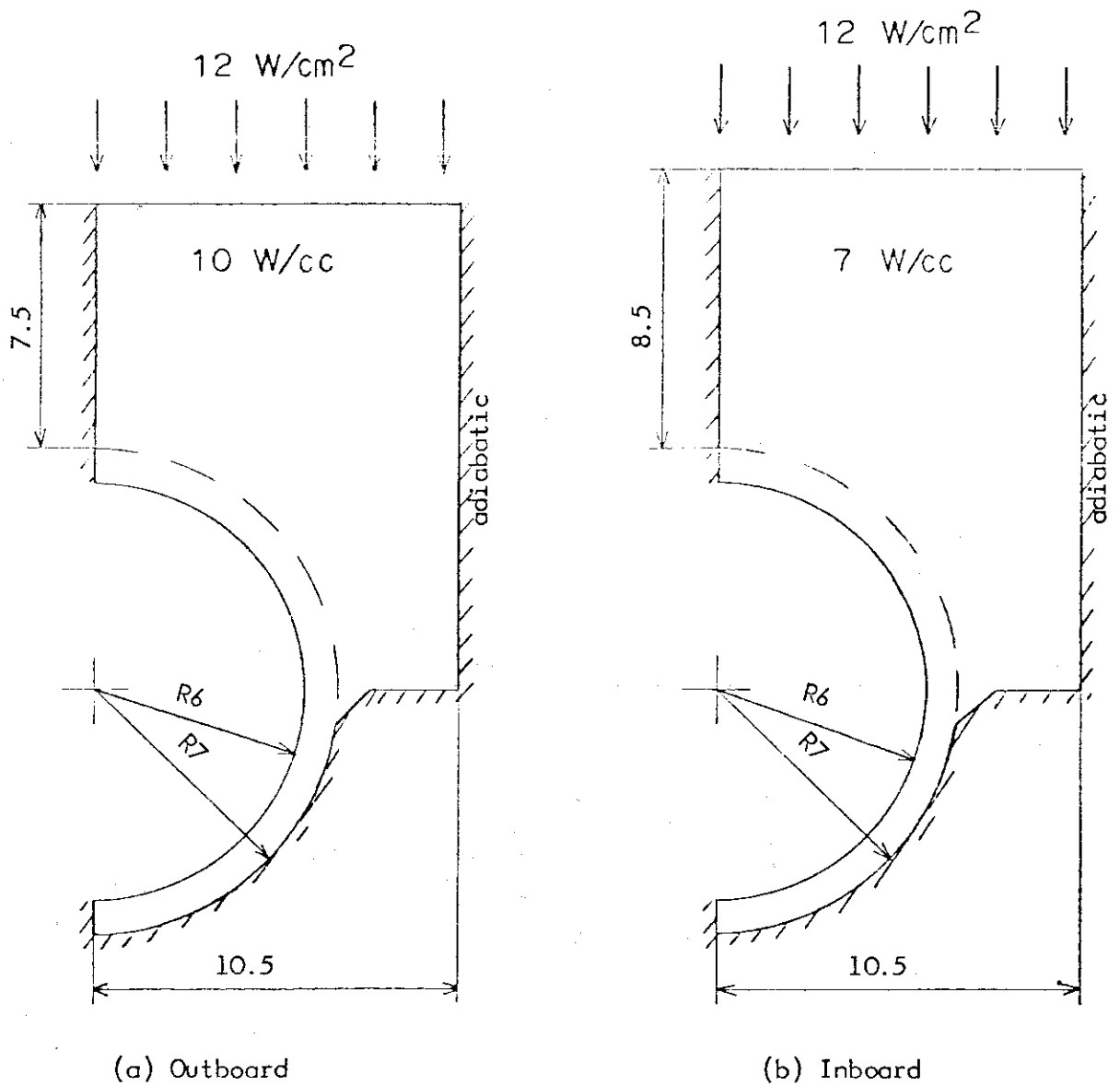


Fig. Analytical Models for Thermal Analyses of First Wall

Appendix

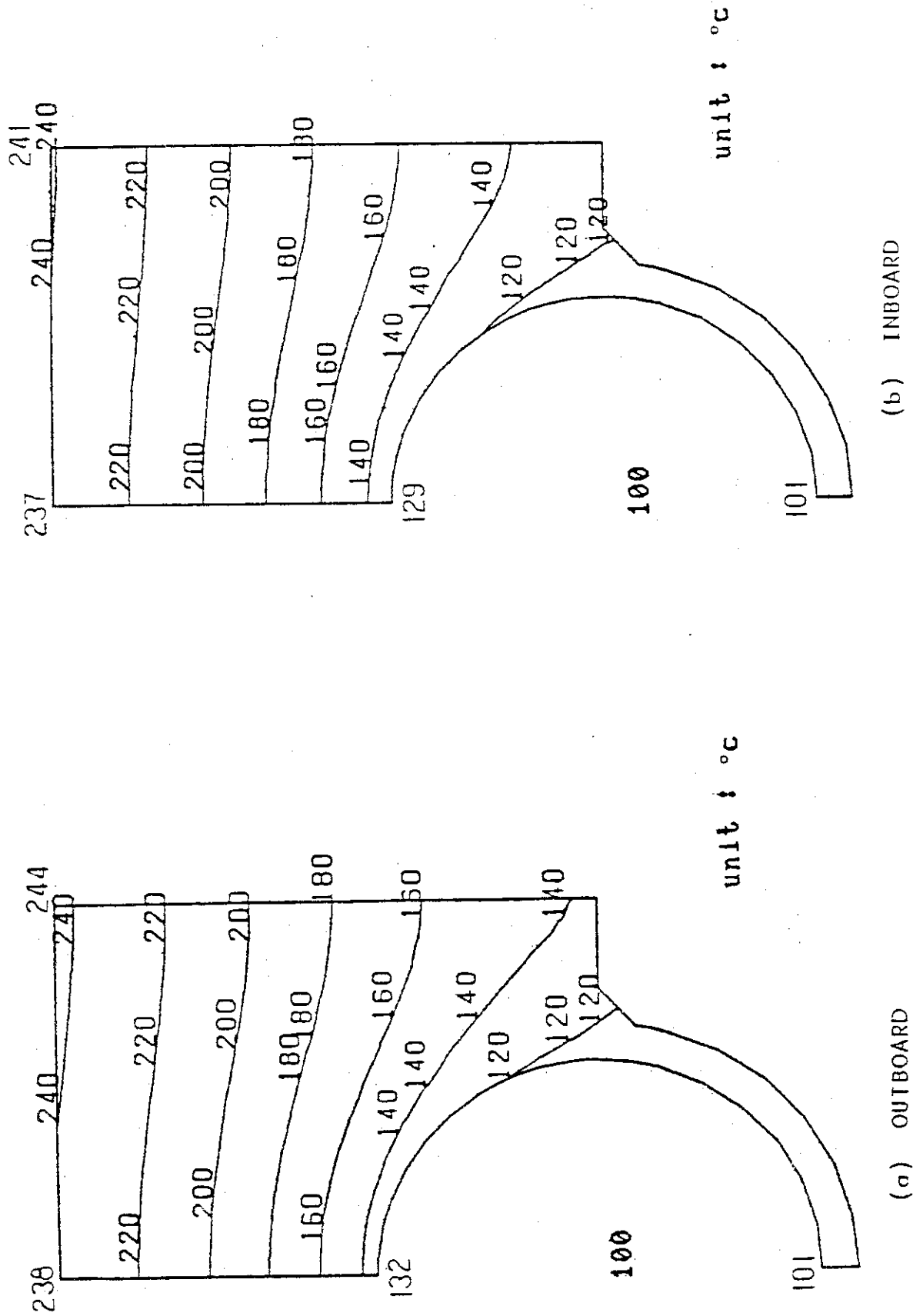


Fig. Temperature Distribution in First Wall of FER

Appendix

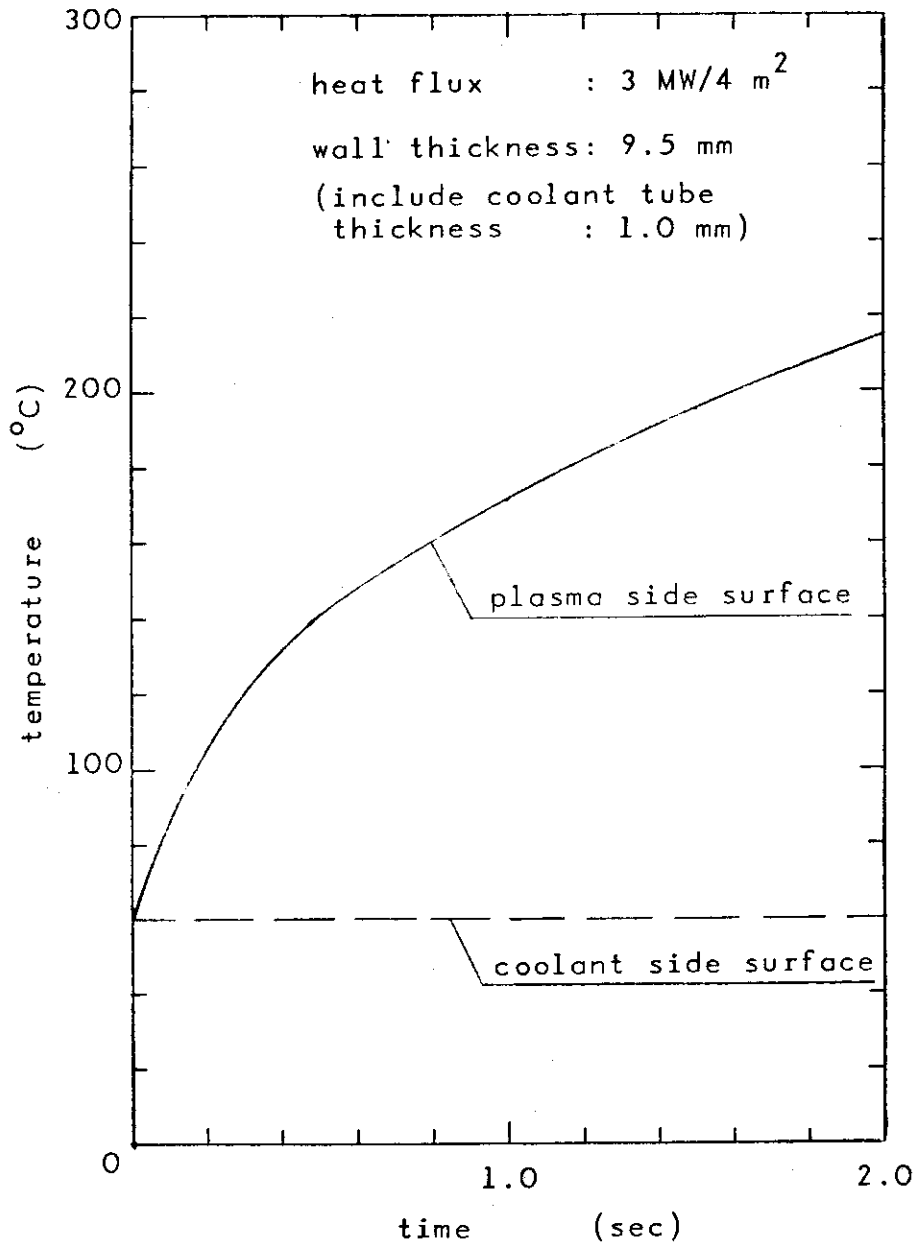


Fig. Wall Temperature during Beam Shine-Through

Appendix

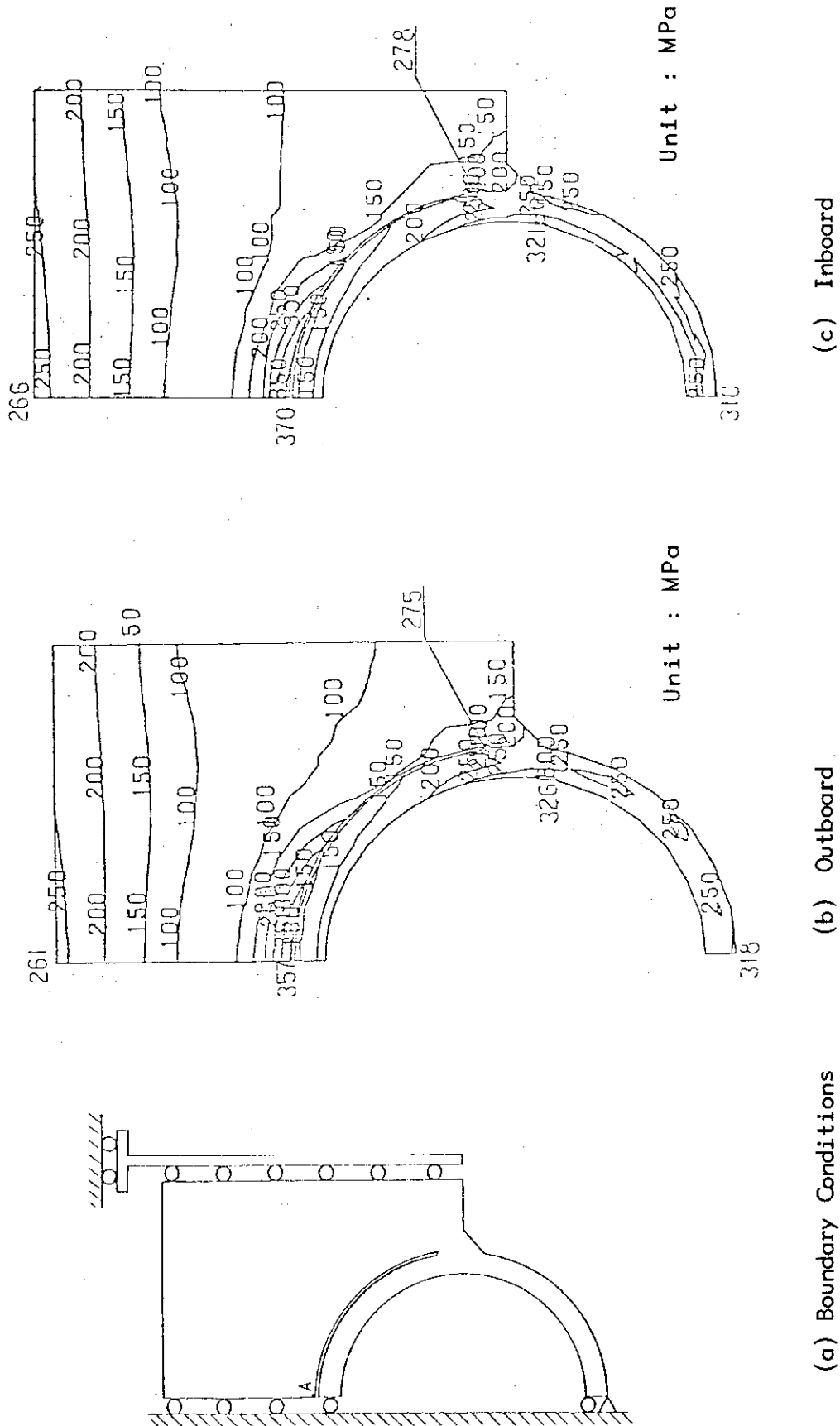
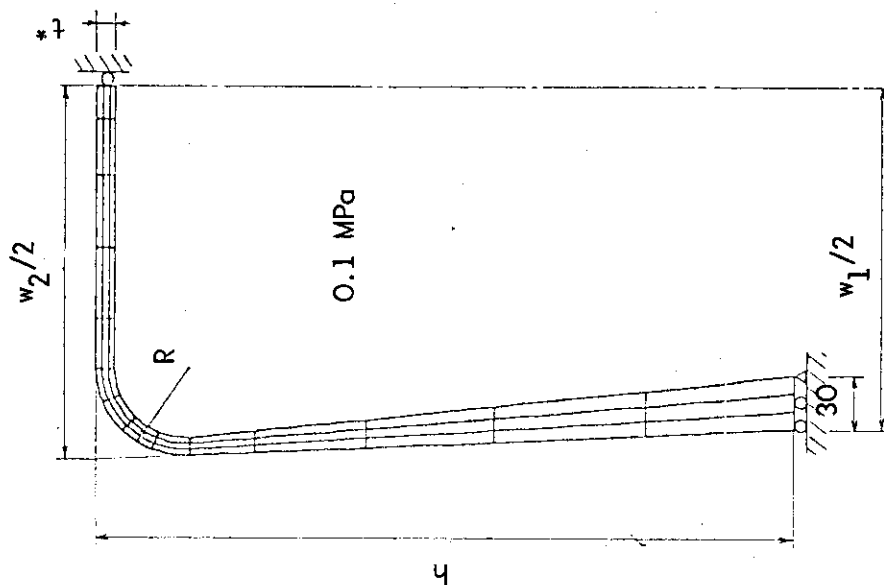
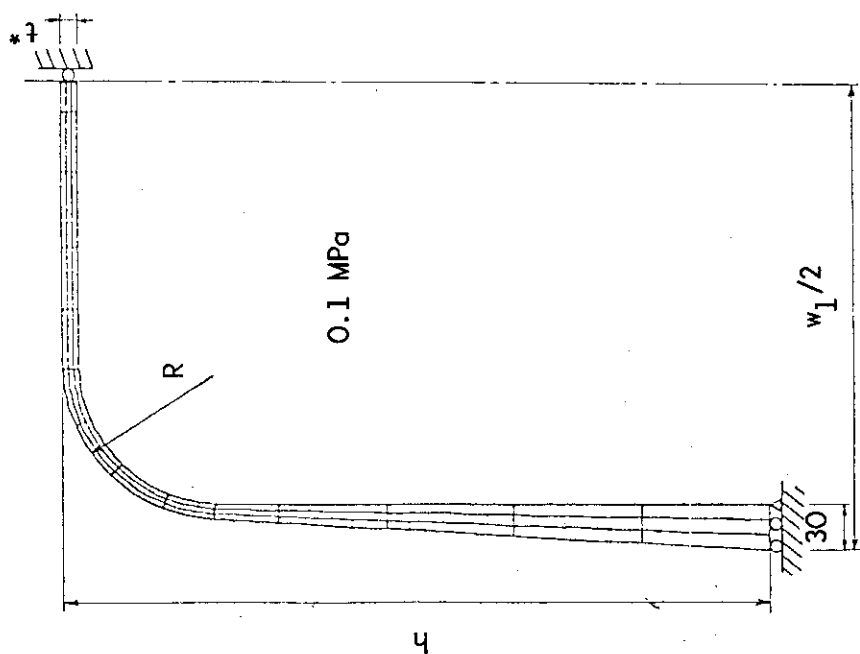


Fig. Boundary Conditions and Distribution of Stress Intensity

Appendix



(b) Inner Blanket



(a) Outer Blanket

Fig. Analytical Model and Boundary Conditions

Appendix

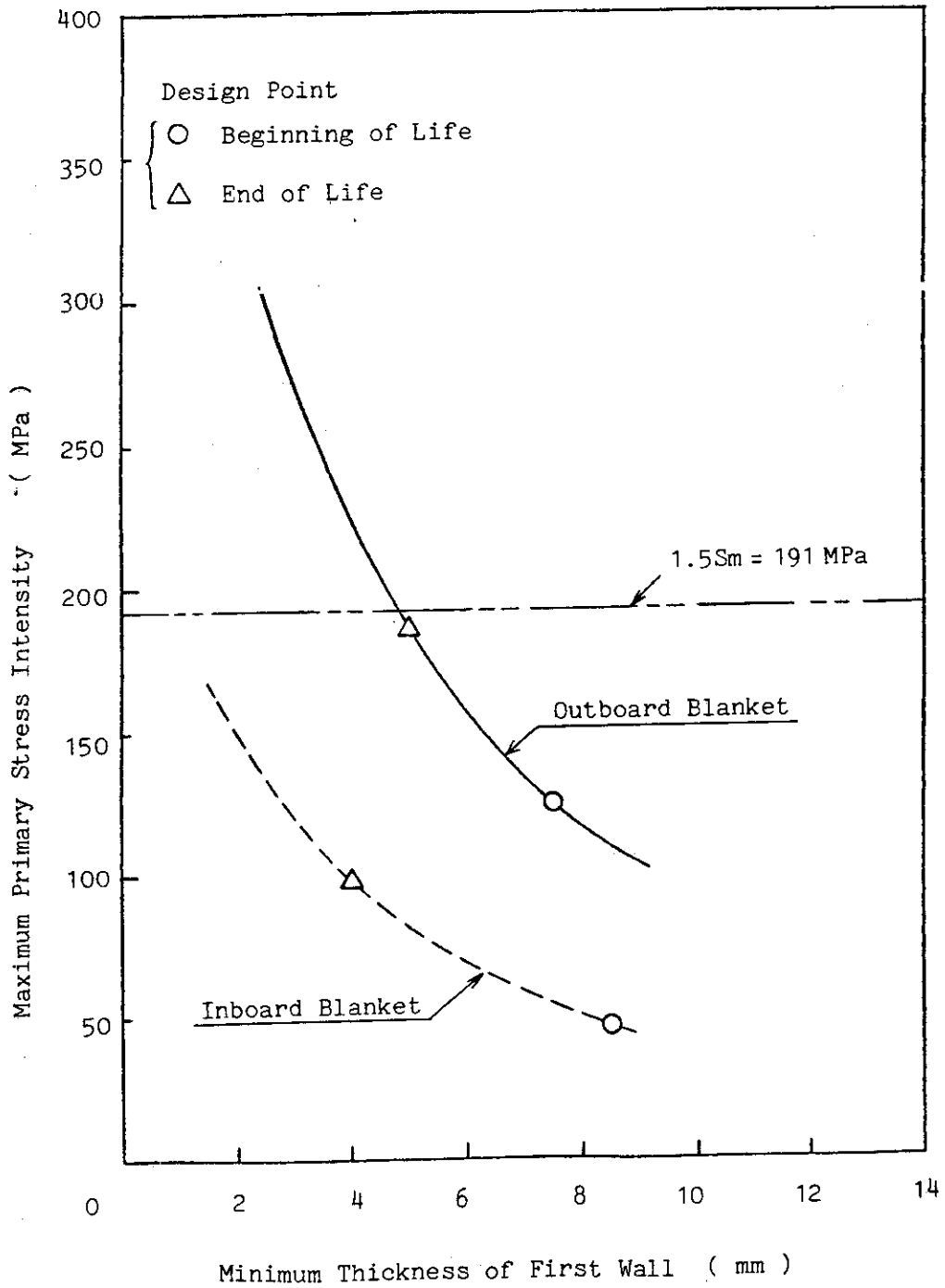


Fig. Maximum Primary Stress Intensities in First Wall.

VI. Technology Issues of the FER Blanket Development

In order to develop a viable blanket concept, data bases for various kinds of materials (structural, coating and armor) under high heat flux and neutron irradiation conditions are required. Feasibility testing data obtained from the structural testing are also required to determine the concept of blanket structure.

1 Material data bases

1.1 Plasma-First Wall Interaction

- First wall candidate materials -

- structural material ; 316 S.S., modified 316 S.S., Aluminium, Mo-alloy,
- armor material ; SiC, Graphite, etc.
- coating material ; Beryllium, etc.

(1) Charged particle

- physical sputtering rate
- chemical sputtering rate
- blistering rate

(2) Intense surface heat flux at plasma disruption

- surface temperature
- melt layer
- surface evaporation
- sublimation

without and with the effect of electromagnetic force and the effect of vapor shield.

1.2 Neutron irradiation data

- (1) Strength and fatigue data of structural material including welding part
- (2) Physical properties (thermal conductivity, specific heat capacity, etc.) of Li_2O , Pb, Be, 316 S.S. and modified 316 S.S.

2 Structural data bases

2.1 First Wall Structure

- Partial models of the candidates -

- integral type or separated type
- surface structure and coolant channel structure
 - : tube-panel, semi-circular-tube-panel and ribbed panel
 - : grooved and non-grooved surface
 - : coating surface

(1) Heat load during burn time

- temperature distribution
- thermal stress and cyclic thermal fatigue
- thermal and mechanical integrities of brazing, coating

(2) Heat load during plasma disruption

- surface temperature
- thermal stress
- thermal shock and its fatigue

(3) Coating technique

(4) Attachment technique of armor

(5) Brazing technique

(6) Fabrication technique

(7) Inspection technique

2.2 Temperature Control of the Breeder

(1) Partial model

- packing forms of Li_2O pebbles, especially near coolant tube
- thermal conductivity of packed bed and temperature distribution in the bed
- flow distribution of the coolant
- sensitivity of helium gap on the temperature control
- fabrication accuracy of the clearance of helium gap
- performance of other candidates of temperature control: ceramic coating, metallic bonding or active control including material selection
- flow distribution of helium purge gas

(2) Full model

- temperature control for the poloidal change of power density
- hot spot
- structure free from thermal expansion

2.3 One Module of First Wall/Blanket Vessel

(1) Construction technique

(2) Test for internal pressure and thermal load

(3) Fatigue test for thermal cycle

(4) Thermal shock test for plasma disruption

(5) Support structure of first wall (separated type)

(6) Safety of blanket by rupture of cooling tube

2.4 One Sector of First Wall/Blanket Vessel/Shield

(1) One turn resistance

(2) Electromagnetic force

(3) Seismic test

(4) Repair and maintenance technique

3 Design standards for a fusion blanket

The philosophy and procedures in ASME Boiler and Pressure Vessel Code will be available to assess the structural strength of the blanket. However, there are some problems to apply the code to fusion reactor design: the classification of components and of service condition (level A, B ---), etc. In order to establish the design standards for a fusion reactor, it is required to clarify the loading condition and the service temperature of the each component, the safety level, and so on.

4 Fabrication of Blanket

Based on state-of-art technologies for the fabrication of blanket, following issues are to be solved in near future.

4.1 Fabrication Technique

Main technologies required for fabrication are mentioned in " V Thermomechanical Design of the FER Blanket ". In these technologies, following issues should be solved.

(1) Precise Machining and Cold Bending of Heavy-section Stainless Steel

Machining of austenitic stainless steel causes work hardening which impairs machinability and precision. Further, cold bending also causes plastic deformation which makes precise joining more difficult after that. Therefore, following research should be performed.

- . Selection of proper machining conditions
- . Material modification of tool for machining
- . Cold bending of full-scale and heavy-section stainless steel

(2) Joining Method for First Wall and Cooling Tube

In this blanket design, it is difficult to join the first wall and cooling tube with integrity. Therefore, full considerations should be paid to the joint design from viewpoint of joining. In this meaning, following research should be made.

- . Proper joint design
- . Development of practical joining method suitable to joint design

(3) Welding of Heavy-section Stainless Steel

Heavy-section stainless steel is welded by EBW (electron beam welding). This welding is carried out in the vacuum chamber for complicated large component which requires mobile gun and beam tracking system to

avoid misalignment of the electron beam. In this meaning, following research should be conducted.

- .Development of mobile gun for large component
- .Development of beam tracking system

4.2 Demonstration of Technologies required

Technologies required for fabrication of the blanket should be established by use of the partial model. In this demonstration, following techniques should be verified.

- .Fabrication technique mentioned above
- .Non-destructive testing

Further, these techniques employed should be finally confirmed to be useful for the fabrication of blanket through the mock-up test.

5 Blanket-Tritium System

5.1 Fabrication technique of Li_2O breeder

5.2 Physical and chemical properties of Li_2O breeder

- hydrolysis reaction rate and weight loss rate in the presence of water vapor in flowing He
- major vapor species over Li_2O and their vaporization pressure in operating temperature range
- effective thermal conductivity in helium atmosphere (including Li_2O pebble packing fraction and wall effect)
- compatibility with structural material

5.3 Integrity assurance of Li_2O breeder

- grain growth, sintering and pore-closure under high temperature and neutron fluence
- mechanical integrity of breeder zone under cyclic thermal condition

5.4 Tritium release rate from Li_2O breeder

- effects on tritium release for a number of variables such as chemical composition of breeder, particle and grain size, temperature, and purge gas flow rate

5.5 Energetic Tritium Permeation

- determining process (diffusion, recombination, etc)

VII. Studies on the Fusion Reactor Blanket Engineering
at Universities in Japan, 1980-1982

Study Items on Fusion Reactor Blanket Engineering at universities in Japan may cover very wide fields. One side of our works on these fields is the contribution to Blanket & Shielding Designs for various conceptual Fusion Reactors, which includes the Reactive Plasma Study Project (IPP, Nagoya Uni.), the Laser Fusion Reactor-Senri (Osaka Uni.), the Heliotron Reactor (Kyoto Uni.), the Tandem Mirror (Tsukuba Uni.) and the D-D Tokamak (Kyushu Uni.). The other side may include the promotion of basic engineering studies on fusion neutronics, thermal-hydraulic study, stress analysis and other miscellaneous items.

The former works were mainly based on the already established nuclear fission reactor design technology with some adjustments, such as a typical neutrons transportation code ANISN and the Nuclear Data File ENDF/B-IV which are widely adopted for nuclear reactor design.

However, the latter works indicate big discrepancies between calculated values based on the conventional technology for fission reactors and some experimental values obtained by some basic studies for fusion reactor design. For the future conceptual design study of fusion reactor, it is clear that we must have specific design methods which emphasize the properties of fusion energy.

To override such technological gaps between the basic studies and the reactor design, it was decided that special financial supports for the development of fusion reactor blanket engineering from the fiscal year of 1983 to 1985 should be provided as Grant in Aids for Fusion Research from the Ministry of Education, Science and Culture.

Contributions to each conceptual design work were already presented at several international meetings, for instance, IAEA Symposium on Fusion Reactor Design at Tokyo in 1981 and at Baltimore in 1982. So, the appendix of this memorandum contains only the summaries of basic studies of 1980 and 1981 in the field of blanket engineering.

Acknowledgement

The authors are greatly indebted to Y. Iso (Director) of Fusion Research and Development Center, K. Tomabechi (Head) and M. Yoshikawa (Deputy Head) of Division of Large Tokamak Development, and Y. Obata (Head) of Division of Thermonuclear Fusion Research for their encouragement and valuable comments.